Novel Controller Designs for VSC-HVDC Networks

Jiebei Zhu

A thesis submitted for the degree of Doctor of Philosophy

to Department of Electronic and Electrical Engineering

University of Strathclyde

June 2013

This thesis is the result of the author's original research. It has been composed by the author and has not been previously submitted for examination which has led to the award of a degree.

Abstract

Future power system will incorporate much higher penetrations of renewable energy than is presently the case. In particular, large offshore wind energy resources, connected to AC power systems via HVDC and VSC converters, are expected to proliferate.

This thesis introduces research in the area of control of multi-terminal HVDC systems, presenting a review of the state of the art and challenges associated with respect to VSC control solutions for HVDC transmission systems. To address one of the identified challenges (effective control of a multi-terminal HVDC system), a direct current matching control strategy is developed and demonstrated. This uses telecommunications to match the input and output powers of the various VSCs. The operation of the scheme is demonstrated through several case studies, and the advantages of the strategy compared to more traditional and other proposed schemes are presented.

Another major challenge associated with future power systems is a reduction in system inertia, due to increased levels of energy being provided from renewable sources, which typically provide little or no inertia to the system. Voltage source converters (VSC), used in high voltage direct current (HVDC) transmission applications, are often deliberately controlled in order to de-couple the interconnected systems to prevent propagation of transients and potential for instability between the systems on either side of the VSC interface. However, this can inhibit the provision of much needed support during transients that would otherwise be available from system inertia provided by rotating plant connected to an interconnected system. Accordingly, a novel VSC-HVDC control system, termed "INEC" (INertia Emulation Control) is proposed, which enables a VSC-HVDC system to provide support that emulates the inertia of synchronous generators (SG). The energy to provide the inertial response is sourced from the capacitance of the HVDC connection, which may be augmented by the installation of additional capacitance. The proposed INEC system allows a VSC-HVDC system with a fixed capacitance to emulate a wide range of inertia constants (H) by specifying the amount of permissible DC voltage variation. The scheme is demonstrated through simulations, and its performance is evaluated for transients that include faults and also changes in load.

Acknowledgements

This research project, sponsored by UK Engineering and Physical Sciences Research Council (EPSRC) and Rolls-Royce plc under a Dorothy Hodgkin Postgraduate Award, has been carried out at the Department of Electronic and Electrical in University of Strathclyde, Glasgow, UK. The sponsors are thankfully acknowledged.

First of all, my great gratitude is given to my first supervisor Dr. Campbell Booth, for his dedication and support of my research activities. His choice of me for this competitive fully funded studentship is appreciated, and his patience and so many weekend working hours spent refining my research papers will be remembered. I also offer personal thank for his care as well as strictness on me. It has also been a privilege to be a student of my second supervisor Professor Graeme Burt and this is much appreciated.

I express my appreciation to Dr. Grain Philip Adam for his generous technical guidance and specific knowledge support, and for his day-after-day work with me, without which the research project would not have progressed so well. Also thanks to Professor Steven Finney for sourcing the staff support for my project. Many thanks go to Dr. Andrew Roscoe for his close engagements and constructive suggestions with my project. My acknowledgements also go to my industrial supervisor Chris Bright of Rolls-Royce plc, for his precious time spent on guiding my research activities and correcting my papers.

Last but not least, I would also like to thank Dr. Stuart Galloway and Dr. Adam Dysko for their encouragement and recognition of me, and my friends Qiteng Hong, Tianyu Luo, Xinyao Li, Jun Xia, Xue Cao, Yushu Zhang, Jiancong Ren, Feng Ding, Kyle Jennett, Douglas Ritchie, Steven Blair, Steven Fletcher, etc. for accompanying me throughout my university life.

Jiebei Zhu
Royal Leamington Spa, UK
June 2013

Contents

Figures

Glossary of Terms

AC	Alternating Current
CCS	Carbon Capture and Storage
CO_2	Carbon Dioxide
CSC	Current Source Converter
CSC-HVDC	Current Source Converter Based HVDC
DC	Direct Current
DCMC	Direct Current Matching Control
DCVD	Direct Current Voltage Droop Control
DCVM	Direct Current Voltage Margin Control
DFIG	Double Fed Induction Generator
EU	The European Union
FACTS	Flexible Alternating Current Transmission Systems
FC	Flying Capacitor Converter
GB	Great Britain
HVDC	High Voltage Direct Current Transmission
HVAC	High Voltage Alternating Current Transmission
IEEE	The Institute of Electrical and Electronics Engineers in US
IET	The Institute of Electrical and Technology in the UK
IGBT	Insulated Gate Bipolar Transistor
INEC	INertia Emulation Control
LCC	Line Commutated Converter
LCC-HVDC	Line Commutated Converter Based HVDC

MMC	Modular Multilevel Converter
MPPT	Maximum Power Point Tracking
MTDC	Multi-terminal DC Transmission System
NPC	Neutral-Point-Clamped Converter
PCC	Point of Common Coupling
POD	Power Oscillation Damping
PSS	Power System Stabiliser
PWM	Pulse Width Modulation
RCL	Circuit Consisting of a Resistor, a Capacitor and a Inductor
Sine	Sinusoidal
SG	Synchronous Generator
SM	Synchronous Machine
SSSC	Static Synchronous Series Compensator
STATCOM	Static Synchronous Compensator
THD	Total Harmonic Distortion
UK	United Kingdom
VSC	Voltage Source Converter
VSC-HVDC	Voltage Source Converter Based HVDC
XLPE	Cross-linked Polymeric Electrical Insulated Cable
WPG	Wind Power Generator

Chapter 1

Introduction

1.1 Research Context

Worldwide demand for electricity is rising. As shown in Figure 1.1, electricity assumptions for different global regions (measured in Mtoe - millions of tons of oil equivalent) have been increasing dramatically over recent decades, and this increase is expected to accelerate markedly in the future. The reasons for this increase are as follows: industrialisation and huge growth in energy-intensive businesses and factories, especially in emerging markets, which require significant amount of electricity in order to operate. As global economies industrialise and their society and infrastructure develops, electricity demand invariably increases. Developing countries such as China and India are experiencing huge growth in terms of industries and electrification of communities. Furthermore, in countries with mature electrical infrastructure, the electrification of heating and transport will also contribute to large growth in demand. Demand growth and the requirement to maintain energy supply security will lead to construction of generating assets, and these will be powered by a variety of energy sources, with an increasing focus on renewable energy sources in the future.

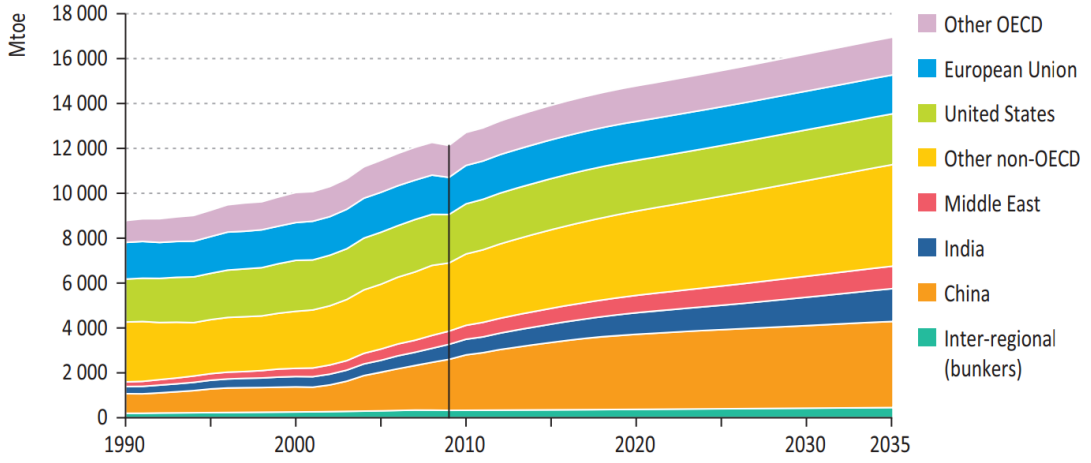

Figure 1.1 World electricity consumption by region [1]

Greater demand for electricity energy is increasing pressure on the availability of natural (predominantly fossil fuel) resources. These pressures are directly reflected on the cost of fuels used to generate electricity. Globally, electric power companies have been struggling to maintain costs at acceptable levels and have been striving to improve efficiency and seek alternative resources. It is important to plan in advance to meet increased energy demands, and there are concerns over whether the future energy supply/demand balance can be met securely [1][2].

Furthermore, climate change has risen to the top of the political agenda and global warming, which is widely acknowledged as being exacerbated by excessive CO_2 emissions, is exposing the planet to significant threats. Many nations have published clear CO_2 reduction proposals: for example the European Union member nations have a target of significantly reducing CO_2 emissions by generating 20% of their total electricity requirements from renewable sources such as wind, hydro, tidal stream, solar and biomass. Market forces will act to determine wholesale electricity prices at a level that discourages conventional, low efficiency fossil-fuelled power plants, and should provide a stimulus to develop renewable energy for new generating capacity, which is likely to lead to a gradual replacement of conventional power plant [4].

The complexity of modern electric power systems is very high, and many aspects of planning and operating systems, comprising generation, transmission, distribution, possibly storage, and interconnections with other systems (possibly via DC interconnectors) must be considered. Some of the main considerations are listed below:

- Where are demand centres and where generation and transmission facilities should be located to meet the demand?

- Where is demand growth going to be and what plans must be drawn up to meet these areas of growth?

Figure 1.2 shows the proposed reinforcements for the UK power transmission system. As a mean of assessing power system stability; it is useful to consider a power transmission system to be sub-divided into areas that are defined by boundaries. Even at present, UK transmission networks are under increasing strain. There are very limited generation connection opportunities in Scotland, Wales and the north of England and, as such, there is a need for major transmission network reinforcement in these areas [6]. As there are abundant wind energy resources in Scotland, the predominant power flow in the UK mainland is increasingly from net generation in the north to net load in the south. It is estimated by the UK transmission system operator National Grid [2] that certain power flow levels across specific north/south boundaries could increase by up to five times their present levels and capacities under certain future scenarios. The transmission system boundaries in England will see less pronounced changes in power transfer requirements, but there is still enough generation development to potentially warrant significant future transmission system reinforcements.

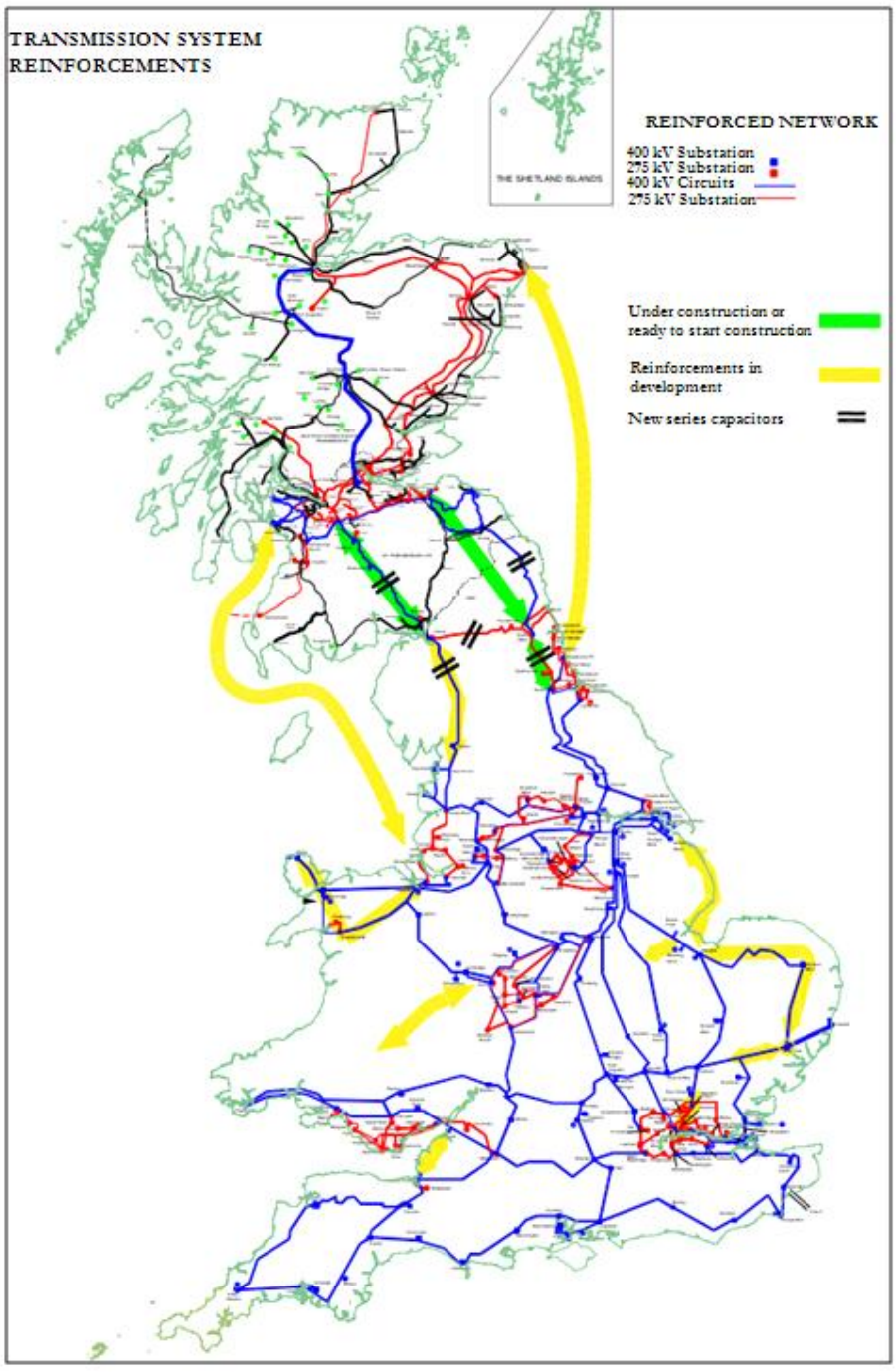

Figure 1.2 Proposed reinforcements for UK transmission power grids [5]

The existing onshore transmission network is operated almost at its maximum capability (in specific locations) so there is a need for re-conductoring and/or increasing the voltage from 275 kV to 400 kV on many circuits. There is also a requirement to expand the network in order to accommodate increasing renewable power penetration (indicated by the green and yellow lines shown in Figure 1.2). Meanwhile, two offshore high voltage DC transmission links are proposed off the western and eastern coasts of the UK to facilitate increased power transfers between north and south. Future

transmission network planning and construction must be carried out optimally to facilitate new renewable generation connections and to reduce grid connection charges.

Presently in the UK, electrical energy generation is primarily sourced from natural gas and coal (307.3 TWh and 302.7 TWh respectively in 2011, as illustrated in Figure 1.3). Nuclear energy also provides a significant proportion of the energy generated (181.7 TWh), while contributions from renewable sources such as wind and hydro remain relatively small. The energy in these fuels is converted to electricity by power stations and delivered to various loads such as industry, domestic and transportation, with relatively high losses associated with energy conversion, and the transmission and distribution systems (resistive heating losses in transmission and distribution systems and losses associated with reactive power exchange).

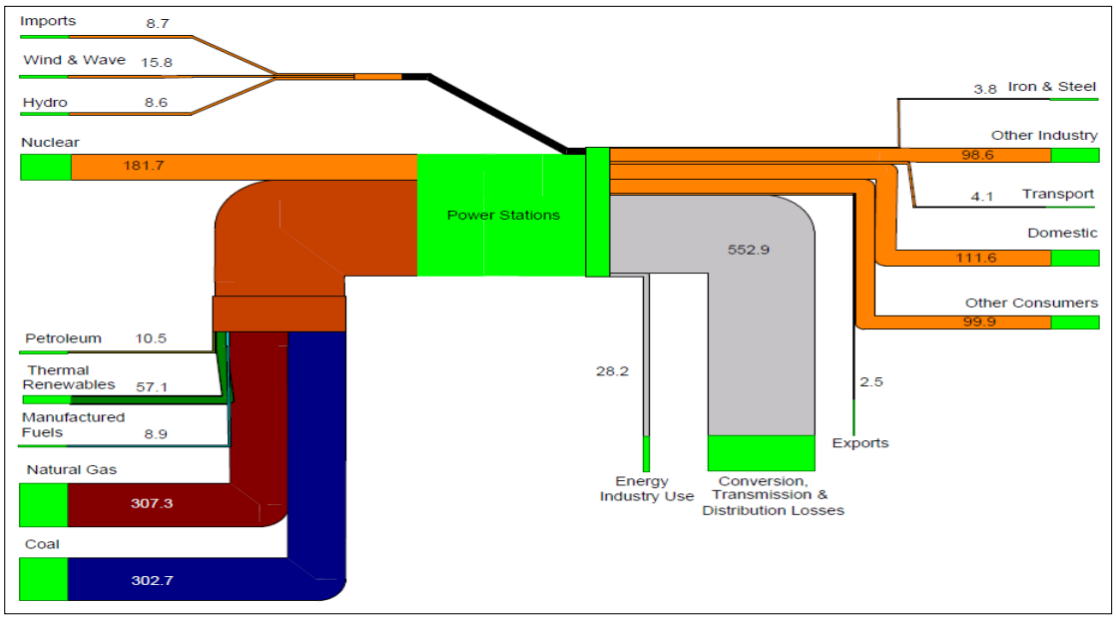

Figure 1.3 UK electrical energy flow composition [7]

As shown in Figure 1.4, electrical energy generation in the UK is currently undergoing a dramatic change. The majority of existing coal fired power plants and a large proportion of gas fired power plants will close successively in the forthcoming decades [9] and the two most significant reductions, in terms of fuel sources, are coal and gas (although the technology of "fracking" and removal of gas from significant reserves that exist in the UK could change this). Nuclear power remains relatively unchanged in present projections up to the year 2028, when it will slightly increase its share due to its high availability and provision of continuous base load power [8]. Renewable energy, particularly offshore wind power, will grow its share of the generation mix and play an

important role in meeting future power demand – this is facilitated by many government policies that incentivise development of wind power. For example, Renewable Obligation Certificates are designed to encourage renewable energy development in the UK by placing an obligation on licensed electricity suppliers in the United Kingdom to source an increasing proportion of electricity from renewable sources (initially set at 3% in 2002/03, 11.1% in 2010/11 and rising to 15.4% by 2015/16) [10][11]. To exploit these market incentives, the certificates can be traded between suppliers that have surplus renewable capacity and those that do not on the basis of a fixed price per MWh [11].

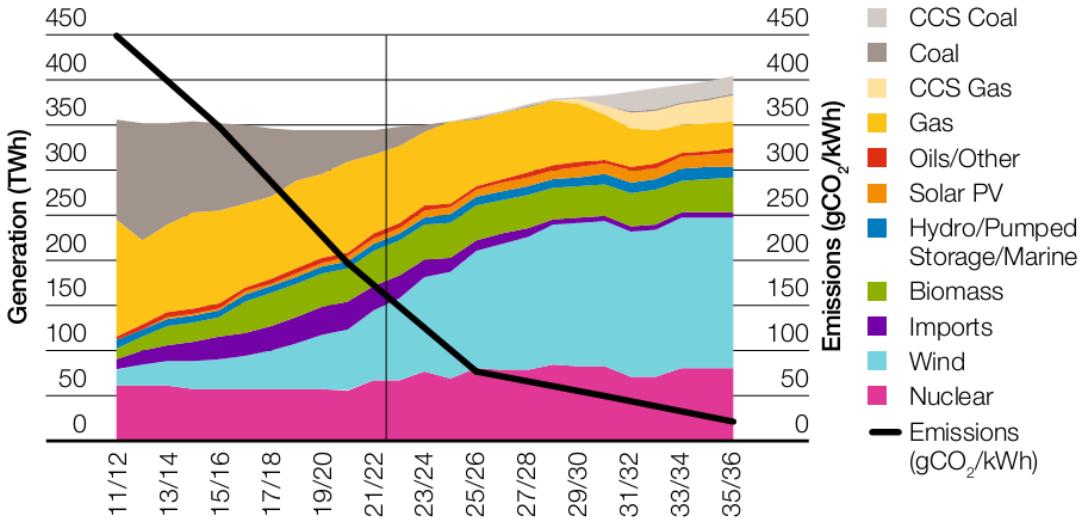

Figure 1.4 Estimated UK future generation by fuel type and carbon intensity [9]

Wind power generators of all sizes have become a familiar sight around the world for a wide variety of reasons, which include their economic, environmental and social benefits (although these benefits are often the subject of debate). The development of wind power is recognised as one of the most promising options for meeting electricity consumption, and carbon reduction, needs of the future. In Europe, wind power is even more crucial, as it is estimated that unless remedial actions are taken, 70% of Europe's energy will be imported by 2025 and Europe will be more dependent on neighbouring countries for gas [13]. The utilisation potential for wind energy is immense, as shown in Figure 1.5, which presents operational wind generation in Europe. Germany possesses the highest capacity of 29 GW, while Spain has 21 GW. In terms of prospective wind power developments, many governments have established targets for using large amounts of wind energy to meet demand (e.g. 20% by 2020 in the EU member states [14]) and reduce CO_2 emissions as part of their attempt to mitigate climate change.

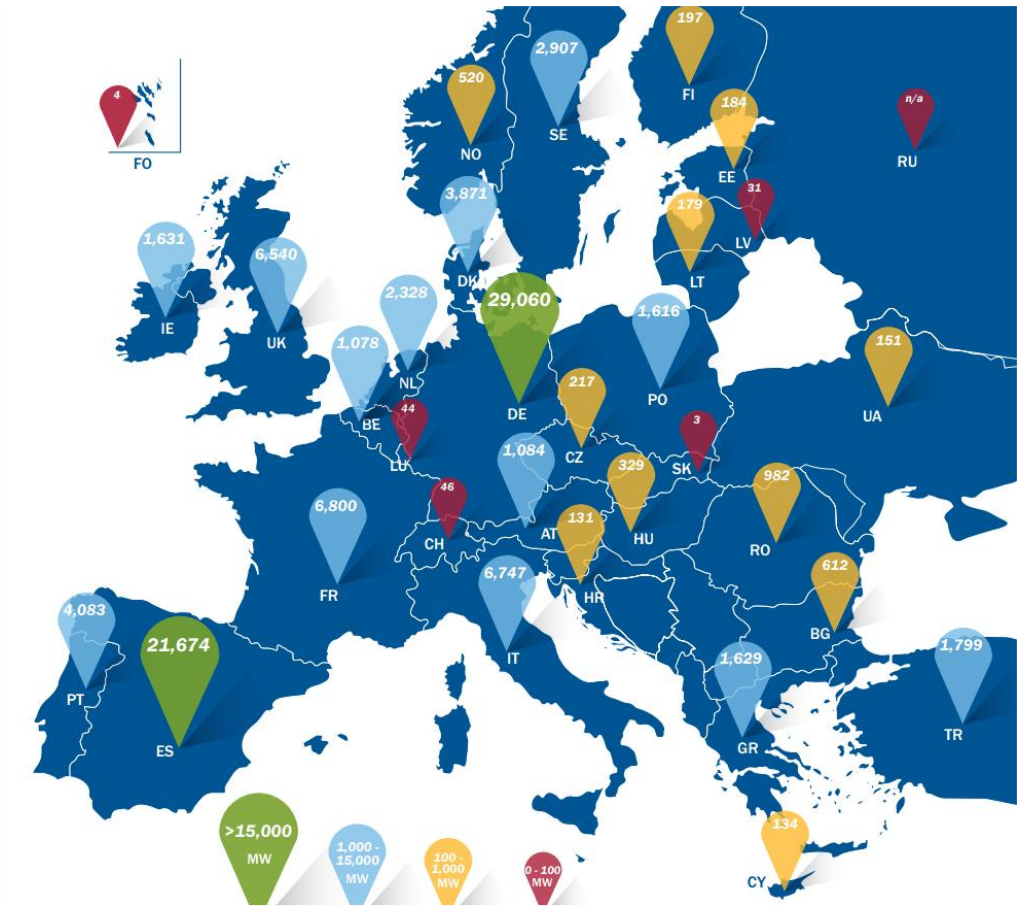

Figure 1.5 Operational installed wind power in Europe in 2011 [12]

As stated in the European Wind Energy Association's "Key Trends and Statistics" report [14], in 2012 there are 132 new offshore wind turbines constructed, with a combined capacity totalling 523.2 MW. In the near future, 35 GW of offshore wind power is proposed in Europe by 2020, and 120 GW by 2030 [15]. The fast pace of European wind power development is evident in Table I, which shows installed wind power during 2011 and 2012.

Nevertheless, wind power is difficult to harvest and is typically dispersed over large geographic areas. The large areas required for wind power generation sites limits the pace of onshore development. It is estimated that a wind-powered equivalent of a typical base load power plant of approximately 1 GW would require an area of 300 square miles to house the necessary turbines and associated equipment. This may also require construction of new transmission infrastructure [8]. Due to limited land availability, public objections and media coverage, the construction of wind farms onshore may be viewed as reaching saturation levels (certainly this is true in the UK) and the

development and exploitation of wind power is now focussed on offshore installations [16].

Table I. Wind power installed in Europe by end of 2011 [12]

	Installed 2011	End 2011	Installed 2012	End 2012
EU Capacity (MW)				
Austria	73	1084	296	1,378
Belgium	191	1,078	297	1,375
Bulgaria	28	516	168	684
Cyprus	52	134	13	147
Czech Republic	2	217	44	260
Denmark	211	3,956	217	4,162
Estonia	35	184	86	269
Finland	2	199	89	288
France	830	6,807	757	7,564
Germany	2,100	29,071	2,415	31,308
Greece	316	1,634	117	1,749
Hungary	34	329	0	329
Ireland	208	1,614	125	1,738
Italy	1,090	6,878	1,273	8,144
Latvia	17	48	21	68
Lithuania*	16	179	46	225
Luxembourg*	1	45	0	45
Malta	0	0	0	0
Netherlands	59	2,272	119	2,391
Poland	436	1,616	880	2,497
Portugal	341	4,379	145	4,525
Romania	520	982	923	1,905
Slovakia	0	3	0	3
Slovenia	0	0	0	0
Spain	1,050	21,674	1,122	22,796
Sweden	754	2,899	846	3,745
United Kingdom	1,298	6,556	1,897	8,445
Total EU-27	**9,664**	**94,352**	**11,895**	**106,040**
Total EU-15	**8,524**	**90,145**	**9,714**	**99,652**
Total EU-12	**1,140**	**4,207**	**2,181**	**6,388**

Integration of offshore wind farms with onshore power systems has resurrected the debate surrounding the use of AC versus DC for power transmission purposes. The story of AC versus DC originates in the days of Thomas Alva Edison, as shown in Figure 1.6, who established a research laboratory at Menlo Park, New Jersey and invented a commercial DC generator and incandescent lamp in 1872 [17]. In 1882, the Peel Street Power Station began providing electrical energy to New York's financial district using six "jumbo dynamos" producing DC, each rated at 100 kW, which provided power to 7,200 lights. The debate at the time also encompassed the safety aspects of the competing AC and DC technologies. Initially, DC was the preferred choice, but its dominance was brief, and George Westinghouse joined with Nikola Tesla

and others to capitalise on the performance and benefits of AC, the main benefit being the ability to easily transform voltage in AC systems and the use of AC induction motors. AC was eventually selected as the technology of choice and has been dominant for more than 100 years. However, DC still possesses important benefits, particularly with respect to improved power transfer capacity, and for bulk power transmission, particularly over long distances and/or in underground or subsea cables. It is clear, however, that DC is more efficient than AC in specific application contexts.

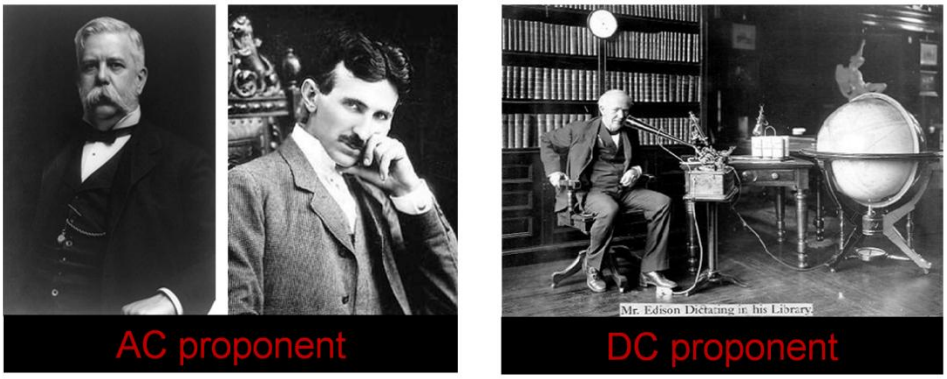

Figure 1.6 From left to right: George Westinghouse, Nikola Tesla and Thomas Alva Edison

As of June 2013, more than 170 HVDC transmission networks have been built worldwide (a project list is provided in Appendix C Table V), with a total capacity of almost 200 GW, and HVDC transmission systems are an increasingly important contributor to successful power system operation [18]. Figure 1.7 illustrates a possible DC grid design in Europe in 2030, showing that large-scale HVDC grids may be in use. This will facilitate international power exchange and trading, and the integration of large amounts of offshore wind power.

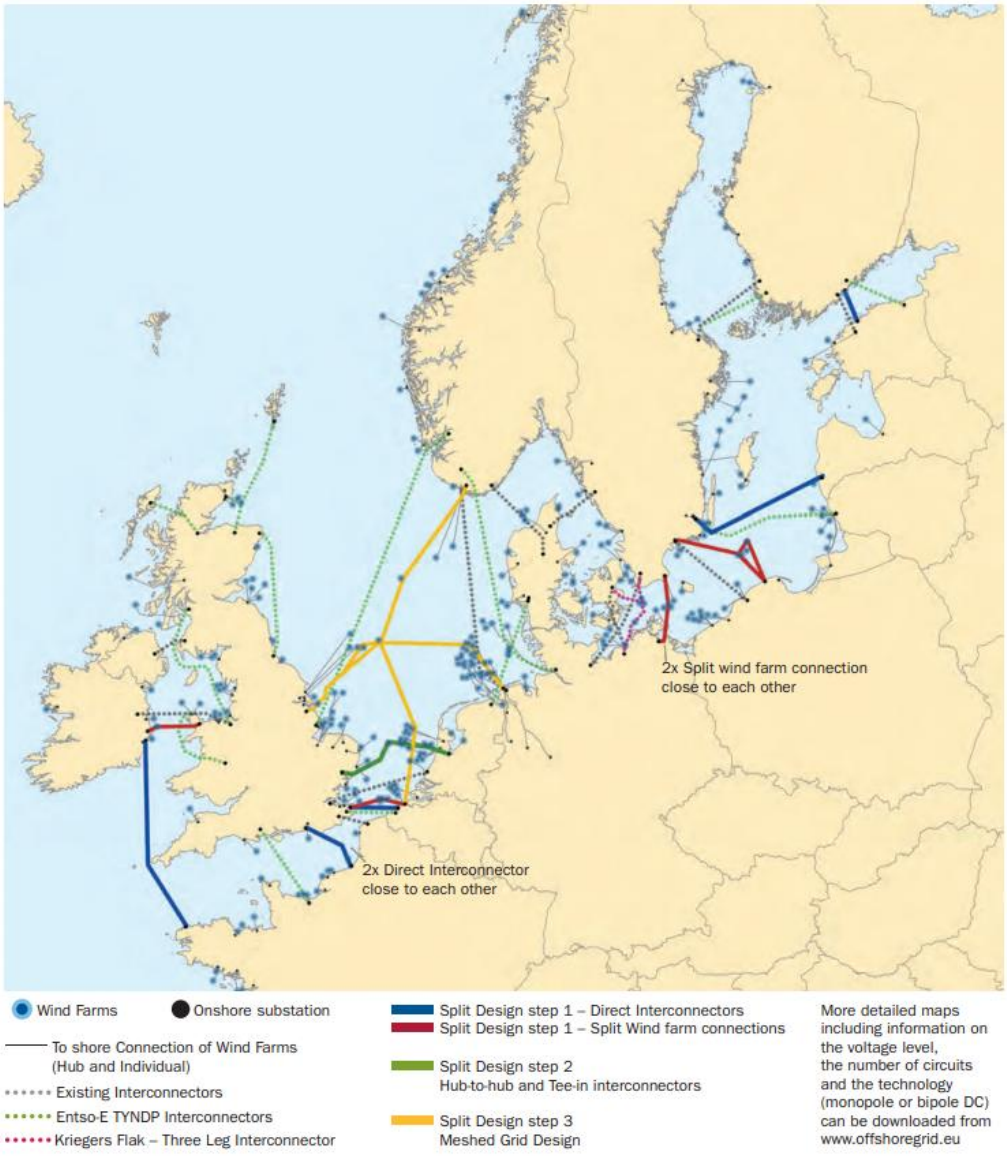

Figure 1.7 Possible layout of European DC grid in 2030[19]

At present, traditional AC transmission networks are highly meshed and tightly interconnected, whereas HVDC transmission systems remain predominantly applied to point to point transfer of power within and between AC systems. For integration of remote offshore wind farms, multi-terminal DC grids are desired to deliver wind power with less electrical losses than AC systems. Furthermore, large pan-European MTDC networks will facilitate the interconnection of UK, European and possibly African AC power systems and provide a vehicle that can act to smooth fluctuations in generation and demand over a massive geographic area. Additionally, this facility would allow power to be transferred and traded between different regions in addition to collecting energy from large offshore wind (and possibly marine) energy sources.

It has come to a time when an offshore "DC Supergrid" to facilitate offshore renewable connections is urgently required. This has been proposed in [20], which will initially build and subsequently expand a European DC Supergrid, centred in the North Sea. It is proposed that this supergrid would be built over three phases, as illustrated in Figure 1.8. To address immediate offshore wind integration issues while providing a staging post for the future in phase 1, the first prototype of DC supergrid is planned to connect North sea-surrounding countries. Energy from wind park modules off the coasts of the UK is collected at the DC super nodes at Firth of Forth, Dogger Bank/Hornsea, Norfolk Bank, which are connected together and interconnected with German and Belgian North Sea Wind park modules and Norwegian hydro power units [20]. The DC grid then can deliver the power to the super nodes at Glasgow, Hull and Zeebrugge, and the super node at London and southern Germany.

Phase 2 and phase 3 of the European DC supergrid as illustrated in Figure 1.8 will be topological extension of the backbone DC grid achieve in phase 1. In phase 2, the DC supergrid has new DC super node at Netherland and further expanded southwards to France. In phase 3, the DC supergrid is proposed to cover many Continental countries (e.g. Poland, Italy, and Spain) and Mediterranean islands. As phase 2 and phase 3 will be realised in far future which involves various uncertainties, they are not introduced here in details.

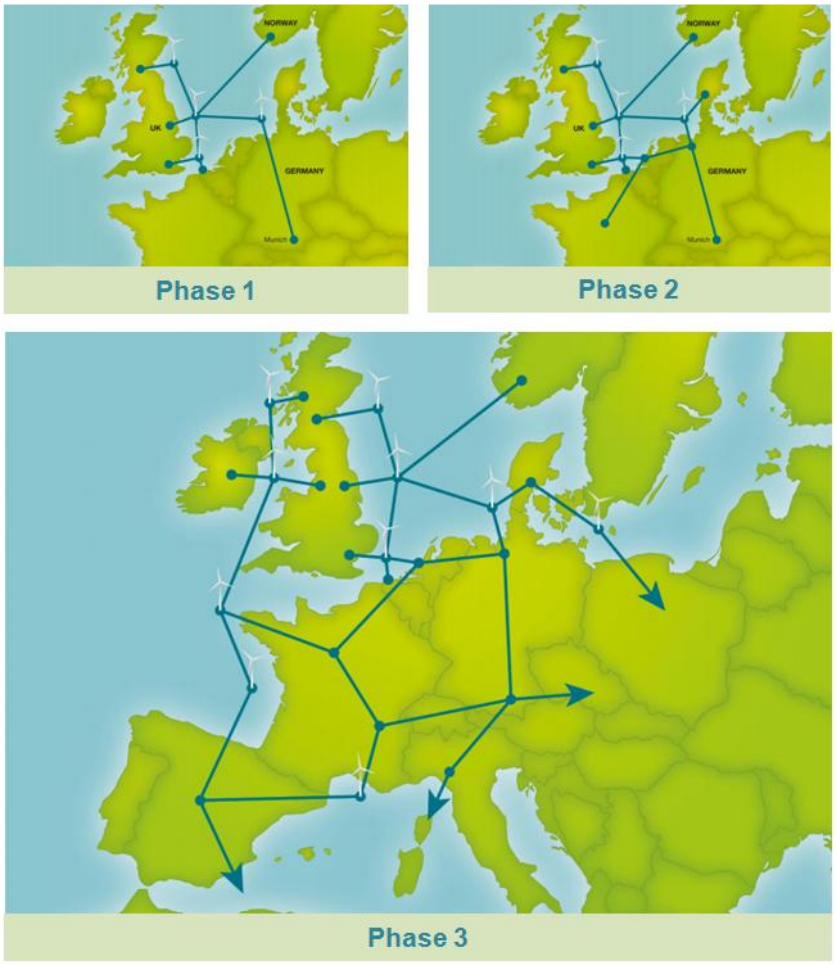

Figure 1.8 Pan-European DC supergrid proposal [20]

1.2 Research Challenges Arising from Increased HVDC Connections

VSC-HVDC transmission systems, and the associated operation, control and protection functions, must be fully understood in order to quantify benefits and ensure that systems will be fit for purpose in integrating renewable energy and that system stability will not be compromised. Associated with this, and also due to the rapid development of renewable generation technologies, future power systems will be faced with a higher level of technical uncertainty and risks, some of which are listed below:

- Decreasing fault levels on the system, as illustrated in Figure 1.9, could compromise the functionality of certain protection devices, due to the implementation of self-commutated power electronics converters. These reductions in fault level will arise as a result of decommissioned conventional plant and increased converter-interfaced sources. This situation may also, in extreme cases, limit the ability of conventional

protection and backup protection to correctly identify and operate for fault conditions on AC networks.

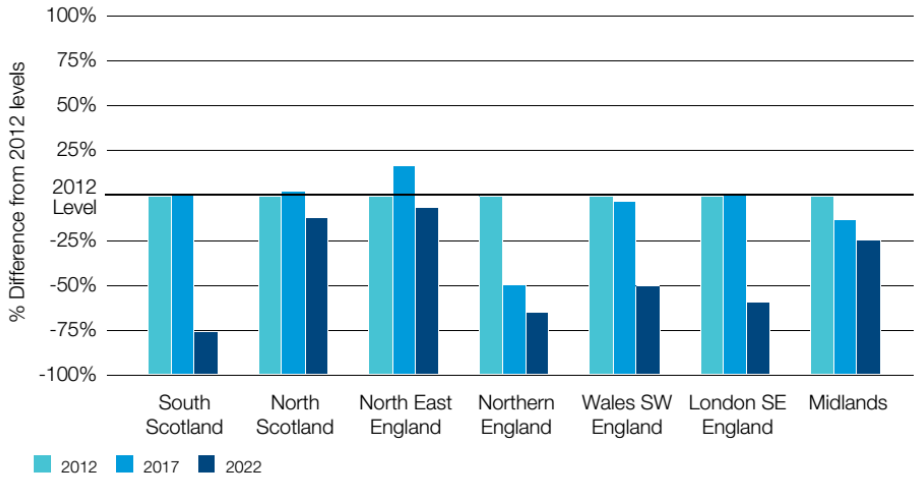

Figure 1.9 Fault level variation for the National Grid's Gone Green Scenario [2]

- Connection of larger amount of distributed generations will change historically unidirectional power flow and flows will become more volatile, both in terms of magnitude and direction of flows. Consequently, managing voltage profiles, particularly in high wind lower demand periods, could become more difficult [2];

- Less predictable renewable power output must be matched sufficiently quickly by balancing conventional generation and/or demand – this could be challenging in some cases.

- Falling levels of conventional synchronous generators in service, particularly in periods of lower system demand, will effectively reduce the system inertia as shown in Figure 1.10 of the change in total UK system inertia (calculated in GVA.s) at different years and during low demand periods, which is given by UK National Grid's Electricity Ten Year Statement. The reduction on system inertia will lead to an increased risk of frequency instability, which in turn negatively impacts upon rate of change of frequency protection (ROCOF) as applied by many distributed generators in the UK.

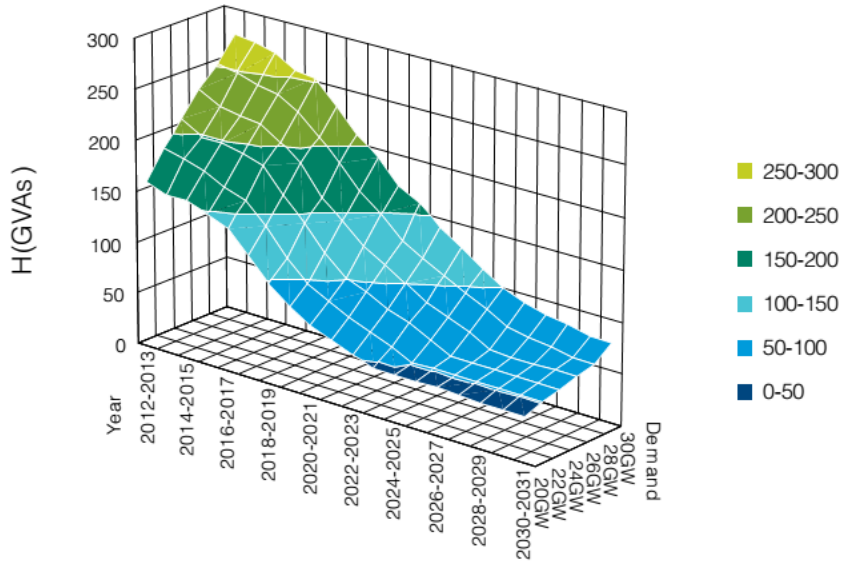

Figure 1.10 System inertia changes for National Grid's Gone Green scenario at 70% wind power output (H= System Inertia, measured by GVA.s) [2]

1.3 Research Aims and Scope

In order to address a number of the challenges previously mentioned, the aim of this thesis is to investigate voltage source converter-based HVDC (VSC-HVDC) transmission systems from the perspectives of modelling, design and understanding their detailed operation, and to propose and demonstrate new control strategies for VSC-HVDC systems to address the identified issues that may impact negatively upon future power system with high renewable power penetrations. The work has five main objectives, and these are summarised below:

- Review elementary power electronic devices, and investigate and compare the relative features of VSC-HVDC and line commutated converter based HVDC (LCC-HVDC);
- Study of VSC-HVDC system design and operation, specifically in terms of component specifications, converter switching mechanisms and control strategies for various connection and application arrangements;
- Identification of research challenges associated with high penetrations of renewable power, coupled via HVDC on to AC systems;

- Design, development and demonstration of a new control philosophy for VSC based Multi-Terminal HVDC (VSC-MTDC) transmission systems;

- Design, development and demonstration of a new inertia emulation control strategy (synthetic inertia) for VSC-HVDC, and a new inertia emulation controller for individual VSC-MTDC terminals.

1.4 Principle Research Contributions

The First principle contribution is the design, development and demonstration of a novel *Direct Current Matching Control (DCMC)* strategy for multi-terminal HVDC (MTDC) transmission systems. The DCMC strategy, which employs communications (although it can also operate when communications facilities are lost) is a more effective alternative to DC voltage droop control and voltage margin control schemes that have been reported by others, which do not use communications. With DCMC, the MTDC is able to dispatch DC power in a far more flexible manner and has the capability to reduce DC system voltage variations due to fluctuations in input and output power arising from a range of transients.

The second main contribution relates to the design and operation of a novel *Inertia Emulation Control (INEC)* strategy for point-to-point VSC-HVDC transmission systems. This control strategy acts to contribute a "synthetic" inertial response to supplied AC systems from the DC system when required, typically during AC grid disturbances. The INEC is distinct from previous work carried out by other researchers, in that it employs the HVDC link capacitance as the source of energy storage for provision of synthetic inertia. With the INEC, the VSC-HVDC inverter is able to effectively stabilise grid frequency, damp power oscillations and enhance system stability.

Finally, the work has progressed to extend the second principle contribution to develop and demonstrate a *Generic Inertia Emulation Control (GIEC)* for any MTDC converter terminal. With no hardware modification, this controller can equip any grid-side MTDC converter terminal with the capability to contribute synthetic inertia to the grid. This will be useful in future applications of MTDC systems and will assist in addressing anticipated reductions in system inertia in the future.

1.5 Associated Publications

Journals:

- Zhu, J.; Booth, C.D.; Adam, G.P.; Roscoe, A.J.; Bright, C., "Inertia emulation control strategy of VSC-HVDC transmission systems," *IEEE Transactions on Power Systems*, vol.28, no.2, pp.1277,1287, May 2013;

- Zhu, J.; Booth, C.D.; Adam, G.P.; Roscoe, A.J., " Current Matching Control for Multi-terminal DC Transmission Systems with Wind Farm Integrations," submitted to *IEEE Transactions on Power Delivery* on June 2012;

Conferences:

- Zhu, J; Booth, C.D., "Future multi-terminal HVDC transmission systems using voltage source converters,", 2010 45th International Universities Power Engineering Conference (UPEC), vol., no., pp.1-6, Aug. 31 2010-Sept. 3 2010;

- Zhu, J.; Booth, C.D.; Adam, G. P., "Current Matching Control system for Multi-Terminal DC transmission to integrate offshore wind farms," *IET Conference on Renewable Power Generation (RPG 2011)*, vol., no., pp.1-7, 6-8 Sept. 2011;

- Zhu, J.; Booth, C.D.; Adam, G.P.; Roscoe, A.J., "Inertia emulation control of VSC-HVDC transmission system,"*, 2011 International Conference on Advanced Power System Automation and Protection (APAP)*, vol.1, no., pp.1-6, 16-20 Oct. 2011.

- Zhu, J.; Booth, C.D.; Adam, G.P.; Roscoe, A.J., "A Generic Inertia Emulation Controller for Multi-terminal HVDC Transmission Systems with Offshore Wind Farm Integrations," submitted to *IET 2013 Renewable Power Generation in September 2013*.

- Zhu, J.; Urdal, H., "Synthetic Inertia Control Strategy for Double-fed Induction Generator Wind turbine Generators Using Energy from DC Capacitor", 12th Wind Integration Workshop 2013, London, UK.

- Urdal, H.; Ierna, R.; Ivanov, C.; Dahresobh, A.; Zhu, J., "System Strength Considerations in a Converter Dominated Power System", 12th Wind Integration Workshop 2013, London, UK.

- Zhang, H.T.; Lai, L.L.; Zhu, J., "A Novel Automatic Load Shedding Scheme to Improve Survivability of Distribution Networks," submitted to *IEEE International Conference on System, Man and Cybernetics in Manchester October 2013*.

1.6 Thesis Outline

The remainder of this thesis is organised as follows:

Chapter 2: A brief introduction to power electronics technology and the associated devices are presented. This includes a description of diodes, bipolar junction transistors, thyristors, metal-oxide-semiconductor field-effect transistor (MOSFET), insulated gate bipolar transistor (IGBT). The historical development of the technologies and their applications are described: the initial main HVDC application, known as LCC-HVDC transmission systems, are briefly analysed, and a more detailed treatment of the relatively recently introduced VSC-HVDC technology is then presented. This includes a description of converter types and configurations, converter components, and information relating to power transfer capabilities. The fundamentals of modelling a VSC-HVDC system and its associated control system are also presented in this chapter – these models form the basis of analyses presented later in the thesis.

Chapter 3: This chapter contains the findings of a literature review focussing on the power system challenges associated with wind power development and interfacing of large scale renewables to AC power systems. The topics reviewed are centred upon power system frequency stability and the associated control schemes that can be used to address any stability concerns. Several primary frequency response inertia emulation control strategies for renewable power generations and HVDC transmission systems, as proposed and reported by others, are critically reviewed. This chapter also contains a review of reported work associated with the benefits that can be provided by VSC converters to power systems, including AC voltage support and active power damping capabilities. To underpin the outcomes of the work reported later in the thesis, the chapter also reviews a number of control strategies for MTDC networks.

Chapter 4: A novel DCMC control scheme for MTDC transmission system using communications for improvement and enhancement of control systems performance is introduced and examples of its operation are presented and analysed. Through

simulation, the performance of the DCMC is compared with conventional control schemes and its superior relative performance and advantages are demonstrated.

Chapter 5: A novel inertia emulation control (INEC) strategy is introduced and its operation demonstrated for both point-to-point VSC-HVDC and VSC-MTDC systems. Simulations validate and verify the performance of the INEC scheme and highlight its abilities to contribute synthetic inertia and therefore enhance power system frequency stability under a range of system conditions and in response to various events.

Chapter 6: This chapter draws a number of conclusions and provides a list of areas of on-going and future activity that can build upon the findings and outcomes of the research work reported in the thesis.

References

[1] International Energy Agency, *World Energy Outlook 2011*. Online available [assessed on 08/10/2012]: http://www.iea.org/Textbase/npsum/weo2011sum.pdf.

[2] National Grid, 2012 Electricity Ten Year Statement. Online available [assessed on 01/05/2013]: http://www.nationalgrid.com/NR/rdonlyres/DF56DC3B-13D7-4B19-9DFB-6E1B971C43F6/57770/10761_NG_ElectricityTenYearStatement_LR.pdf

[3] Davis, G., *Meeting Future Energy Needs: Choices and Possibilities*. Online available [assessed on 09/10/2012]: http://www.nae.edu/Publications/Bridge/EngineeringEnergyandtheFuture/MeetingFutureEnergyNeedsChoicesandPossibilities.aspx.

[4] White, D., *Reduction in Carbon Dioxide Emissions: Estimating the Potential Contribution from Wind-power*, Dec 2004. Online available [assessed on 11/10/2012]: http://www.ref.org.uk/Files/david.white.wind.co2.saving.12.04.pdf.

[5] UK Electrical Network Strategy Group, *Our Electricity Transmission Network: a Vision for 2020*, July 2009. Online available [assessed on 13/10/2012]:http://www.decc.gov.uk/assets/decc/11/meeting-energy-demand/future-elec-network/4263-ensgfull.pdf.

[6] Barnacle, M.; Ault, G., *Network Reinforcements for Scotland and the Rest of the UK and Possible Solutions for This*. Fraser of Allander Institute Quarterly Economic Commentary, Special I (3). pp. 9-12, 2012.

[7] MacLeay, I.; Harris, K.; Annut, A., *Digest of United Kingdom Energy Statistics 2012*. Online Available [assessed on 13/10/2012]: http://www.decc.gov.uk/assets/decc/11/stats/publications/dukes/5949-dukes-2012-exc-cover.pdf.

[8] South Mississippi Electric Report, *Energy Costs on the rise*. Online available [assessed on 13/10/2012]: http://www.smepa.coop/news/smepa_insert_august08.pdf.

[9] National Grid, *UK Future Energy Scenarios*. Online Available [assessed on 29/07/2013]:

http://www.nationalgrid.com/uk/Gas/OperationalInfo/TBE/Future+Energy+Scenarios/

[10] Parliamentary Office of Science and Technology, *Renewable Energy*. Published in Oct 2001, retrieved in Jun 2011. Online Available [assessed on 19/10/2012]: http://www.parliament.uk/documents/post/pn164.pdf.

[11] UK Government, *National Renewable Energy Action Plan for the United Kingdom*. Online Available [assessed on 21/10/2012]: https://www.gov.uk/government/uploads/system/uploads/attachment_data/file/47871/25-nat-ren-energy-action-plan.pdf

[12] The European Wind Energy Association, *Wind in Power 2012 European Statistics*, February 2013. Online Available [assessed on 21/10/2012]: http://www.ewea.org/fileadmin/files/library/publications/statistics/Wind_in_power_annual_statistics_2012.pdf

[13] Gordon, S., "*Supergrid to the rescue*," Power Eng., vol. 20, no. 5, pp. 30–33, October 2006.

[14] The European Wind Energy Association, *The European Offshore Wind Industry - key trends and statistics 1st half 2012*. Online Available [assessed on 26/10/2012]: http://www.ewea.org/fileadmin/ewea_documents/documents/publications/statistics/EWEA_OffshoreStats_July2012.pdf.

[15] European Wind Energy Association (EWEA), *Pure Power: Wind Enery Scenarios up to 2030*. Online Available [assessed on 27/10/2012]: http://www.ewea.org/fileadmin/ewea_documents/documents/publications/reports/purepower.pdf.

[16] Bassi, S.; Bowen, A.; Fankhauser, S., *The case for and against onshore wind energy in the UK*, Policy brief 2012, The Grantham Research Institute on Climate Change and the Environment & The Centre for Climate Change Economics and Policy. Online Available [assessed on 28/10/2012]: http://www2.lse.ac.uk/GranthamInstitute/publications/Policy/docs/PB-onshore-wind-energy-UK.pdf.

[17] Long, W.; Nilsson, S., "HVDC transmission: yesterday and today," *IEEE Power and Energy Magazine*, vol.5, no.2, pp.22-31, March-April 2007.

[18] Wikipedia, *List of HVDC projects*, Online Available [assessed on 29/10/2012]: http://en.wikipedia.org/wiki/List_of_HVDC_projects.

[19] Decker, J.D.; Kreutzkamp, P., *Offshore Electricity Grid Infrastructure in Europe*, Offshore Grid Report, Oct 2011. Online Available [assessed on 30/10/2012]: http://www.ewea.org/fileadmin/ewea_documents/documents/publications/reports/OffshoreGrid__report.pdf.

[20] Friends of the Supergrid, *Supergrid Phase 1*. Online available [assessed on 01/11.2012]: http://mainstream-downloads.opendebate.co.uk/downloads/Supergrid-Phase-1-Final.pdf

Chapter 2

Power Electronics and HVDC Transmission Systems

2.1 Introduction

HVDC transmission systems are attractive as they have inherently lower losses for large distance bulk power transmission, and permit asynchronous operations between two or more connected AC power systems. A number of HVDC projects have been committed globally and far more projects are under consideration for construction. Furthermore, the rapid development of converter technologies has broadened the range of applicability of HVDC systems to include underground and offshore applications, and use in voltage stabilisation and reactive power compensation schemes.

In this chapter, an introduction to the semiconductor devices used within power electronics is presented, and an overview of different HVDC transmission technologies is provided, covering configurations, switching operations, output power quality and their relative advantages and disadvantages. Specific details of the latest generation of HVDC converter technologies are described: voltage source converter (VSC). The VSC's topologies, transformers, phase reactors, AC filters, DC capacitors and DC cables are all introduced. A brief overview of VSC operating principles in terms of sinusoidal pulse width modulation (PWM) methods and VSC power transfer characteristics is presented.

In addition to power electronic devices, this chapter also introduces the modelling of VSC converters. The functions of VSC-HVDC inner current control and various outer controllers are described in detail in the subsequent sections.

2.2 Semiconductor Devices

Power electronics, which provides the basic building blocks for HVDC transmission technology, is effectively the application of solid-state semiconductor-based electronics to facilitate the conversion of electric power. In modern electric power systems, power electronics converters are invariably present wherever there is a need for modification of voltage, current or power. Power electronic converters are rated from a few mW as used for mobile phone applications to thousands of MW as employed in HVDC transmission applications.

In terms of the historical development of the technology, power electronics was effectively "born" with the implementations of the mercury arc rectifier, invented by Peter Cooper Hewitt in 1902 [1]. In 1948, when the bipolar junction transistor (BJT) was

invented by William Shockley, the cost and size of power electronics were reduced with increased transistor efficiency, opening up a new era of applications for power electronics [8]. In 1956, the Silicon Controlled Rectifier (SCR) was introduced by General Electric, marking the point where semiconductor power electronics really began to proliferate. More advanced technologies, such as the Metal Oxide Semiconductor Field-effect Transistor (MOSFET) and Insulated Gate Bipolar Transistor (IGBT) became commercially available in 1970s and 1980s [2], further improving the power ratings and switching speeds of devices.

As a host of new converter topologies have been introduced, it is essential that the characteristics of the available power devices are put in perspective. To do this, a brief summary of the terminal topologies, voltage, current and power behaviour and their switching speed capabilities are presented in this chapter. Presently available power semiconductor devices can be classified into three groups according to their degree of controllability [2]:

- **Diode**: on- and off-states are controlled by the power circuit;
- **Thyristor**: on-state is triggered by a control signal but off-state must be achieved by the power circuit;
- **Controllable switches** (including MOSFET, GTO, IGBT, etc.): on- and off-states are both triggered by control signals.

2.2.1. Diode

In power electronics, a diode is an uncontrolled two-terminal electronic component with an asymmetric electrical characteristic. A p-n junction, as an elementary material for a diode, is connected to its two terminals, having low resistance (ideally zero) to the flow of current in one direction and high resistance (ideally infinite) in the other direction. It is a common device used for rectification and circuit directional current control [2].

Figure 2.1 presents a p-n junction and its electrical characteristics. It is constructed from a single crystal that is modified in two separate regions. "Acceptor" impurity atoms are incorporated into one part to produce a p-region in which the majority of carriers are "holes" (as opposed to electrons), and "donor" impurity atoms are incorporated into the other part to produce an n-region in which the majority of carriers are electrons [3]. A p-

n junction, at the boundary between p-region and n-region, is formed by joining together the p- and n-type semiconductors. Holes concentrated on the p-region have a natural tendency to diffuse to fill the crystal uniformly, whereas electrons on the n-region have the natural tendency to diffuse from the n-region [3]. By a technique referred to as **doping**, a small charge transfer creates a double layer with an excess of (-) ionised electrons on the p-region side and (+) ionised holes on the n-region, as shown in Figure 2.1. This layer possesses an electric field from n to p which inhabits the natural diffusion and thereby maintains the separation of these two carriers type [3].

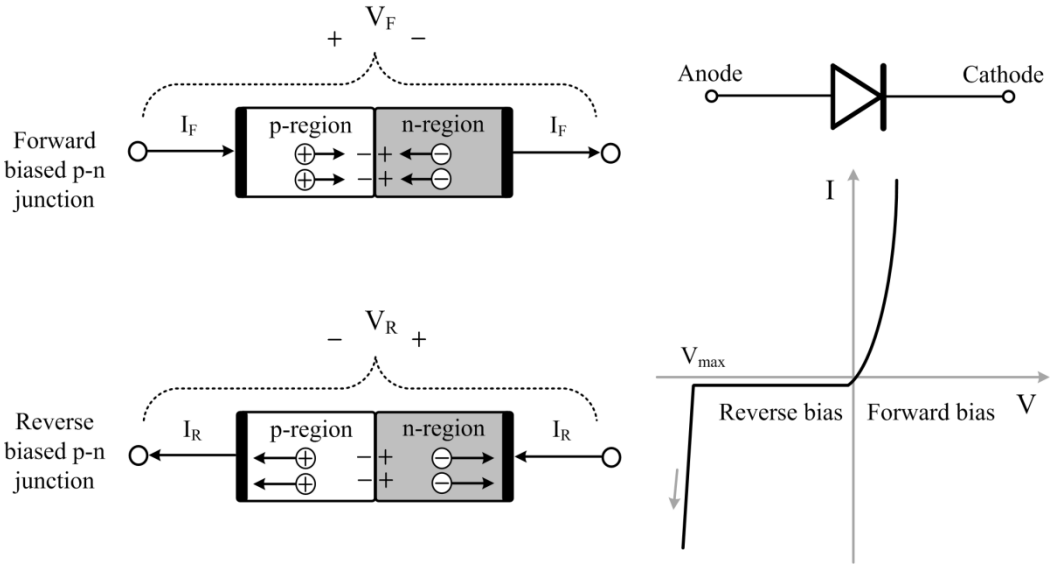

Figure 2.1 Diode and its p-n junction structure and characteristic

When the forward biased voltage is applied across the p-n junction, offsetting the electric field in the middle layer, electrons in the n-region tend to diffuse into the p-region, leaving positively charged ions in the n-region and negatively charged holes in p-region. In this way, the p-n interface loses neutrality, and becomes charged and conductive [4]. In the opposite sense, when the reverse biased voltage is applied across the p-n junction, the electric field tends to counteract the diffusion and inhibit conduction [4]. Hence, as observed in Figure 2.1, there is little resistance in a diode with forward biased voltage and very large resistance when a reverse biased voltage is applied. In addition, if the reverse biased voltage exceeds a threshold, which is termed the "breaking-over voltage", then an "avalanche" of electron carriers is trigged, leading to damage or destruction of the device [4].

2.2.2. Bipolar Junction Transistor

A bipolar junction transistor (BJT) is a three-layer (n-p-n or p-n-p topologies are available) device which consists of two p-n conjunctions as illustrated in the left chart of Figure 2.2. The schematic in the left chart of Figure 2.2 shows the three terminals of an n-p-n type transistor. At first glance, it may be assumed that the two p-n junction function like two diodes.

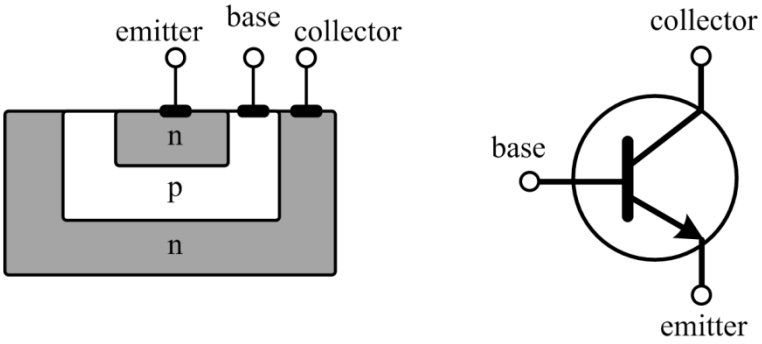

Figure 2.2 The bipolar transistor and its p-n junction structure

To turn on the transistor, a positive voltage in the base with respect to the emitter is needed to forward bias the base/emitter junction. The collector must supply voltage with higher potential with respect to the base; therefore, the base/collector junction is reverse biased and the transistor is completely turned on [5]. The electrons are injected from the emitter and accelerated by the electric field to allow current flow in the external circuit from the collector to the emitter, whose magnitude depends on the electron concentration gradient and is in turn controlled by the forward biased voltage of the emitter-base conjunction [4]. The collector–emitter current can be viewed as being controlled by the base–emitter current (current control), or by the base–emitter voltage (voltage control) [8].

Due to the p-n conjunction interactions, the switching response of the transistor is slow and the conduction resistive losses are high [6] compared to diodes. In order to carry high currents in the main switch circuit, the injected base current is large, resulting in additional losses. As BJT devices exhibit relatively high losses, they are normally not used as independent power switches, but are usually embedded within other switch configurations to control the current [5].

2.2.3. Thyristors (SCR, GTO, etc.)

A thyristor, also referred as a silicon-controlled rectifier (SCR), is a current "valve" with two discrete states: conducting or blocking current. When a reverse voltage is applied across the thyristor (the anode is negative and the cathode is positive), the operating state that only allows conduction of a very small reverse current is referred as the **blocking state**, which is shown on the left-hand side of the V-I characteristic in 0. When the voltage the device across is forward, there are two states, one of which, referred as the **off state**, still permits a small forward current to conduct in absence of a gate signal, the other of which, referred as the **on state**, permits conduction of a large current in presence of a gate signal. The gate signal, which can be either electrically triggered or triggered optically [4], must be sufficiently large (greater than the threshold current I_s as shown in the V-I characteristic of Figure 2.1) to maintain conduction.

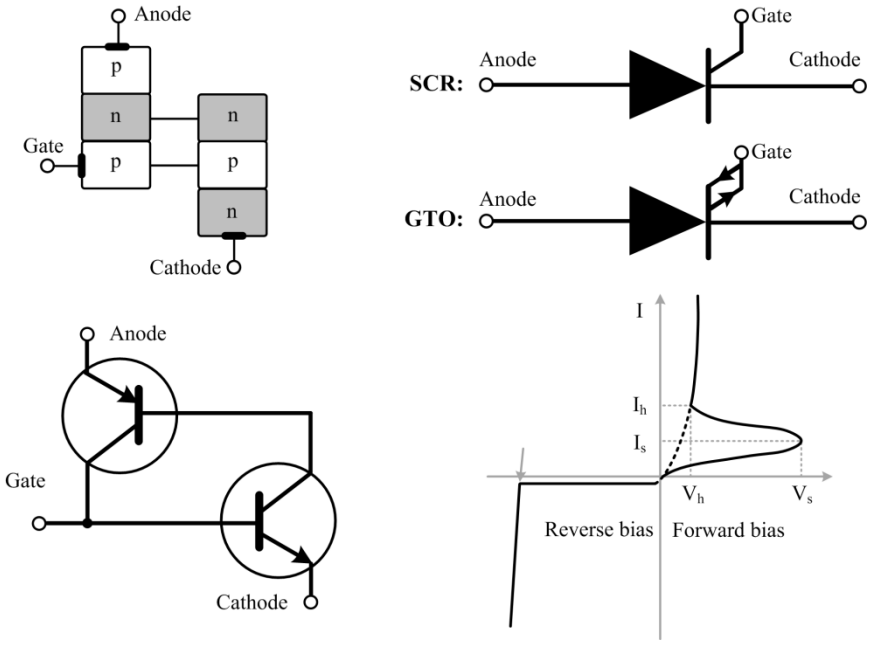

Figure 2.3 Thyristor and its p-n junction structure and transistor representation

An SCR essentially consists of an ordinary p-n rectifier and an n-p-n transistor, which are combined into one unit to form a four-layer three-terminal p-n-p-n device. It is normally visualised as being separated into two transistors as shown in the first chart of Figure 2.3.

When the reverse biased voltage is applied to the SCR (negative anode voltage and positive cathode voltage), the two emitters in the two transistors are reverse biased and there are no injections of carriers from the emitters [4]. This is referred as the **blocking state** as shown on the left hand of Figure 2.3. With forward biased voltage but in the absence of gate current signal, the top p-n junction as shown in Figure 2.3 is forward biased while at the central p-n junction a space-charge region builds up that only permits a small group of electrons to flow across the junction [4]. This is referred as the **off-state**, with its characteristic as shown in the right-hand solid line of Figure 2.3.

To trigger the **on-state** of the SCR, the injection of a positive current to the gate is required, which must be sufficiently large to keep it in the conductive state. Another condition to turn the device on is at the presence of large forward voltage (the break-over voltage) which clauses a conducting state with an almost exponential on-state characteristic [4]. The SCR **cannot** be turned off by a gate signal, only passively by a reverse-biased voltage [4].

Unlike an SCR-type thyristor, a gate-turn-off (GTO) thyristor, with the symbol as illustrated in the top right chart of Figure 2.3, can not only be turned on by a positive gate signal, but can also be turned off by a negative gate signal, and can therefore be regarded as a fully controlled switch.

2.2.4. MOSFET

The metal–oxide–semiconductor field-effect transistor (MOSFET) is a device which is commonly used for the purpose of power switching and signal amplification. Compared to transistors and thyristors, its main advantages are that the base current for the MOSFET's gate is relatively small (almost zero) and the switching commutation speed is relatively high (with switching times range from tens of nanoseconds to a few hundred microseconds) [2]. The MOSFET, similar to the BJT, is a three-terminal device where the voltage on the gate controls the current flow between the collector and emitter terminals. The electric field produced by the **gate** voltage modulate the conductivity of the semiconductor channel between the main current carrying terminals normally called the **drain** and the **source**, as illustrated in Figure 2.4.

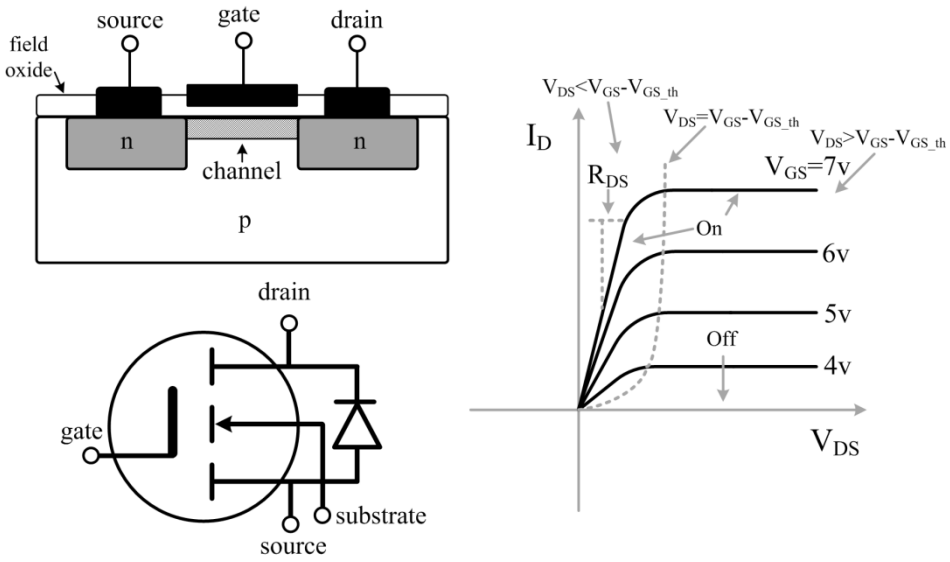

Figure 2.4 MOSFET and its representative symbol

The V-I characteristic of a MOSFET is demonstrated by the left-hand side chart of Figure 2.4. When the gate-source voltage V_{GS} is below the threshold voltage V_{GS_th}, the MOSFET is in off state and no current flows between the drain and the source. In this chart it shows four threshold voltages of 7v, 6v, 5v and 4v, whose values strongly depend on the manufacturing variations, for example the oxide thickness and junction depth [7].

When VGS increases beyond V_{GS_th}, for the smaller drain-source voltage V_{DS} ($V_{DS}<V_{GS}-V_{GS\_th}$), the drain current I_D starts to flow in proportion to V_{DS}. This operation mode is consequently referred to "ohmic mode" where the MOSFET can be regarded as a constant resistance R_{DS} as shown in the characteristic chart [7]. For higher V_{DS} ($V_{DS}>V_{GS}-V_{GS\_th}$), I_D tends to saturate and no longer increases in proportion with the voltage. As a result, the drain current I_D becomes independent of V_{DS} and determined solely by the gate voltage V_{GS}.

2.2.5. IGBT

The Insulated Gate Bipolar Transistor (IGBT) is a three-terminal switch device combining the advantageous characteristic of p-n-p Transistors for high-current low-saturation-voltage high power efficiency, with the useful characteristics of MOSFETs in terms of ability for fast gate-drive switching [4]. It can be modelled as a p-n-n transistor driven by a power MOSFET.

The basic structure of an IGBT is almost identical to that of a MOSFET except that the P injecting layer at the bottom is as illustrated in Figure 2.5 [9]. For an IGBT, a

forward-blocking state can be transferred to a **forward-conducting state** by applying a positive voltage with a sufficient magnitude [9]. This forms a conducting channel which connects the n emitter to the n drift region in which the electrons' mobility is high as illustrated in Figure 2.5. Electrons are transported from the n emitter to the n drift region whereby the junction between the p collector and the n drift becomes forward-biased. A high density of carrier holes is injected from the p collector to the n drift region to gather a high concentration of holes and electrons which drastically enhance the conductivity of the n drift region [9]. When a negative voltage is applied to the gate, the junction between the p collector and the n drift regions is reverse-biased so that a **reverse-blocking state** is triggered [9].

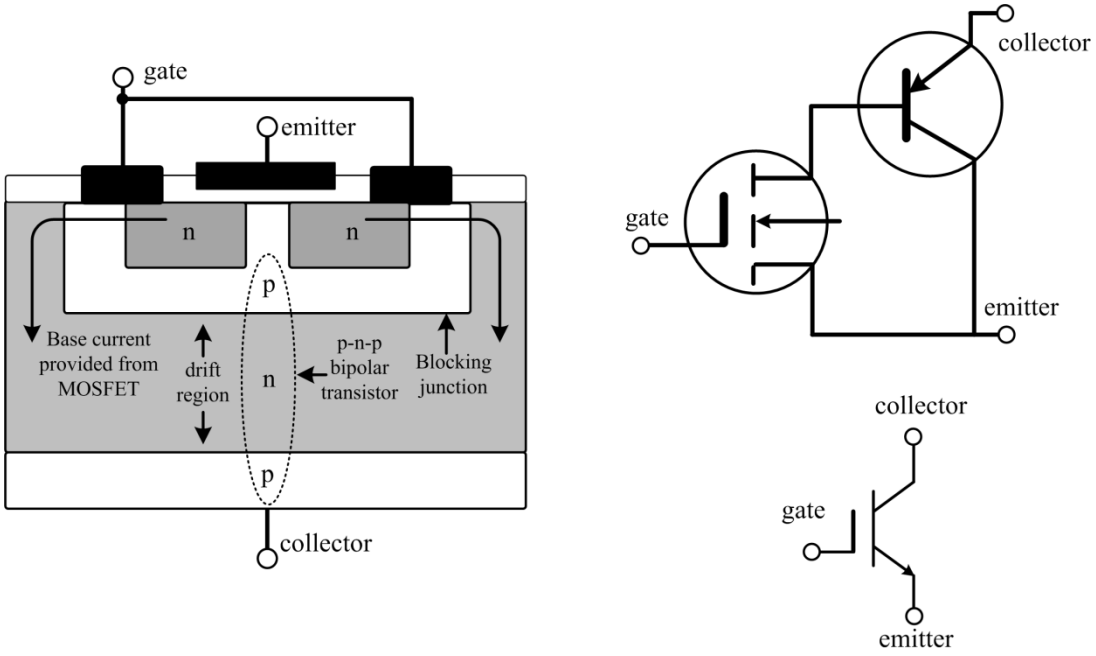

Figure 2.5 IGBT and its representative symbol

As with GTOs, the IGBT can block in both forward and reverse directions. As for transistors, it has a low on state voltage drop and consequently low power losses. Operating currents can be relatively high, in excess of 1500 A, and switching voltages of up to 3000 V can be catered for [4]. Because it is able to switch rapidly, it can be used to synthesise complex waveforms and act as an ideal power switch in power converter applications such as motor electric drives and HVDC transmission systems.

2.3 Current Source Converter based HVDC Transmission Systems

Two basic converter technologies are used in modern HVDC transmission systems. These are the long-established line-commutated current source converter (CSC, also sometimes known as LCC) and self-commutated voltage source converter (VSC), as illustrated in Figure 2.6 and Figure 2.8 respectively.

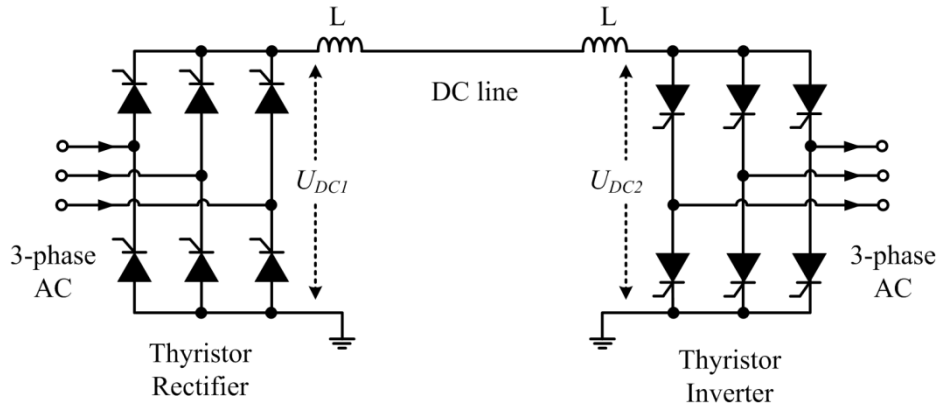

Figure 2.6 CSC-HVDC system: basic monopole configuration

The first CSC-HVDC link, based on mercury arc valves, was commissioned in 1954 [11]. In the 1960s, a major evolution came in the form of the silicon-controlled thyristor and following that period substantial progress was been made in terms of ratings and reliability of thyristor valves [11]. Today, the CSC HVDC remains as the most cost-effective solution for large-power long-distance transmission and it has contributed to more than 80 GW of installed HVDC links worldwide [4].

The basic building blocks of CSC-HVDC, as illustrated in Figure 2.6, is the three-phase full-wave bridge referred to as a six-pulse or Graetz bridge [10]. By firing an incoming thyristor with the correct polarity of line voltage, the thyristor can be switched (or commutated) to conduct current. The outgoing thyristor (i.e. the thyristor that is moving from conductive to blocking state) is commutated naturally without the need for any firing pulse, by the line voltage. Two aspects are essential to the CSC-HVDC systems:

- The presence of an established synchronous AC voltage to serve as a commutating voltage;

- In order to successfully achieve turn-off switch by means of line commutation, the associated AC line voltage, serving as the commutating voltage for the incoming thyristor, must has the polarity that will reverse-bias the outgoing thyristors [1].

For the CSC-HVDC system, the DC current is always unidirectional, but the DC voltage can be reversed by controlling thyristor firing angles. Therefore, the active power flow can be managed in a bidirectional sense if required. However, the CSC-HVCD link will always act to absorb reactive power, leading to a poor power factor, as the commutation is achieved by the AC voltage source and the current therefore always lags the voltage. Consequently, CSC applications require large reactive power compensation in the form of shunt capacitors (usually rated at 50%-60% of the converter MW rating as demonstrated in [2]). As the level of active power transfer changes, the corresponding reactive power change causes AC voltage fluctuations which may lead to voltage instability. Therefore, in order to avoid instability, a strong AC grid voltage source is required and this is defined by a high short circuit ratio [2].

A converter transformer is normally required to connect the CSC to the grid. Due to the converter transformer's leakage inductance, there is inevitably inductance between the converter and the connected AC grid. The inductance acts to reduce the rates of change of current and lengthens the converter's commutating time, introducing difficulties in terms of controllability of the converter turn-off process. The delayed turn-off period of the thyristor results in considerable current waveform distortion, as shown in Figure 2.7. Even though the thyristor configuration is simple, large filtering devices are required and the cost is consequently high [2]. In most modern CSC-HVDC systems [10], a series-connected supplementary CSC with a 30º displaced voltage phase [10], referred to as twelve-pulse CSC, is used to counteract the high levels of AC current harmonics and reduce requirements for filtering devices. The 30º phase displacement is achieved by coupling one bridge with a wye-connected secondary winding and the other bridge with a delta-connected secondary winding [4]. In this way, although low-order characteristic harmonics still exist on both of the bridges and transformer windings, they are 180º out of phase and therefore act to cancel each other [4].

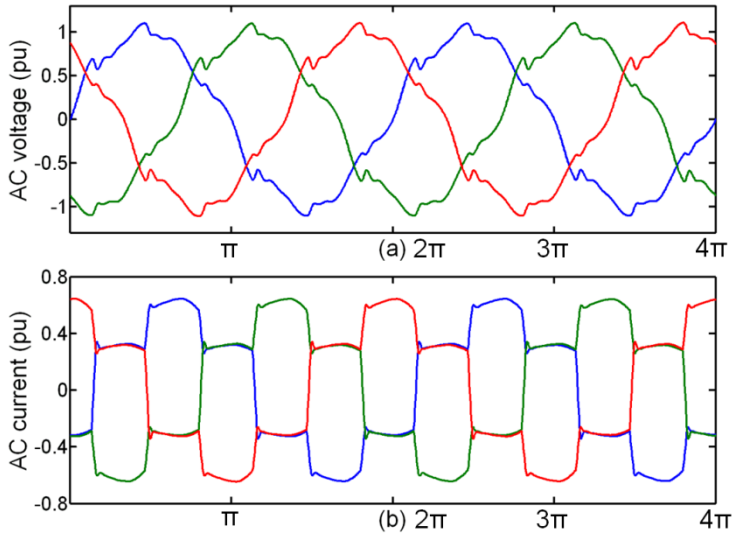

Figure 2.7 Six-pulse CSC grid voltage and output current

The CSC with series-connected capacitors, known as a capacitor-commutated converter (CCC), was introduced in the 1100 MW Garabi HVDC connection project between Argentina and Brazil around the year 2000 [12]. The series capacitors are used to generate reactive power and provide an element of the voltage required for converter commutation, so voltage stability is improved and the CCC can be operated when connected to a weak power system [12]. However, as verified in [12], with unbalanced grid voltages, arising, for example, from a single-phase-to-earth fault, the CCC's capacitors are incorrectly charged leading to longer periods of recovery of the capacitor voltage following the fault.

2.4 Voltage Source Converter based HVDC Transmission System

The Insulated Gate Bipolar Transistor (IGBT), which was initially developed for motor drives and related applications, found its way into HVDC applications as illustrated in Figure 2.8 from the 1990s [10]. The IGBT based converter, which is able to generate perfect sinusoidal voltage waveforms at its terminals using high-frequency Pulse Width Modulation (PWM) techniques, is referred to as a Voltage Source Converter (VSC).VSCs for power transmission applications first appeared in 1997, with the experimental Hellsjön–Grängesberg project in Sweden [11]. Three major VSC-HVDC manufactures: ABB, Siemens and Alstom, have their own trademarks of "HVDC Light", "HVDC Plus" and "HVDC MaxSine" respectively [11][12]. VSC-HVDC systems have now reached a maximum power transfer capability up to 1 GW, with DC voltages of up to ±300 kV being possible. With a stable DC voltage aided by DC side capacitors, VSCs

can use Pulse Width Modulation (PWM) techniques to create the desired AC side voltage waveforms with controllable amplitudes and relative phase angles. To modify the voltage waveforms, the PWM pulse patterns are changed accordingly by control systems in a near-instantaneous fashion.

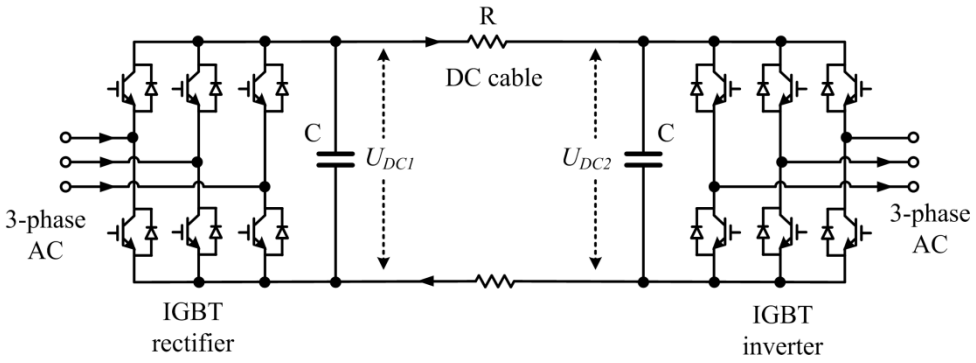

Figure 2.8 VSC-HVDC system: basic monopole configuration

Compared with the CSC-HVDC, the VSC-HVDC converters have a number of advantages, such as ability to provide reactive compensation and grid voltage support, a reduced relative size of converter and reduced AC filter size. These advantages make VSC-HVDC ideally suited for weak power systems, especially for onshore grid integration of offshore wind farms.

2.5 VSC-HVDC System Components

This subsection present a description of the critical components of a VSC, as systems employing VSC form the main focus of investigation for the remainder of the dissertation. The modelling of VSC-HVDC system in the following chapters involves these elements including converter configurations, phase reactors, AC filters, DC capacitors etc. Proper design of all VSC components is vital in ensuring proper converter operation and stability.

2.5.1 VSC configurations

VSC-HVDC systems employ IGBTs as the fundamental components. The IGBT valve is either turned off (non-conducting) or electron-saturated (completely conducting), with a small voltage drop across the semiconductors [1]. Rated voltage required for VSC-HVDC system is beyond the ratings of a single IGBT valve, so the IGBT valves are normally connected in series, as illustrated in Figure 2.9. The series-connected IGBTs can be fired synchronously to acting as a single switch bridge. For instance, a VSC-

HVDC scheme with DC voltage of ±150 kV normally has up to 300 serially-connected IGBTs [1].

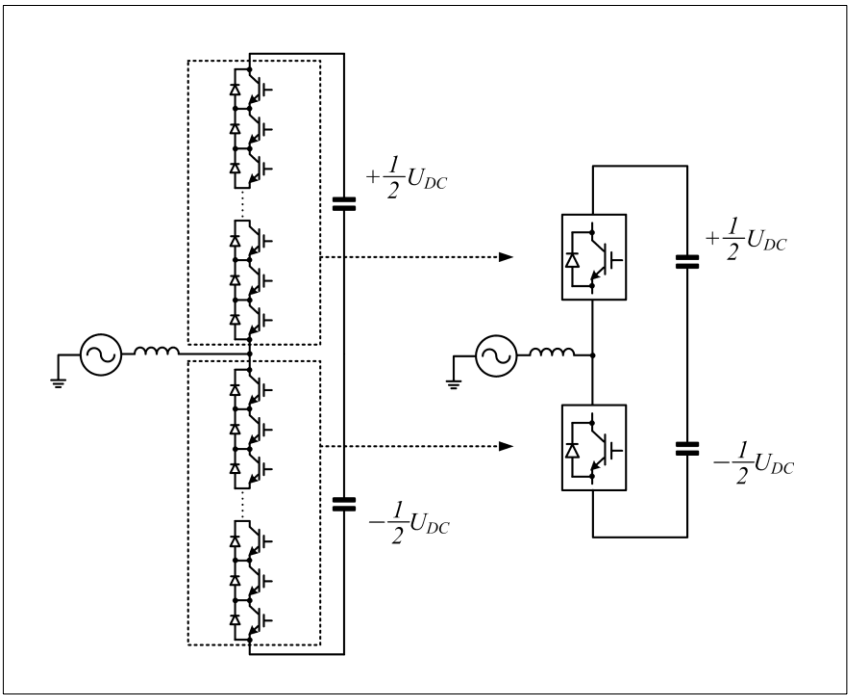

Figure 2.9 Series-connected IGBTs (left) and commonly seen simplified representation (right)

The simplest VSC configuration employs two-level six-pulse three-phase bridges, as show in Figure 2.10(a). This configuration has been extensively used from low- to high-power applications. With a stably established DC voltage U_{DC}, the two-level VSC generates two voltage levels +0.5 U_{DC} and -0.5 U_{DC} for AC side phase commutation using high frequency PWM techniques. Through AC side phase reactors, transformers and harmonic filters, the AC voltage waveforms produced are nearly sinusoidal, with a relatively much higher quality than those produced by CSCs. The VSC output voltage waveform can be further improved by applying multi-level VSCs, which have high order voltage steps than +0.5 U_{DC} and -0.5 U_{DC} from two-level VSCs.

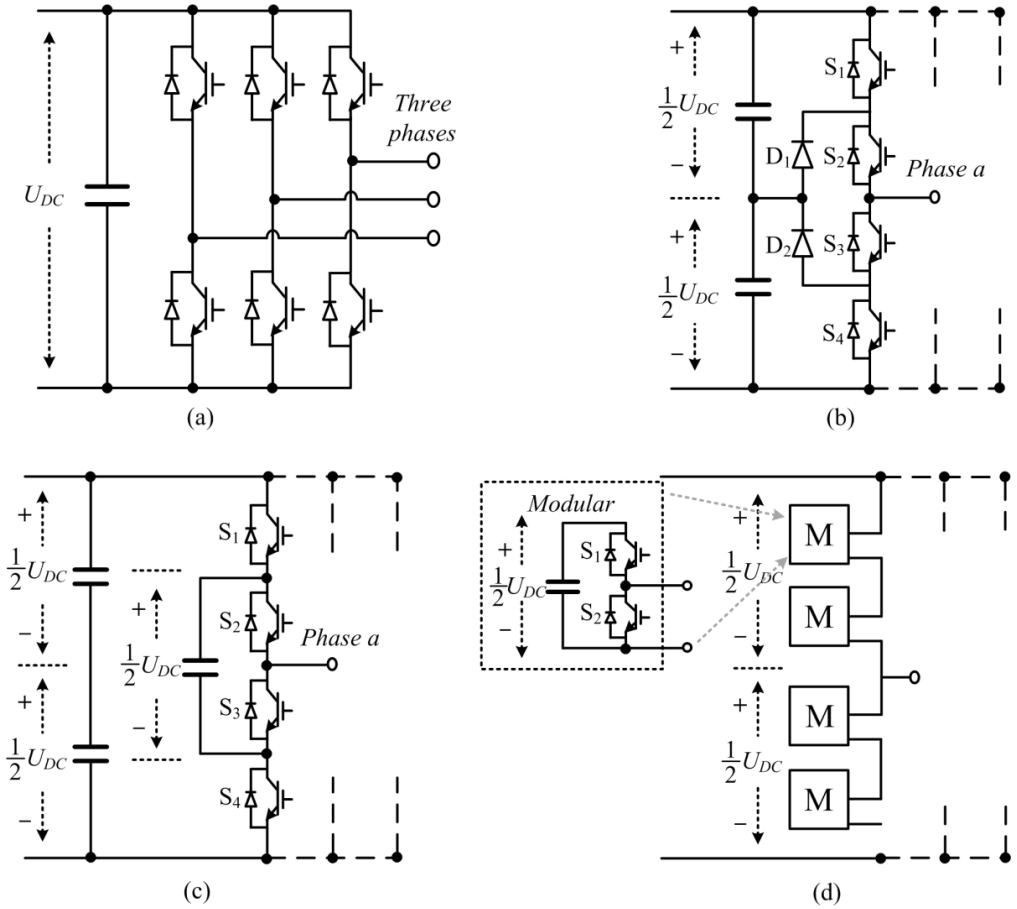

Figure 2.10 (a) conventional two-level VSC; (b) three-level diode-clamped neutral-point-clamped; (c) three-level flying-capacitor VSC; (d) three-level modular VSC.

Multi-level VSC with unique structures allows the HVDC system to operate with lower harmonic content. This positive feature of multilevel VSCs means that the use of transformer and filter devices can usually be avoided [13]. In the following section, three types of multi-level VSC are introduced. For simplicity, the operating mechanisms for each type with three-level bridges are introduced in both text and via Figure 2.10(b)(c)(d). The types of VSC considered are:

- Diode-clamped neutral-point-clamped (NPC) converter;
- Flying capacitor (FC) converter;
- Modular multi-level converter (MMC).

The NPC converter, as shown in Figure 2.10(b), uses 12-pulse diode-clamped neutral-point-clamped bridges [15]. Switches S_1 and S_4 are major valves, while S_2 and S_3 are the valves to clamp the output potentials to the neutral, together with the two diodes

D_1 and D_2 in the central DC link. The phase voltage potential at $+0.5U_{DC}$ is produced by switching on S_1 and S_2, the voltage at $-0.5U_{DC}$ is produced by switching on $S_3$and S_4 and the one at $+0.5U_{DC}$ is produced by switching on S_1 and S_3. Therefore, phase AC voltages at three levels $+U_{DC}$, 0 and $-U_{DC}$ are obtainable.

A potential replacement for the diode-clamped NPC converter is the FC converter [16][17] (also as known as floating capacitor converter), as shown in Figure 2.10(c). The voltage increment between the two capacitors determines the size of the voltage steps that can be produced in the output voltage waveform. Regarding the FC switching sequences, switching S_1 and S_2 on and S_3 and S_4 off produces an output voltage potential $+0.5\ U_{DC}$. Conversely, switching $S_1$and S_2 off and S_3 and S_4 produces an output voltage potential $-0.5\ U_{DC}$. In contrast, switching $S_1$and S_3 on and $S_2$and S_4 off (or switching $S_1$and S_3 off and $S_2$and S_4 on) balances out the capacitor voltages to results in an output voltage potential of 0.

The MMC converter, also referred to as an M2C converter, employs IGBT bridges in modules, as illustrated in "M" in Figure 2.10(d). The MMC distributes the total DC voltage potential across every switching module. It includes two groups of switches: the main switch S_2 and the auxiliary switch S_1 for each switching module, as shown in the enlarged frame in Figure 2.10(d) [18]. To produce an output voltage $+0.5U_{DC}$, all upper main switches and all lower auxiliary switches are turned on. To produce an output voltage $-0.5\ U_{DC}$, all upper auxiliary switches and all lower main switches are turned on. There are four different switch combinations for producing output voltage of 0 for this three-level MMC converter, which is achieved by balancing the voltage potential of switched capacitors at the output connection point.

2.5.2 A brief comparison of VSC with CSC

Compared with the CSC, which has been in commercial use in 1950s and is well established in several HVDC projects [19], VSC is a relatively new technology. VSC technology is now becoming popular because it is able to eliminate many of the disadvantages associated with the CSC. These are listed in the following Table I:

Table I Comparison of CSC and VSC technologies [4][19]

	CSC	VSC
Technology maturity	Mature	Developing
Adopted valve	Thyristor	IGBT
Converter station footprint	200m×120m×22m (100%)	120m×60m×22m (40%)
Converter transformer design	Special design required	Conventional design
Commutation failure	May occur	Rarely occur
AC harmonic filter	Large filters	Small filters
Power rating	Up to 8000 MW	Up to 1000 MW
Power flow reversal	Not easy, required an interruption	Easy
Converter losses	0.5% to 1%	1% to 3%
Minimum DC power	5% to 10%	No minimum
Established voltage required	Yes	No
Reactive power Compensation	Yes	No
AC voltage support provision	No	Yes
DC voltage rating	Up to ±800 kV	Up to ±350 kV
DC fault stability	Inherent limiting by DC inductors	DC capacitors feeding faults

The major operating difference between VSCs and CSCs is that the VSC is self-commutated and this allows it to construct voltage waveforms at any phase angles, either leading or lagging; while the CSC is line commutated and can only produce voltage waveforms that lag the system voltage. Therefore as seen in Table I, the VSC does not require reactive power compensation and can even provide reactive power to support the system voltage. VSC does not require an established grid voltage, whereas CSC requires large reactive power compensation devices and a strong grid.

Furthermore, as the VSC is switched at a relatively much higher frequency than the CSC (1 kHz to 20 kHz), the VSC is capable of outputting near-perfect sinusoidal voltage waveforms and consequently requires little or no filtering. In contrast, the CSC's output

voltages contain significant lower-order harmonics which require large filter devices to reduce their presence.

For VSC, DC power/current flow can be easily changed, without a requirement to change DC voltage polarity. This facilitates the DC power flow control required in a multi-terminal HVDC network. CSC requires an interruption to its operation and the entire HVDC system must be brought offline and then online again to accomplish a one-time directional change of the DC power flow.

However, CSC does possess advantages over VSC. The relatively much higher power rating of a CSC converter station, with capacities up to 8 GW, is a major advantage; with only 1 GW possible for a VSC converter station presently. CSC also has robustness against overcurrent conditions (e.g. caused by short circuits), while significant overcurrent is normally fatally damaging to VSC switches [4]. The CSC's power loss is relatively lower than that associated with VSC. In the future, it is expected that VSC systems will become available with increased power ratings. It is also anticipated that designs that are more fault-tolerant and robust to overcurrent may also become available, and switching losses will also decrease as novel designs are developed and introduced.

2.5.3 Phase reactors

A VSC is normally not connected to the AC grid directly. Phase reactors as shown in Figure 2.11 for each phase act as inductive coupling reactances for VSC grid connections. They are very important to the VSC operation because of the following functions:

- Limiting the fault current from the VSC;
- Reducing the harmonic current content from the VSC;
- Stabilising the AC current and enabling active and reactive power control.

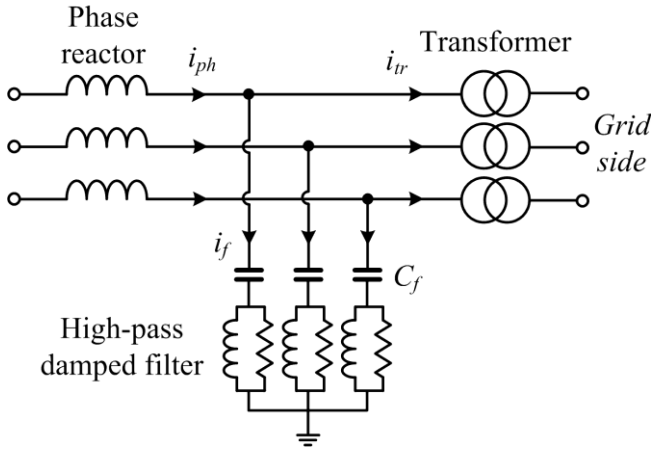

Figure 2.11 LCL structure for a VSC - AC side

Knowledge of the required parameters of the phase reactors must be established before a VSC control system is configured and able to provide precise P&Q control. The combined inductance of the phase reactors and transformer is computed according to the converter's AC side base impedance:

$$L = L_{ph} + L_{tr} = x_{ph} \cdot \frac{Z_{base}}{\omega_0} = x_{ph} \cdot \frac{V_{AC}^2}{2\pi f_0 \cdot S_{VSC}} \tag{1}$$

where L refers to the total inductance including the reactor inductance L_{ph} and transformer inductance L_{tr}, x_{ph} refers to the typically-employed value of inductance in pu with base inductance, which is effectively the inductance of the VSC as "seen" from the grid (normally 0.3 pu, as demonstrated in [20]), f_0 is the nominal grid frequency, V_{AC} is the nominal rms AC voltage and S_{VSC} is the rated active power rating of the VSC.

As well as the phase reactor, the converter transformer naturally provides the same effect as phase reactors when used to couple the VSC with the grid. This is why the transformer's inductances are taken into account in (1). Even though the phase reactors and transformers are normally designed to withstand high-frequency voltage stresses arising from the VSC switching actions, it is good practice to place a shunt high-pass damped filter between the phase reactors and transformer, as shown at the bottom of Figure 2.11. The shunt filter is introduced in the next subsection.

2.5.4 AC Filter

The converter's output voltage contains harmonics associated with the PWM switching frequency. The requirement for a highly sinusoidal output voltage waveform

from the VSC requires the addition of a shunt AC filter. As shown in Figure 2.11, the high-pass damping filter is situated at the mid-point between the phase reactors and the transformer. It allows high-frequency currents to be filtered by diverting into low-impedance shunt capacitive paths [21]. The improvement in the quality of the voltage waveform can be demonstrated by (2). Equation (2) is changed to another format of (3), which is then used to derive (4) which can calculate by how much the filtered voltage is improved (by allowing current to be exchanged with the filter).

$$C_f \frac{dv_f}{dt} = i_{pf} - i_{tr} = i_f \tag{2}$$

$$dv_f = \frac{1}{C_f} i_f dt \tag{3}$$

$$v_f = v_{f0} + \frac{1}{C_f}\int i_f dt = v_{f0} + \frac{i_f}{C_f s} \tag{4}$$

where C_f refers to the filter capacitance, $v_{f0}$and v_f are the original and filtered voltages a tthe mid-point between reactors and transformer, i_f refers to the current flowing to the filter, i_{pf} refers to the phase reactor current, and i_{tr} refers to the transformer current, as shown in Figure 2.11.

Figure 2.11 illustrates a three-phase RCL filter at the bottom which is commonly used in VSC technologies. The objectives is that frequencies at the VSC's PWM carrier frequency (normally within a range between 1 kHz and 20 kHz depending on VSC applications) and the double frequencies associated with the PWM carrier frequency are to be filtered out [22]. The selection of AC filter parameters depends on the converter switching frequency and the VSC base impedance [23]:

$$\begin{cases} Z_f = x_f \cdot Z_{base} = x_f \cdot \dfrac{v_f^2}{2\pi f_0 \cdot S_{VSC}} \\ L_f = \dfrac{Z_f}{2\pi f_{sw}}, C_f = \dfrac{L_f}{Z_f^2} \end{cases} \tag{5}$$

where Z_f is the filter impedance, x_f is the ratio of filter impedance (0.15 in [23]) in VSC base impedance, f_0 is the nominal grid frequency, S_{VSC} is the VSC power rating, L_f and C_f are the filter inductance and capacitance required for filtering the specific switching frequency f_{sw}.

VSC switching frequency only contains high-order harmonics; therefore the filter facilities are not largely required for reactive power compensation. The design of filters for VSCs is a complicated task, which must take account of various factors.

2.5.5 DC capacitor

Technically speaking, the primary objective of DC capacitors within a VSC-HVDC application is to provide a low-inductance path for commutating current from being on to being off [24], as AC side high inductive impedance is cancelled out by the DC side capacitor at the turn-on state. It also acts to reduce voltage ripple on the DC link, through its energy storage capabilities.

Disturbances from both the DC network (e.g. a DC power increase) or from the AC grid (e.g. an AC side fault) will cause the DC voltage to momentarily vary. The DC capacitor limits the rate of voltage variation due to its damping effect on applied voltage changes [25]. The magnitude of this damping effect obviously depends on the size of the capacitor, and is characterised by the capacitor time constant for a DC network [26]:

$$\tau = \frac{W_E}{S_{VSC}} = \frac{\frac{1}{2} CNU_{DC}^2}{S_{VSC}} \tag{6}$$

where W_E represents the electro-static energy stored in the capacitor, S_{VSC} represents the VSC rated power capability, C is the capacitance of a single DC capacitor and N is the total number of capacitors installed on the DC link (for a three-level neutral-point clamped VSC-HVDC network, N=2) and U_{DC} is the nominal DC voltage.

The capacitor time constant approximates to the period needed to charge the capacitors in the DC network from zero to rated voltage [26], when the converter is supplied with rated power S_{VSC}. The capacitor time constant τ can be increased by selecting larger values of capacitance to have an increasingly restrictive effect on DC voltage ripples and variations. The motivation for doing this is clearly demonstrated in [20], which in principle chooses the value of capacitance to avoid DC voltage instability:

$$C = \frac{S_{VSC}}{U_{DC}^2} \cdot \frac{2 \cdot \xi_D}{\omega_{vc}} \cdot \frac{1}{\delta_D (1 - \delta_D)} \tag{7}$$

where ξ_D is the damping provide by the capacitor (greater than 0.707 provides satisfactory performance), ω_{vc} is the DC voltage controller bandwidth (normally 2π*30

rad/s), δ_D is the voltage drop requirement in per unit across the converter (the converter is regarded as a pure resistance, this value is normally less than 0.05pu).

2.5.6 DC cables

Modern polymeric insulating material (XLPE – cross-linked polyethylene) cables, as illustrated in Figure 2.12, employed for VSC-HVDC system are stronger, lighter and relatively cheaper than the traditional mineral-insulated mass-impregnated cables typically used for LCC-HVDC system [27]. XLPE cables for VSC-HVDC are available with ratings of up to 1200 MW at DC voltages of up 320 kV. The data for XLPE is found in [28], which is summarised in the following Table II. This is used as the basis for simulations presented later in this dissertation:

Table II Technical data for XLPE cable [28]

Diameter of conductor mm	**Diameter of cable mm**	**DC resistance (20 °C copper) Ω/km**	**Inductance mH/km**	**Capacitance μF/km**
20.4	76.7	0.0601	0.45	0.14
26.2	79.1	0.0366	0.41	0.17
33.7	85.4	0.0221	0.37	0.21
42.8	97.9	0.0151	0.35	0.26
49.8	105.5	0.0113	0.34	0.29
54.4	110.3	0.0090	0.33	0.31
62.0	118.5	0.0072	0.32	0.34

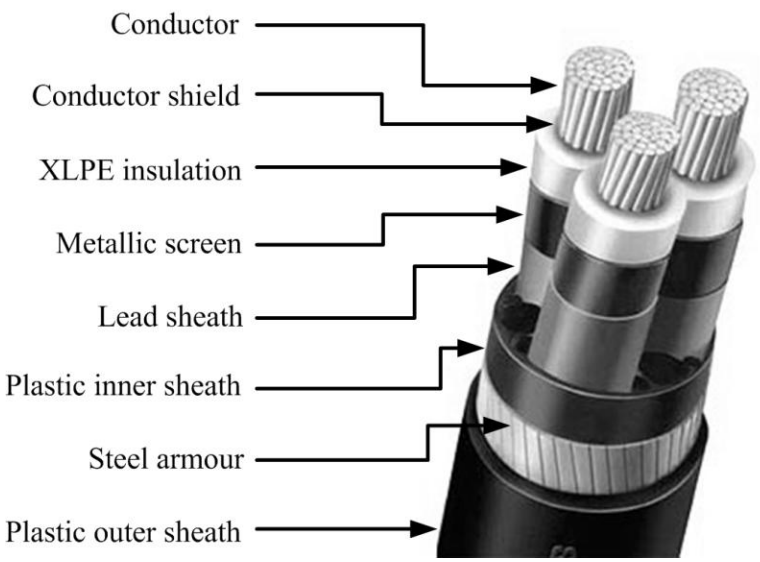

Figure 2.12 XLPE power cable [29]

2.6 VSC Operation

As already stated, a VSC is operated to generate desired voltage waveforms within the converter's capability using high-frequency switch-triggering signals to the switches that are provided using PWM technique. In this subsection, PWM techniques and P&Q capabilities and control are described.

2.6.1 PWM operating principles

VSCs are typically controlled using a sinusoidal PWM technique [4]. The sine PWM is a carrier-based technique which employs a sawtooth modulating waveform (carrier) with a fixed frequency, as shown in the single-phase diagrams of Figure 2.13. The instances where positive and negative switches reversed are determined by the intersections between the voltage reference (represented as the black dashed line) and the carrier (represented as the black sawtooth) for each phase.

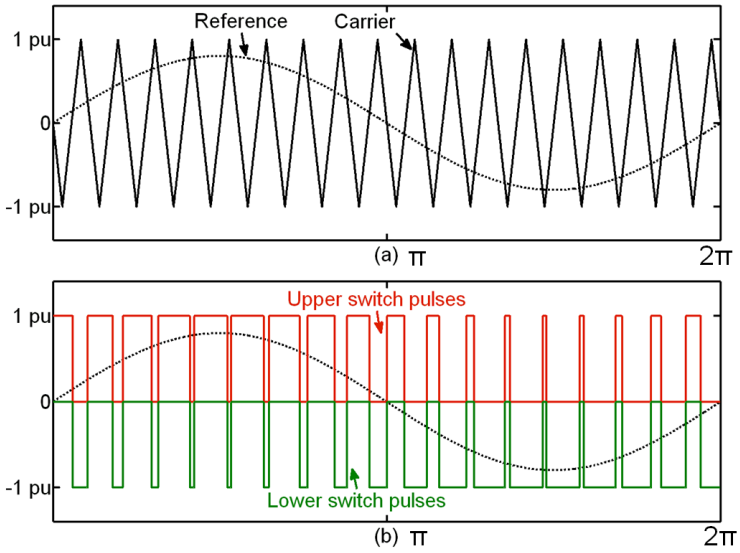

Figure 2.13 One leg of a two-level converter PWM: (a) Carrier with reference (b) Converter output voltage

For a typical two-level VSC switching bridge, the upper and lower valves must be switched on and off in a coordinated manner, i.e. one must be on while the other is off and vice versa. The PWM sampling frequency is the same as the carrier frequency as illustrated in (a) and (b) of Figure 2.13, whereas the output voltage frequency is controlled by the voltage reference. The amplitude of the output voltage v_{out} is generated in the following way:

- When $V_{reference} > V_{carrier}$, $v_{out} = U_{DC}/2$;
- When $V_{reference} < V_{carrier}$, $v_{out} = -U_{DC}/2$.

This converter side voltage signal consists of various durations of "on and off" periods, which when passed through the phase reactor and transformer will produce sinusoidal-like output waveforms.

2.6.2 Decoupled VSC power flow control

With the functionality of PWM technique, the VSC is able to produce voltage waveform at converter side at any desired phase angle and amplitude, within capabilities of the devices. Referring to the voltage at VSC grid point of common coupling (PCC), the active and reactive power flow through the reactor and transformer can be fully controlled by modulating the converter side voltage, effectively influencing the power flow control of AC transmission and distribution network, which is typically defined as:

$$P = \frac{v_c \cdot v_g \cdot \sin\delta}{\omega L} \tag{8}$$

$$Q = \frac{v_g \cdot (v_g - v_c) \cdot \cos\delta}{\omega L} \tag{9}$$

where v_c is the converter side voltage, v_g is the grid side voltage, δ is the converter side phase angle with respect to the grid side phase angle, ω is the grid voltage angular speed and L is the combine inductance of the VSC reactor and transformer.

The relevance of converter side voltage at various phase angles and amplitudes is shown in the phasor diagrams of Figure 2.14. The solid black line represents the grid voltage, which is unlikely to change significantly in a stiff power grid. Therefore it acts as a "slack" bus with fixed amplitude and voltage angle (on the y-axis). The dashed black line represents the VSC generated voltage waveforms; four scenarios are graphed to determine the VSC active and reactive power flow. Figure 2.14(a) illustrates the scenario where the VSC voltage angle leads grid the voltage angle (δ positive) and the VSC voltage amplitude v_c is larger than the grid voltage amplitude v_g. The active power and reactive power flow from the VSC to the grid are both positive, which can be demonstrated by (8) and (9), and also the position of grid voltage and current ig. The other three scenarios are demonstrated in Figure 2.14(b)(c)(d) in the same way as Figure 2.14(a).

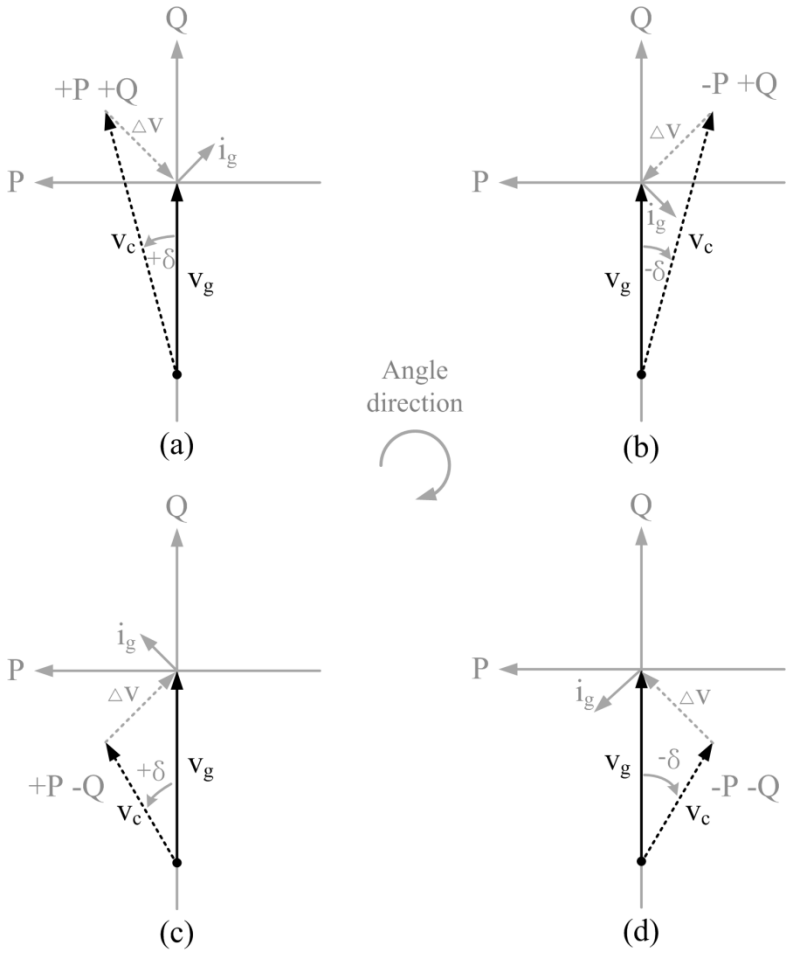

Figure 2.14 Voltage phasor demonstration for power flow

In conclusion, if the converter side voltage v_c is phase-leading with respect to the grid side voltage v_g, as shown in Figure 2.14(a) and (c), then the active power flows from the converter to the grid. Conversely, if v_c is phase-lagging with respect to v_g, as shown in Figure 2.14(b) and (d), the active power flows from the grid to the converter. In terms of reactive power control of the VSC, if the voltage amplitude v_c is larger than v_g, as shown in Figure 2.14(a) and (b), then the converter is providing reactive power. Conversely, if v_c is smaller than v_g, as shown in Figure 2.14(c) and (d), the converter is consuming reactive power.

2.6.3 VSC active and reactive power capability

While the control of a VSC's P&Q is flexible, as demonstrated in the subsection above, there are three factors that limit a VSC's power transfer capability [30] and these are summarised below:

- The maximum current through the IGBTs. This give rise to a maximum MVA circle in the power plane, as shown in Figure 2.15 which is established by multiplying the maximum current and the VSC's nominal PCC voltage. Due to the limited overcurrent capability of a VSC, if the grid PCC voltage drops, then the MVA circle is also accordingly impaired, as shown by the dashed line of Figure 2.15.

- The nominal VSC DC voltage rating. The maximum VSC AC side voltage is generated by modulating the established DC voltage. As demonstrated in subsection 2.6.2, there is a direct link between VSC reactive power flow, and PCC and converter-side AC voltage amplitude. If the difference between DC voltage rating and nominal PCC AC voltage is sufficiently low, the reactive power capability is limited in order to avoid over-modulation of the DC voltage, beyond which the VSC generates distorted AC voltage waveforms;

- The maximum DC current through the cables.

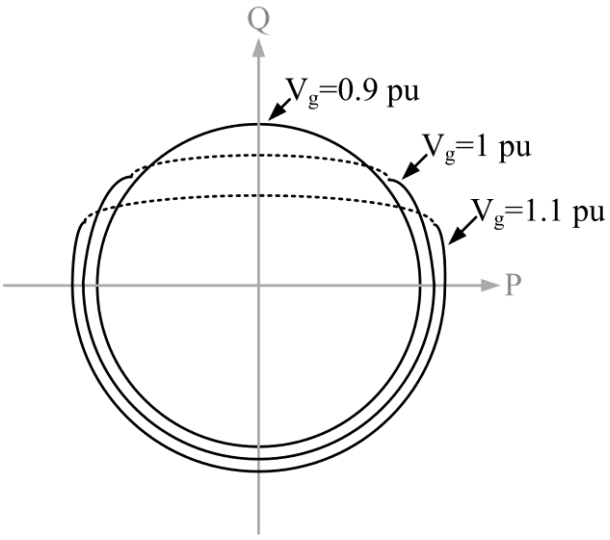

Figure 2.15 Active and reactive power capability

These limits are shown in Figure 2.15, where higher grid voltage amplitudes impair the circle representing the VSC's power capability. This is due to the nominal DC voltage, the transformer's voltage ratio and the voltage drop across the phase reactor and the transformer. When available, tap changers of the transformer play an important role in boosting the reactive power capability [1] and they need to be deliberately designed to suit the VSC for grid support purposes.

As demonstrated previously, the VSC can alter the operating point almost instantaneously anywhere within the circle in Figure 2.15. For instance, fast reversal of the active power flow is possible by changing DC current without changing the DC voltage polarity. Reactive power control is achieved by regulating the grid voltage amplitude. These advantages are of great benefit to the power industry, especially to provide various grid support functions (e.g. damping low- and high-frequency power oscillations, provision of synthetic mechanical inertia, and provision of grid voltage support). These VSC applications will be introduced in Chapter 3.

2.7 Modelling of a VSC-HVDC and the Associated Control System

A detailed model of a VSC-HVDC system with a comprehensive control system is required to fully investigate performance and to research and develop new features to address identified challenges. Accordingly, this section outlines the model that has been developed in this research and which underpins much of the research outcomes reported in later chapters of the dissertation.

A VSC-HVDC transmission system is unlike LCC-HVDC transmission system, which always requires reactive power compensation in order to function [17]. As described in the previous section, a VSC-HVDC system allows independent control of active and reactive power in four quadrants. This feature greatly promotes the freedom of control, and offers benefits for offshore wind farm integration such as reactive power compensation and black-start capability. Cascaded control loops underpin this feature and are at the core of VSC-HVDC control systems.

The cascaded control loops consist of an inner current vector controller and various outer controllers, as shown in Figure 2.16. The inner current vector controller exerts primary actions for computation of voltage vectors for the PWM process, and its functionality is completed by auxiliary outer controllers. The outer controllers include the active power controller, reactive power controller, DC voltage controller, AC voltage controller, frequency controller and inertia emulation controller (the inertia emulation controller has been developed as a result of the research reported in this dissertation and is described in detail later).

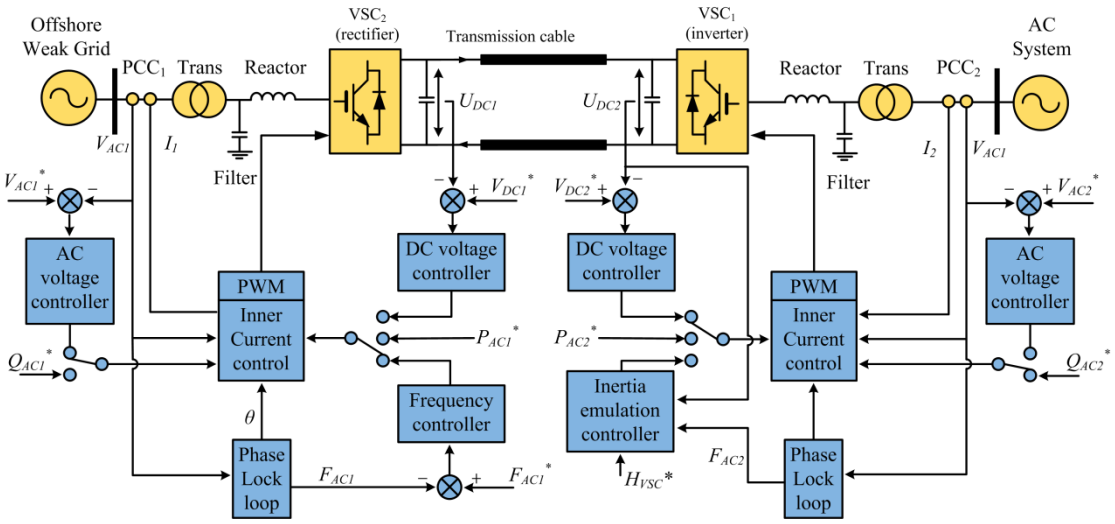

Figure 2.16 Inner current control and outer controllers for a VSC-HVDC system

In general, the inner current controller regulates active and reactive components of converter current individually. The references of active and reactive current components are provided by the output of outer controllers and are input to the inner current controller. It is obvious not all the outer controllers are selected. Individual controllers may be selected depending on the specific requirements of the HVDC applications.

2.7.1 Modelling of a VSC

For a VSC-HVDC transmission system, each converter can act as either a rectifier or an inverter, as power flow through the converter can be controlled and can be bidirectional. Therefore, the analysis of the VSC when operating as an inverter is carried out in this case. The operation of a VSC in rectification mode is identical to inversion, with the only difference being that the power transfer references are opposite in terms of polarity. Figure 2.17 and Figure 2.18 illustrate a three-phase VSC equivalent model and a single-diagram representation of the VSC with AC and DC property included. The AC/DC electrical dynamics of the VSC converter is presented as:

$$\begin{cases} v_{a1} - v_a = Ri_a + L\dfrac{di_a}{dt} \\ v_{b1} - v_b = Ri_b + L\dfrac{di_b}{dt} \\ v_{c1} - v_c = Ri_c + L\dfrac{di_c}{dt} \\ i_{dc1} - i_{dc} = C\dfrac{dU_{dc}}{dt} \end{cases} \tag{10}$$

where v_{a1}, v_{b1} and v_{c1} are the phase voltages at converter side; v_a, v_b and v_c are the phase voltages at AC grid side; i_a, i_b and i_c are the currents that flow to the grid; R and L are the aggregated resistance and inductance of the phase reactor and transformer; C is the capacitance of the DC link capacitor.

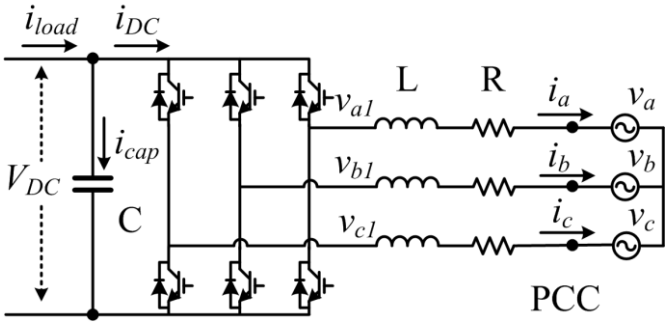

Figure 2.17 Three-phase VSC equivalent model

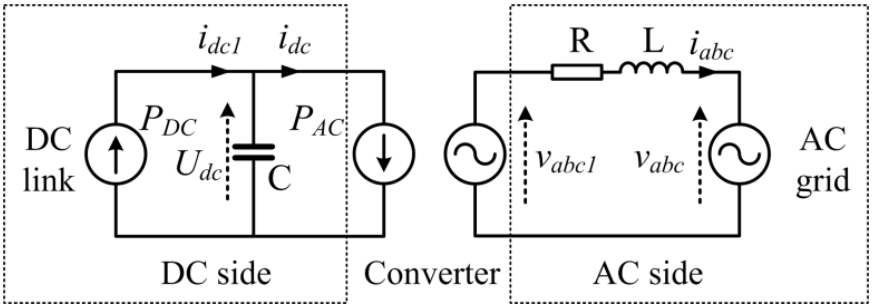

Figure 2.18 Single-line representation of a VSC

Through application of a Park Transformation (refer to Appendix A), the first three equations in (10) are transferred to two distinct DC quantities within a rotating dq reference frame, which rotates at the same angular frequency as the grid voltage:

$$\begin{cases} v_{d1} - v_d = Ri_d + L\dfrac{di_d}{dt} - j\omega i_q \\ v_{q1} - v_q = Ri_q + L\dfrac{di_q}{dt} + j\omega i_d \end{cases} \tag{11}$$

where v_{d1} and v_{q1} refer to the converter voltage vectors, v_d and v_q refer to the grid voltage vectors, i_d and i_q refer to the vectors of the current through the reactor and transformer, ω refers to the angular speed of grid frequency.

The angular speed of grid frequency ω is provided by a phase-locked loop which is used to synchronise the output voltage from the converter with the grid voltage. When

the network voltage at the PCC remains constant and balanced, the grid q-axis voltage is equal to zero. Therefore, equation (11) can be written as:

$$\begin{cases} v_{d1} = v_d + Ri_d - j\omega Li_q + L\dfrac{di_d}{dt} \\ v_{q1} = Ri_q + j\omega Li_d + L\dfrac{di_q}{dt} \end{cases} \tag{12}$$

The instantaneous active and reactive power at the grid connection point in dq coordinates is given by:

$$\begin{cases} P = \dfrac{3}{2}(v_d i_d + v_q i_q) = \dfrac{3}{2} v_d i_d \\ Q = \dfrac{3}{2}(v_q i_d - \frac{3}{2} v_d i_q) = -\dfrac{3}{2} v_d i_q \end{cases} \tag{13}$$

From equation (13), the active and reactive power can be controlled independently by regulating the d-axis and q-axis current at the grid connection points.

2.7.2 Inner current control

Inner current control is shown graphically in Figure 2.19. The objective of the inner current control is to provide and update reference voltage vectors v_{d1}* and v_{d1}* for the VSC. In order to regulate the current vectors i_d and i_q through the phase reactors, the inner current control loops use the feed-forward loops to function according to (11). The S-functions of (12) with applications of proportional-integral controllers are expressed in (14):

$$\begin{cases} v_{d1}^* = v_d - \omega Li_q + k_p(i_d^* - i_d) + \dfrac{k_i}{s}(i_d^* - i_d) \\ v_{q1}^* = \omega Li_q + k_p(i_q^* - i_q) + \dfrac{k_i}{s}(i_q^* - i_q) \end{cases} \tag{14}$$

The choices of proportional and integral gains will be within an acceptable range of values, which can be manually tuned based either upon experience/judgement or using software tools based on root locus or lambda tuning methods. The analysis concerned with inner current control dynamics and stability can adopt the following S-function which is derived from (11) (assuming two PI controllers has the same values in terms of k_p and k_i for i_d and i_q):

$$G(s)=\frac{i_d}{i_d^*}(or=\frac{i_q}{i_q^*})=\frac{\frac{k_p}{L}+\frac{k_i}{L}}{s^2+\frac{R+k_p}{L}s+\frac{k_i}{L}} \tag{15}$$

The details of feed-forward inner current control loops based on (14) are presented in Figure 2.19. Reference voltage vectors v_{d1}* and v_{q1}* are transferred to three-phase values in abc coordinates for PWM process.

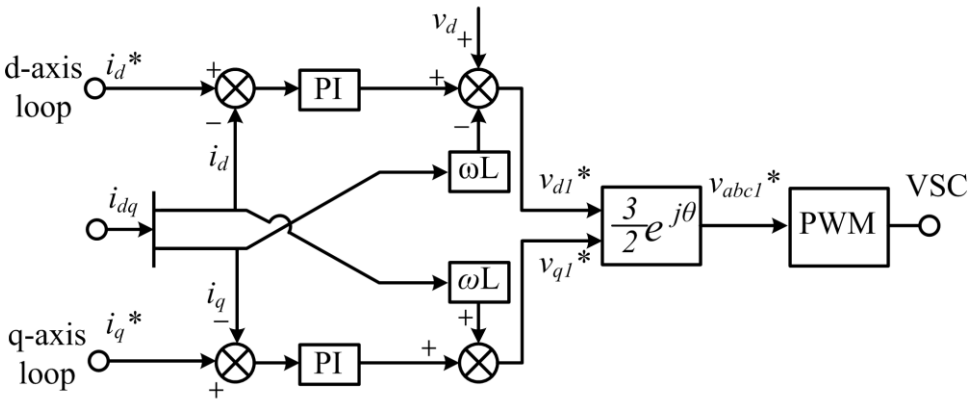

Figure 2.19 Feed-forward inner current control loops

2.7.3 Outer controllers

As previously mentioned, there are a range of outer controllers for VSC-HVDC system, and they can be classified according to their function. The functions considered in this research include: active power controller, reactive power controller, DC voltage controller, AC voltage controller, frequency controller and inertia emulation controller. The following text provides brief descriptions along with relatively simple simulation demonstrations for each controller type.

i. Active power controller

As demonstrated in subsection 2.7.1, the active power at the grid connection point is estimated by (13). With the active power controller, the d-axis current reference i_d* is computed according to:

$$i_d^*=\frac{2P^*}{3v_d} \tag{16}$$

In actual implementations, a PI controller is used to regulate d-axis current according to the d-axis current reference i_d*, as shown in Figure 2.20. The S-function of the open-loop active power controller is expressed as:

$$i_d^* = k_p\left(\frac{2P^*}{3v_d} - i_d\right) + \frac{k_i}{s}\left(\frac{2P^*}{3v_d} - i_d\right) \tag{17}$$

The active power reference P* is specified by system operators. The output of the PI controller is input to the inner current control.

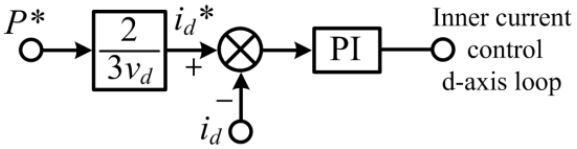

Figure 2.20 Active power controller

ii. Reactive power controller

The reactive power controller has a similar principle of operation as for the active power controller. According to (13), the q-axis current reference i_q* is computed as:

$$i_q^* = \frac{2Q^*}{3v_d} \tag{18}$$

The S-function of the open-loop reactive power controller with a PI controller is expressed as:

$$i_q^* = k_p\left(\frac{2Q^*}{3v_d} - i_q\right) + \frac{k_i}{s}\left(\frac{2Q^*}{3v_d} - i_q\right) \tag{19}$$

As shown in Figure 2.21, reactive power reference Q* is also specified by system operators. The output port of the PI controller is connected to the input port of inner current control.

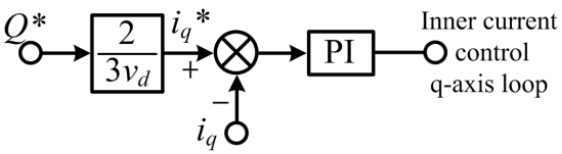

Figure 2.21 Reactive power controller

iii. DC voltage controller

The active power transmitted through the converter DC side is given as:

$$P_{DC} = U_{DC} i_{DC} \tag{20}$$

Assuming the VSC is lossless, power balance between the converter's AC and DC sides results in:

$$i_d^* = \frac{2U_{DC} i_{DC}}{3v_d} \tag{21}$$

The DC link capacitor as shown in Figure 2.17 and Figure 2.18 has dynamic properties that result in the DC voltage varying with changes of input current in accordance with:

$$C\frac{dU_{DC}}{dt} = i_{DC1} - i_{DC} \tag{22}$$

where i_{DC1} is the DC load current from the DC system and i_{DC} is the converter side DC current.

Combining (21) and (22) yields:

$$i_d^* = \frac{2U_{DC}}{3v_d}(i_{DC1} - C\frac{dU_{DC}}{dt}) \tag{23}$$

From (23), it is clear that variations in DC link voltage are directly linked with d-axis reference current on the AC side grid connection point. In order to regulate DC link voltage, the DC voltage controller controls the d-axis current. The nonlinearity of (23) is eliminated by a PI controller. The S-function of the DC voltage is then given as:

$$i_d^* = -k_p(U_{DC}^* - U_{DC}) - \frac{k_i}{s}(U_{DC}^* - U_{DC}) \tag{24}$$

Equation (24) is the control logic for the inverter which has a proportional relationship between U_{DC} and i_d. If a DC voltage controller is applied to a rectifier which has an inverse proportional relationship between U_{DC} and i_d, then the minus sign should be omitted. The DC voltage controller loop is shown in Figure 2.22.

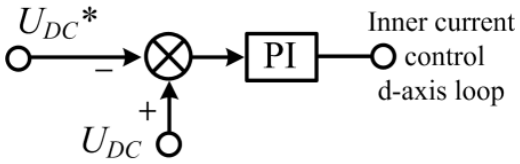

Figure 2.22 DC voltage controller

iv. AC voltage controller

On the AC side of a VSC, the amplitude of voltage drop across the impedances of the phase reactor and transformer $R+j\omega L$ is approximated as follows:

$$\Delta v = |v_{AC1}| - |v_{AC}| = \frac{RP + \omega LQ}{v_d} \tag{25}$$

where v_{AC1} is the amplitude of the converter AC side voltage, and v_{AC} is the amplitude of the grid connection point voltage.

In the phase reactor and transformer, reactance ωL is significantly larger than resistance R. Therefore from (25), the reactive power flow Q through the reactor and transformer determines the resultant voltage at the grid point. The control of AC voltage amplitude is reliant on the reactive component i_q of the current at the grid connection point.

The voltage amplitude $|v_{abc}|$ at the grid connection point can be estimated by the relevant voltage vectors v_d and v_q:

$$|v_{AC}| = \sqrt{v_d^2 + v_q^2} \tag{26}$$

The S-function of AC voltage controller is given as:

$$i_q^* = k_p(|v_{AC}|^* - \sqrt{v_d^2 + v_q^2}) + k_i(|v_{AC}|^* - \sqrt{v_d^2 + v_q^2}) \tag{27}$$

The AC voltage controller loop is shown in Figure 2.23.

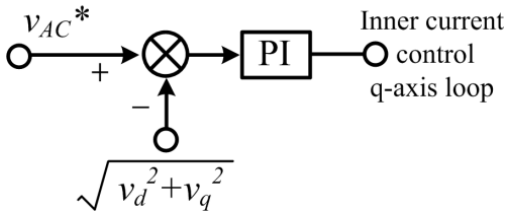

Figure 2.23 AC voltage controller

v. Frequency controllers

The power-frequency characteristic of a power system is defined as the effect of change of loads or generations in overall system frequency:

$$\Delta f = -R_{Droop}\Delta P \tag{28}$$

where R_{Droop} is the value of the droop gain which is the characteristic for a specific power system.

Depending on the specific application, there are two primary types of frequency controllers that are normally applied to VSC-HVDC systems.

Frequency controller I (droop type):

Frequency controller I is used for the supply to a power system with an established frequency. To compensate any power imbalance in a system which is reflected in changes in system frequency as shown in (28), frequency controller I adjusts the active component of transmitted current i_d according to the system frequency f which is estimated by the PLL in the control system, as illustrated in Figure 2.24:

$$i_d^* = -k_p(f^* - f) \tag{29}$$

where K_p is the proportional gain, and is also often referred to as the droop value of the frequency controller. f_0 is the nominal grid frequency.

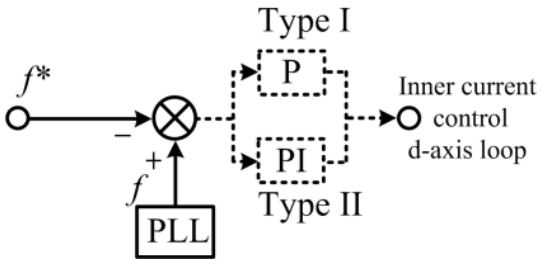

Figure 2.24 Frequency controller I and II

There is a steady-state error associated with such controllers as only proportional control is used in frequency controller I. The selection of the droop value depends on the degree of required frequency support and the power transfer capability of the VSC-HVDC transmission system.

Frequency controller II (converging type):

Frequency controller II is used for the supply to a system that does not contain any other power sources or frequency control capabilities within that system. It normally has a fixed frequency reference to regulate the power balance of the system. To absolutely control the frequency of a power system, a PI controller is employed to eliminate steady state errors:

$$i_d^* = -k_p(f^* - f) - \frac{k_i}{s}(f^* - f) \tag{30}$$

vi. Inertia emulation controller

This type of outer controller enables the VSC to contribute a virtual inertial response, in a similar fashion as a synchronous generator would provide inertia due to its stored kinetic energy. This is one of the major contributions of this research work, and details of the inertia emulation controller will be discussed in Chapter 5.

2.8 Summary

In this chapter, power electronic devices including diodes, bipolar junction transistors, MOSFET, thyristors and IGBT are first of all briefly introduced. Then an overview of VSC-HVDC converters, including converter topology, phase reactor, AC filter, DC capacitor and DC cable has been presented. PWM techniques, used to control VSC operation, have also been introduced. It has been shown that control of VSC active and reactive power flows are effectively decoupled, and a voltage phasor demonstration was presented to investigate scenarios where different VSC converter voltages were used. The active and reactive power capability of VSC-HVDC converters was demonstrated.

This chapter also introduced the control structure for a VSC-HVDC system. The control system firstly demonstrates the relatively faster inner current control. Following on from this, a number of relatively slower outer controllers, including active power controller, reactive power controller, DC voltage controller, AC voltage controller, frequency controller and inertia emulation controller, were described. This chapter has provided the underpinning theory of VSC-HVDC converter control systems and acts as a basis for the following chapter, where a literature review of VSC-HVDC system applications and novel VSC-HVDC control strategy designs is presented.

References

[1] Thompson, M.T., *Introduction to Power Electronics*. Thompson Consulting Inc. Online Available [assessed on 06/12/2012]:http://www.thompsonrd.com/notes%2001%20introduction%20to%20power%20electronics.pdf.

[2] Mohan, N.; Undeland, T.M.; and Robbins, W.P., *Power Electronics: Converters, Applications and Design.* 3rd ed. NJ: John Wiley & Sons, Inc. 2003.

[3] Kittel, C., *Introduction to Solid State Physics*. 8th ed. John Wiley & Sons, Inc. 2005.

[4] Arrillaga, J., Liu, Y.H., Watson, N.R., *Flexible Power Transmission-The HVDC Options*, 2007.

[5] Delmar Learning. *The Bipolar Transistor*. [On-line]. Available: http://webtools.delmarlearning.com/sample_chapters/04.pdf[Mar 7th, 2013].

[6] ON Semiconductor (2005). *Thyristor Theory and Design Considerations Handbook*. [On-line]. Available: www.onsemi.com/pub/collateral/hbd855-d.pdf [Mar 1st, 2013].

[7] Kharagpur, P., *Class Lecture Topic: Power Semiconductor- Metal Oxide Semiconductor Field Effect Transistor*. [On-line]. Available: http://nptel.iitm.ac.in/courses/webcourse-contents/iit%20kharagpur/power%20electronics/pdf/l-6(dk)(pe)%20((ee)nptel).pdf

[8] Horowitz, P.; Hill, W.,*The Art of Electronics*. Cambridge University Press.ISBN978-0-521-37095-0.Online Available [assessed on 12/12/2012]: http://books.google.com/books?id=bkomdgwfa28c&pg=pa113&dq=bjt+charge+current+voltage+control+inauthor:horowitz+inauthor:hill.

[9] Sattar, A., *Insulated Gate Bipolar Transistor (IGBT) Basics*, IXYS Corporation, Online Available [assessed on 15/12/2012]: www.ixys.com/documents/appnotes/ixys_igbt_basic_i.pdf.

[10] Bahrman, M.P.; Johnson, B.K., "The ABCs of HVDC transmission technologies," *IEEE Power and Energy Magazine* , vol.5, no.2, pp.32-44, March-April 2007.

[11] Long, W.; Nilsson, S., "HVDC transmission: yesterday and today," *IEEE Power and Energy Magazine,* vol.5, no.2, pp.22-31, March-April 2007.

[12] Gole, A.M.; Meisingset, M., "Capacitor commutated converters for long-cable HVDC transmission," *Power Engineering Journal*, vol.16, no.3, pp.129-134, June 2002.

[13] Flourentzou, N.; Agelidis, V.G.; Demetriades, G.D., "VSC-Based HVDC Power Transmission Systems: An Overview", *IEEE Trans. on Power Electrons.,* vol.24, no.3, pp.592-602, March 2009.

[14] Adam, G.P.; Anaya-Lara, O.; Burt, G.M.; Telford, D.; Williams, B.W.; McDonald, J.R., "Modular multilevel inverter: Pulse width modulation and capacitor balancing technique," *IET Power Electronics , vol.3, no.5, pp.702-715*, September 2010.

[15] Nabae, A., I. Takahashi; Akagi, H., "A new neutral-point-clamp PWM inverter, "*IEEE Trans. Ind. Appl.*, vol. IA-17, no. 5, pp. 518–523, Sep.1981.

[16] Bhagwat, P. M.; Stefanovic, V. R., "Generalized structure of a multi-level PWM inverter,*" IEEE Trans. Ind. Appl.*, vol. IA-19, no. 6, pp. 1057–1069, Nov. 1983.

[17] Meynard, T. A.; Foch, H., "Multi-level conversion: High voltage choppers and voltage-source inverters, " in Proc. IEEE Power Electron. Spec. Conf., 1992, pp. 397–403.

[18] Adam, G.P.; Anaya-Lara, O.; Burt, G.M.; Telford, D.; Williams, B.W.; McDonald, J.R., "Modular multilevel inverter: Pulse width modulation and capacitor balancing technique," *IET Power Electronics*, vol.3, no.5, pp.702-715, September 2010.

[19] National Grid Plc., Factsheet: High Voltage Direct Current Electricity- Technical Information, Online Available [assessed on 07/01/2013]: http://www.nationalgrid.com/nr/rdonlyres/7d099982-c937-4257-aeeb-6a7cd0757b79/50189/20100621_hvdc_detailed_factsheet_final.pdf

[20] Karlsson P., *DC Distributed Power Systems - Analysis, Design and Control for a Renewable Energy System*, Lund University. Department of Industrial Electrical Engineering and Automation. Sweden 2002. ISBN 91-88934-25-X.

[21] MathWorks, *Three-phase Harmonics filters*. Online Available [assessed on 07/12/2012]:

http://www.mathworks.co.uk/help/physmod/powersys/ref/threephaseharmonicfilter.html

[22] MathWorks, *VSC-Based HVDC Link*, Online Available [assess on 13/12/2012]: http://www.mathworks.co.uk/help/toolbox/physmod/powersys/ug/f8-9059.html.

[23] Agap, A.; Dragan C.M., "Multiterminal dc connection for offshore wind farms," Master's thesis, Aalborg University, 2009.

[24] ABB, *It's time to Connect*, Technical description of HVDC Light® technology. ABB - Grid Systems -HVDC. SE-771 80 Ludvika, Sweden.

[25] Bird, J., *Electrical and Electronic Principles and Technology*, Elsevier Limited 2010, Page 63-76.

[26] Du, C.Q.,"VSC-HVDC for Industrial Power Systems," Ph.D. dissertation, Dept. Energy and Enviro., Chalmers Univ. of Technol., G¨ oteborg, Sweden, 2007.

[27] Alstom Grid, Multi-terminal HVDC system for large offshore wind park grid integration, 2010.

[28] ABB, *XLPE Land Cable Systems User´s Guide*, pp.16-22, Online Available [assessed on 05/07/2011]: http://www05.abb.com/global/scot/scot245.nsf/veritydisplay/ab02245fb5b5ec41c12575c4004a76d0/$file/xlpe%20land%20cable%20systems%202gm5007gb%20rev%205.pdf.

[29] XLPE Insulated DC High-Voltage Submarine Cable, Online Available [assessed on 05/06/2012]: http://www.caledonian-cables.com/product/Submarine_Cables/XLPE-DC.html

[30] Johansson, S.G.; Asplund, G.; Jansson, E.; Rudervall, R., "Power System Stability Benefits with VSC DC-Transmission Systems," CIGRE Conference, 2004, Paris, France.

Chapter 3

Review of research relating to operation and control VSC-HVDC technologies for integration of renewable energy sources

3.1 Introduction

Modern electric power systems are evolving into an era where not only conventional generation and transmission technologies are being used, but also new technologies such as smart grid technologies (smart meters, demand side management and transmission line dynamic rating systems, etc.), wind, wave and tidal power generation, solar farms and flexible AC transmission systems (FACTS) are beginning to come into play and replacing the conventional technologies. Particularly in Europe, wind power generation is expected to play a critical role in meeting future power demand.

Encompassing issues associated with renewable generation integration, this chapter reviews various emerging VSC control technologies. VSC is increasingly employed as interfaces for renewable power generation (e.g. wind power generators) and also as transmission measures for offshore wind farms and power system interconnectors (e.g. HVDC systems). First of all, challenges raised by offshore wind power transmission are specifically demonstrated in terms of system impact and power delivery options. As future power systems are likely to suffer the risk of lacking system mechanical inertia due to the conceivable high penetration of renewable energy, the second part of this chapter moves to review the impact of renewable energy and HVDC systems in terms of system frequency control and ability to contribute "synthetic" inertia. Thirdly, the advantages associated with various VSC applications are presented. Finally, the typical control strategies for a multi-terminal HVDC grid are reviewed.

3.2 "Renewable Dense" Power Systems

The renewable power generation (mainly wind power in the Europe) are characterised by inherent uncertainties, with output often fluctuating and being stochastic in nature. Although wind power forecast techniques are continuously being improved, there can still be significant deviations between forecasts and reality. This implies that power reserve in the short term need to be considered [1], and transmission network reinforcements and construction programmes may be required to accommodate a large amount of wind power. For example, the installations of electrical energy storage such as fuel cells, spinning reserve and hydro pumped storage plants may be required to manage the fluctuating wind energy sources and to ensure that the balance between load and generation levels is maintained.

Consequently, there is a significant challenge presented to power transmission operators in terms of monitoring and controlling future power systems. New transmission technologies such as High Voltage Direct Current (HVDC) transmission systems and Flexible Alternating Current Transmission systems (FACTS) may be employed to address various challenges such as power losses and reactive power compensation. In the following literature review, the major challenges regarding to the offshore wind power developments and the proposed technical solutions with focuses on VSC control systems will be demonstrated:

3.3 Offshore Transmission Options: HVAC or HVDC

3.3.1 HVDC options against conventional HVAC

Currently most European offshore wind farms are connected to the grids using HVAC [4]. For example, the large-scale 172.8 MW Gunfleet Sands wind farm and 300 MW Thanet wind farm in the United Kingdom are both connected to onshore by HVAC. These operational offshore wind farms in Europe in [6] are mostly located at a distance of less than 12 km from the onshore network. There are two transmission technologies available for offshore wind farm integrations: HVAC or HVDC. Nevertheless, since both technologies have advantages and disadvantages, the specific situation in terms of network configuration and wind farm power rating dictates that the integration solution for an offshore wind farm needs to be analysed and optimised on a case by case basis.

The technical-economic choice for HVAC or HVDC primarily depends on the transmission distance involved. Figure 3.1 illustrates the impacting factors considered for the cost analysis, including AC&DC terminals, lines and power losses. It appears that due to the relatively high expense for HVDC converter stations, the DC solution in term of transmission terminals is more expensive for short distances. Nevertheless, DC submarine cables rated to transfer a similar amount of power to their AC counterparts are relatively cheaper than three-wire AC submarine cables (for long-distance AC cables the intermediate reactive power compensation also needs to be taken account [3]). In addition, with sufficiently long distance, DC power losses are less than AC power losses, which contributes to the relatively lower cost of the HVDC solution above certain distances. In [2], the authors conclude that for the integration of a 100 MW offshore

wind farm, the HVDC solution is more expensive and has higher power losses than HVAC for transmission distance up to 60 km, whereas HVDC appears to be competitive for distances in excess of 60 km.

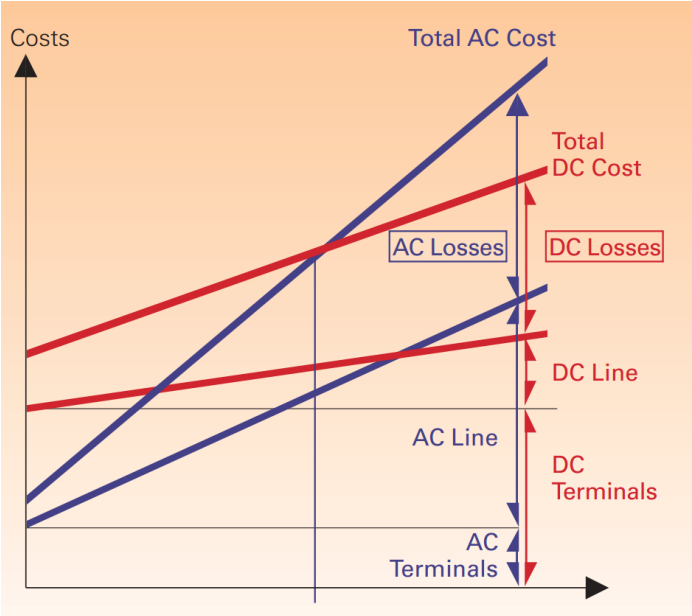

Figure 3.1 Cost versus transmission distances [3]

In the near future there will be more remote offshore wind farms as well as international interconnections requiring longer transmission networks and stronger power flow controllability. The capacitive charging current of HVAC due to large shunt capacitance may threaten transmission stability and require large amounts of reactive power compensation. In such circumstances, HVDC technology may be the best choice for extending and growing the capacities of offshore transmission networks.

3.3.2 Control strategies for multi-terminal HVDC grids

An example of a multi-terminal DC transmission (MTDC) grid is illustrated in Figure 3.2, where three wind farms are integrated to feed three independent power systems. The basic parameters for a DC grid such as DC voltage level and active power flow are listed in Table I with comparisons being included against typical AC power grids. For an AC power grid, voltage frequency ω is a global indication for the balance of generations and loads, whereas for a DC power grid the overall DC voltage level is the used as the indicator and control input for provision of balance between power inputs and outputs of all converters in the system. When computing active power flows between two AC buses, the relative voltage angle difference between the buses, δ, defines the amount of

real power transfer between the locations, while the active power flow between two DC terminals in a DC grid is only determined by the DC voltage difference between the sending and receiving locations. As the DC voltage is not alternating ($\omega=0$ when calculating inductive impedance $X=\omega L$), the DC network inductance can be neglected and only resistance R is considered for electric power losses. Furthermore, obviously the concept of reactive power does not exist in a DC system, further reducing the complexity of controlling power flow between locations and losses in the system.

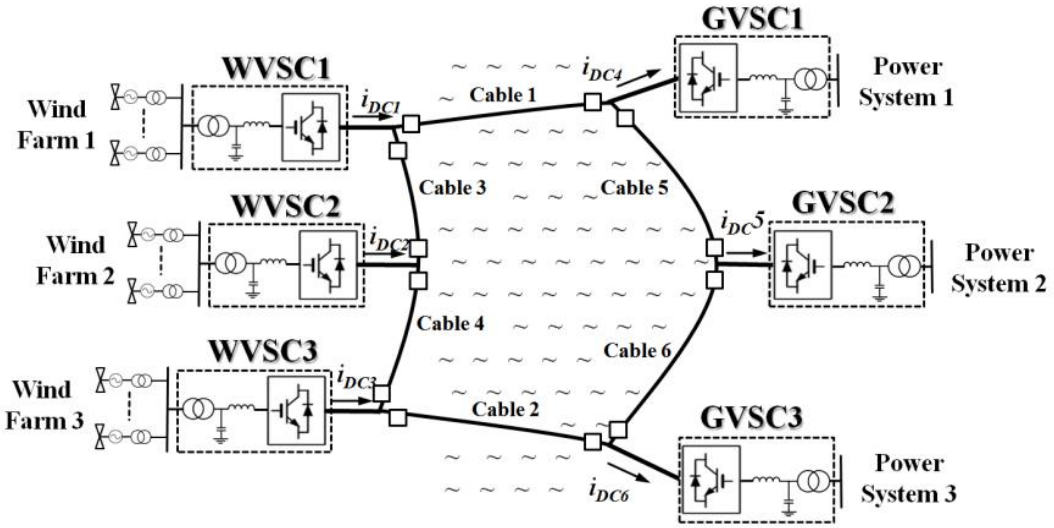

Figure 3.2 A six-terminal DC transmission grid example

Table I Comparison of AC and DC parameters

AC Parameters	**DC parameters**
Frequency ω	Target DC voltage U_{DC}
Voltage change $v \cdot sin(\omega t + \delta)$	Voltage change ΔU_{DC}
Impedance $R + jX$	Resistance R
Real Power $\frac{v_1 \cdot v_2 \cdot \sin\delta}{X}$	Real Power $\frac{U_{DC} \cdot \Delta U_{DC}}{R}$

In terms of the control strategy for the whole MTDC network, the individual VSC converters are controlled under a "master" control framework, as illustrated in Figure 3.3, so that all the converters are co-ordinately operated. As DC voltage level is regarded important for a MTDC system, it has to be maintained stable by at least one VSC converter station. With this basic principle, the control philosophies fall into two distinct routines, which are so-called “DC voltage margin control strategy” and “DC voltage droop control strategy”.

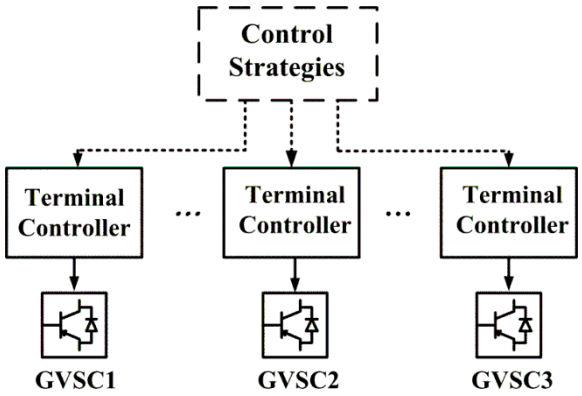

Figure 3.3 Relationships between the MTDC control strategy and local control

i. DC voltage margin control

A voltage margin control strategy is proposed in [42]-[44] to reduce the reliance on communications. It designates a grid connected VSC (GVSC) to regulate the DC voltage and other GVSCs to operate at their local active power references, while allows wind farm side VSC (WVSC) to track maximum active power according to wind speed. As illustrated in Figure 3.4, GVSC2 is the DC voltage regulator which maintains the DC voltage at a constant level and compensates the active power balance in the MTDC network. At the loss of GVSC2, to provide redundancy another GVSC ($GVSC_1$ or $GVSC_3$) will detect the DC voltage variation and come up to regulate the DC voltage at a different level (higher heavy line for $GVSC_1$, lower heavy line for $GVSC_3$ in the case of Figure 3.4). The triggering DC voltage levels for the shift of DC voltage regulator should be discriminative so that all the GVSCs will operate at a coordinated order while securing the DC voltage stability of the MTDC network.

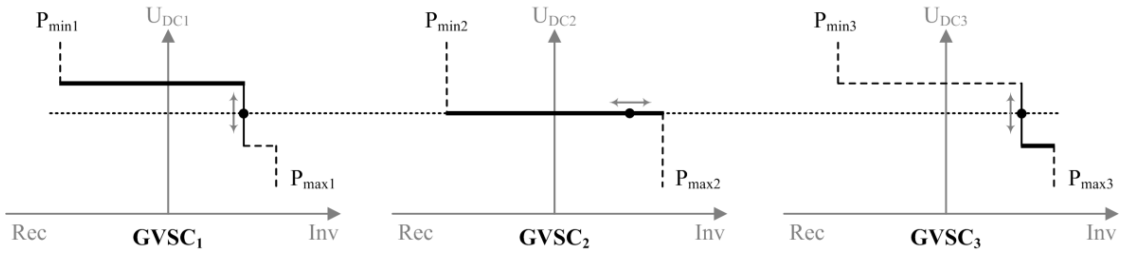

Figure 3.4 UDC-P characteristic of MTDC voltage margin control strategy

The DC voltage margin control strategy, however, has its drawback that it exposes the DC voltage regulating converter and associated AC side equipment to increased power variation stresses and the risk of DC over-voltage. This is because only one converter is designated to balance the power for the entire network, which is less desirable from a power security perspective.

ii. DC voltage droop control

Rather than voltage margin control designating a single GVSC as a DC voltage regulator, a voltage droop control strategy is proposed in [45]-[47] to operate all the GVSCs as DC voltage regulators. The operational DC voltage levels are drooped to share the output power by the MTDC network characteristic of DC voltage – active power, which is computed by the parameters (primarily the resistances among DC nodes) of the network. For the example of Figure 3.5, the droop is applied to $GVSC_1$ and $GVSC_3$, assuming the resistances between $GVSC_2$ and $GVSC_1$ and the resistance between $GVSC_2$ and $GVSC_3$ are fixed, the power flow via $GVSC_1$ and $GVSC_3$ DC nodes to $GVSC_2$ will depend on the operational DC level of $GVSC_1$ and $GVSC_3$. As shown in Figure 3.5, if $GVSC_1$ drops its DC voltage level, more DC active power flow will flow to $GVSC_1$ via the end circuits of $GVSC_2$ and $GVSC_3$.

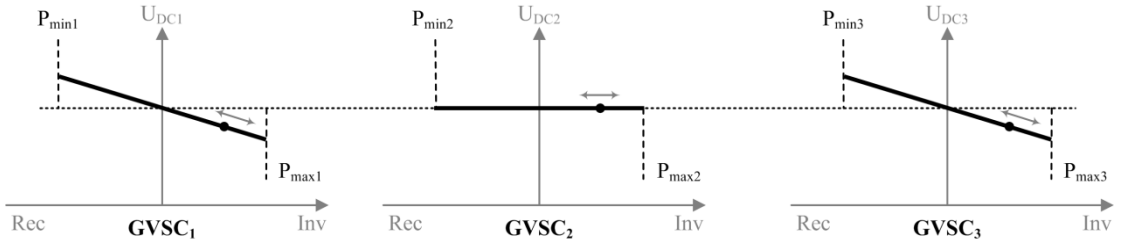

Figure 3.5 UDC-P characteristic of MTDC voltage droop control strategy

However, the major disadvantage associated with the DC voltage droop control is that, in order to achieve multiple control tasks, the droop characteristic may be highly complex as illustrated in [46]. In addition, the droop characteristic may be long-term effective, varying according to the circumstances (e.g. DC cable resistances).

3.4 Power System Frequency Responses

Power system frequency is an important indicator for any instantaneous imbalance between generations and demand. One of the major concerns relating to the with the rapid development and increase of renewable power relates to system frequency stability, as most of renewable power generation contribution little or no inertial and frequency response with power electronics converter interface.

In this section, in order to design frequency control methodologies, the elementary dynamic model of the system frequency is detailed, including the dynamics of the generators, frequency dependent load and the combination of the two elements. The main practices that are adopted for frequency control in most power systems are introduced. Following on from this, the synchronous generator model with frequency and voltage control is demonstrated, along with the behaviour of frequency-dependent loads. A combined generator and load model is presented. Finally, the mechanical inertia of synchronous generators is introduced and its impact on frequency transients is presented.

A nominal frequency is defined as a constant value (for instance, 50 Hz in continental Europe and China, 60 Hz in America). Any deviations from nominal frequency will arise due to imbalances between the instantaneous generation and consumption of electric power, which has an accelerating or decelerating effect on conventional synchronous machines (before control action intervenes). In this subsection, the frequency dynamics of generators and load are discussed independently and combined to form the frequency dynamics of an "uncontrolled" power system; but of course control systems will act to ensure that frequency remains largely stable-this is also summarised.

3.4.1 Inertial behaviour of system generators

After a major disturbance in a power system, e.g. an instantaneous loss of a large power generation plant, the frequencies at different nodes in the power system will vary with a similar trend, as all of the synchronous generators are interconnected. Therefore an average frequency, which determines the trend of all local generator frequencies, can be defined by one lumped generator representing all the generators. The frequencies of the different machines may experience comparatively small variations over the average frequency, as shown in Figure 3.6 which is derived from a simple two-machine power system.

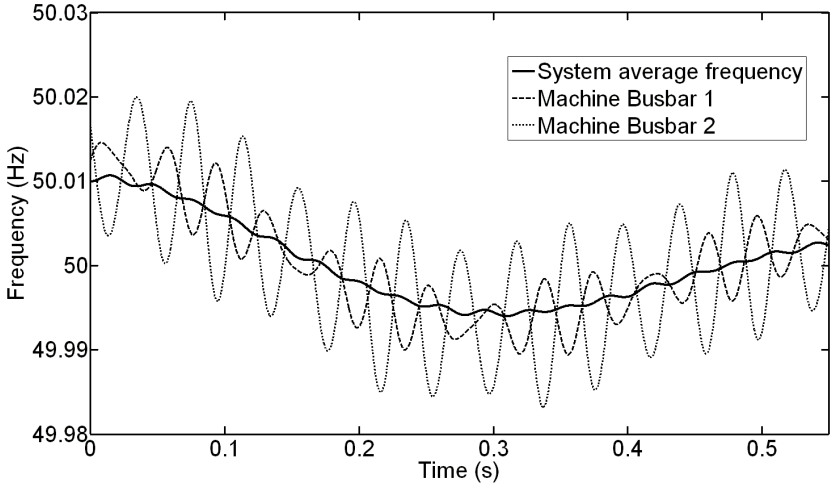

Figure 3.6 System average frequency and frequencies at different locations

In order to derive a complete frequency dynamic model for a large-scale power system which consists of n SMs, the well-known swing equation for a specific synchronous machine i (SM) is first of all used to demonstrate the machine dynamic behaviour:

$$\frac{2H_i}{\omega_0}\cdot\frac{d\omega_i}{dt} = T_{Mi} - T_{Ei} = T_{Ai} \tag{1}$$

where ω_0 is the nominal system angular speed (rad/s), T_{Mi} and T_{Ei} are the mechanical and electrical torques ($N\cdot m$) of machine i, T_{Ai} is the accelerating torque of machine i and H_i is the inertia time constant which is defined by (2):

$$H_i = \frac{\frac{1}{2}J_i\omega_{Mi}^2}{S_i} \tag{2}$$

where J_i is the moment of inertia ($kg \cdot m^2$), ω_{Mi} is the angular shaft speed of the SM i (rad/s) and S_i is the rated machine capacity (MVA).

In pu values, (1) can be converted to (3) by relating the torques with active powers:

$$\frac{2H_i}{\omega_0} \times \frac{d\omega_i}{dt} = P_{Mi} - P_{Ei} = P_{Ai} \ (pu) \tag{3}$$

where P_{Mi} and P_{Ei} are the machine i mechanical and active power ($N \cdot m$), P_{Ai} is the machine i accelerating active power.

Equation (3) can also be written in SI units by dividing active power with the machine power base S_i:

$$\frac{2H_i}{\omega_0} \times \frac{d\omega_i}{dt} = \frac{P_{Mi} - P_{Ei}}{S_i} = \frac{P_{Ai}}{S_i} \quad (SI) \tag{4}$$

$$\frac{2S_iH_i}{\omega_0} \times \frac{d\omega_i}{dt} = P_{Mi} - P_{Ei} = P_{Ai} \ (SI) \tag{5}$$

For a tightly interconnected power system containing n generators, there are small variations of individual machine speeds as the rotors "swing" during dynamic disturbances, but the system can be viewed as behaving as a single entity for analytical purposes. In [7], this is defined as an "inertial centre" which has an average angular speed $\bar{\omega}$:

$$\bar{\omega} = \frac{\sum_{i=1}^{n} \omega_i H_i}{\sum_{i=1}^{n} H_i} \ (pu) \tag{6}$$

All of the n generators in the power system can be consolidated into one single unit. A summation of (5) for the n generators yields:

$$\sum_{i=1}^{n} 2S_iH_i \cdot \frac{1}{\omega_0} \times \frac{d\bar{\omega}}{dt} = \sum_{i=1}^{n} P_{Mi} - \sum_{i=1}^{n} P_{Ei} = P_A \ (SI) \tag{7}$$

$$\frac{d\bar{\omega}}{dt} = \frac{\omega_0}{\sum_{i=1}^{n} 2S_iH_i} \cdot \left(\sum_{i=1}^{n} P_{Mi} - \sum_{i=1}^{n} P_{Ei}\right) = \frac{\omega_0}{\sum_{i=1}^{n} 2S_iH_i} \cdot P_A \ (SI) \tag{8}$$

where P_A is the overall instantaneous active power mismatch for the entire system.

Equation (8) can be put into the pu value as presented in (9) which is identical to [7]:

$$\frac{d\bar{\omega}}{dt} = \frac{(\sum_{i=1}^{n} P_{Mi} - \sum_{i=1}^{n} P_{Ei})}{\sum_{i=1}^{n} 2H_i} = \frac{P_A}{\sum_{i=1}^{n} 2H_i} \quad (pu) \tag{9}$$

From (9) it can be observed that the impact of any power imbalance in a system P_A will be shared by all of the n generators. Without frequency controls and generator governor actions, the mean changing rate of the network angular speed $\bar{\omega}$ will be determined by the aggregated system inertias, particularly during transient disturbances.

3.4.2 Primary frequency control of system generators

Stable frequency is important for power system operations. The quality of power delivery requires a stable frequency. Considerable frequency deviations may cause damages of system elements. If the frequency is excessively low (lower than 47-48 Hz in a 50Hz system), this could lead to damaging vibrations in steam turbines, while in comparison with thermal units hydro power plants are more robust in coping with frequencies down to 45 Hz [8]. In order to maintain grid frequency as constant as possible, energy reserve and frequency response should be adequately provided to keep the frequency during disturbances at an acceptable level. Low frequency may also adversely affect loads and voltage profiles throughout the system.

Figure 3.7 presents a simplified synchronous generation (SG) with network frequency response. The SG consists of a turbine which provides mechanical power to the shaft, and an electrical generator with inertia of H which is connected to the power grid. The SG primary control action is achieved by regulating the mechanical power of the power turbine (e.g. thermal turbine or hydro turbine) according to the real-time difference between the grid frequency and the frequency set point. For instance, for a steam synchronous generator, a servo-motor detects the frequency deviation, adjusts the valve through which the pressure energy in steam is transferred to mechanical torques and drive the turbine to vary the speed of the rotating masses. In this way, the turbine dynamics play a critical role in determining the system frequency response.

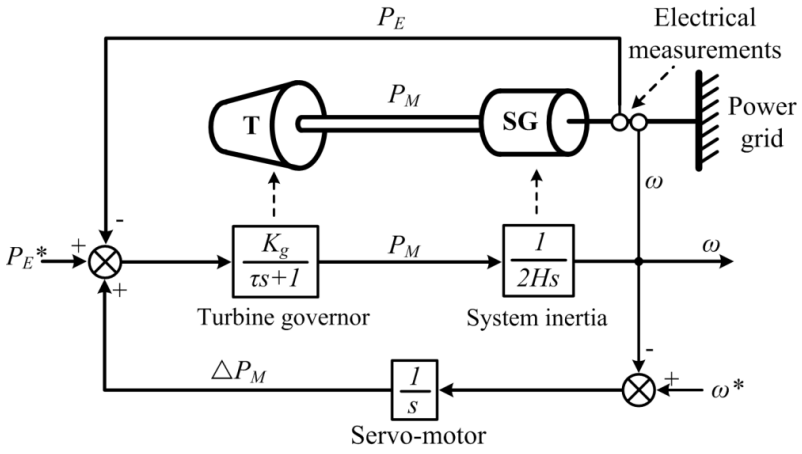

Figure 3.7 Simplified diagram of a system with inertial response and frequency control

The objective of primary frequency control is to bring the frequency back to acceptable values within a short period of time. There are inevitable errors because all generator turbines participating in primary frequency control typically employ purely proportional droop gains [9]. In practice, there is a power/frequency characteristic K as shown in (10) which measures the load-frequency sensibility of a specific power system. In the UK, National Grid currently uses a continuous value of 2% (of the total load) MW/Hz; this figure was established through previous investigations [10].

$$K = -\frac{\Delta P_L}{\Delta f} \tag{10}$$

3.4.3 Frequency dependent loads

Load can be either frequency-dependent or frequency-independent. Frequency-dependent loads, typically rotating machines, are clearly observable in a large-scale power system. Together with synchronous generators, they provide an additional damping effect on frequency variations. A frequency-dependent model is given by:

$$P_L^f - P_L^{f_0} = \Delta P_L = K_L \Delta\omega + H_L \frac{d\omega}{dt} \tag{11}$$

where P_L^f refers to the real-time loading, $P_L^{f_0}$ refers to the nominal loading, ΔP_L refers to the loading changes and H_L refers to the inertia of rotating masses. In the s-domain (10) can be transferred to (12):

$$\Delta P_L = K_L \Delta\omega + H_L \mathrm{s} \Delta\omega \tag{12}$$

The dynamic model of a complete power system is derived as shown in Figure 3.8, which illustrates the importance of inertias of both generation and load in determining the power system dynamics.

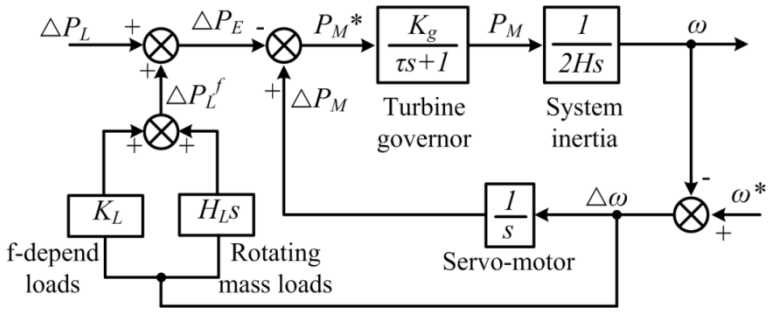

Figure 3.8 Simplified model of a power system

3.5 Study of Interactions between Renewable Energy Source Converters and Onshore Power Systems

3.5.1 Impacts of renewables and HVDC systems on system stability

Fluctuations in large amount of integrated wind power generations can cause the system to which they are connected to experience substantial frequency swings. As shown in Figure 3.9 of British grid frequency response, a short-term imbalance of system energy caused by an instant power loss of 1000 MW generation will result an instant drop in network frequency. During the first 10 sec, generators' inertias arrest the frequency from dropping to unacceptable levels (according to the GB grid code the minimum allowable frequency is 47 Hz [10], however frequencies in excess of this (but less than 50 Hz) may still have a detrimental effect on generators' dynamics. For longer-term recovery, as shown in the post-10-sec frequency of [12], a substantial level of energy reserve should be scheduled in the system to respond and ensure a return to nominal frequency. The reserve can be composed of dynamic responsive generation (spinning reserve) and non-generation measures (demand side management). The primary frequency response is delivered at approximately 10s and is normally maintained for at least a further 20 seconds, and the secondary frequency response is delivered subsequent to primary time scales to raise the grid frequency to the nominal value 50 Hz – this can be required for times of up to 30 min after an event [12].

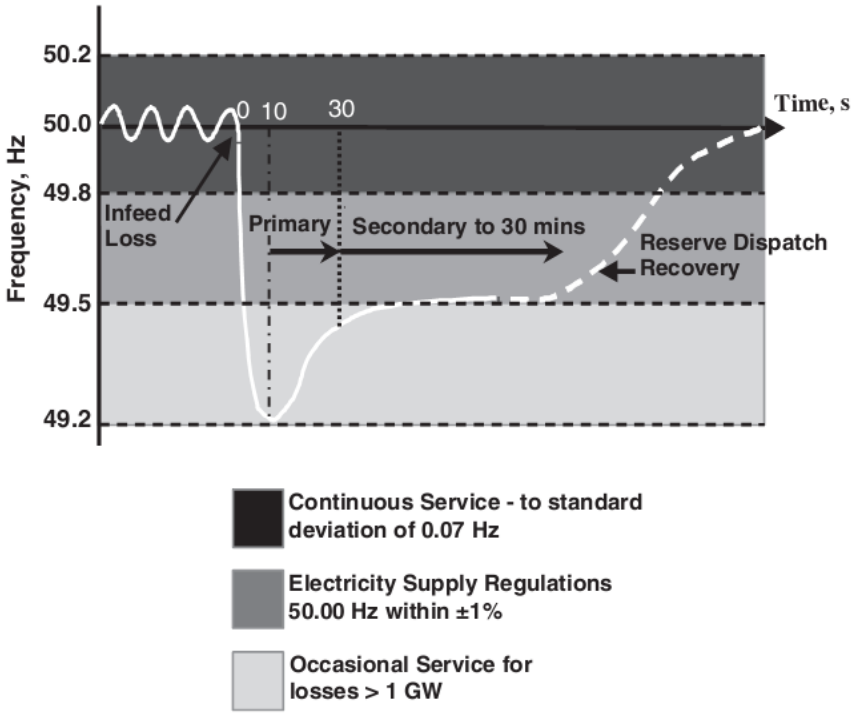

Figure 3.9 Frequency response on the UK grid [12]

The concerns with increasing connections of wind generation with little or no inertial response contribution are that they will act to reduce values of the system aggregate inertia. However, in order to facilitate renewable generation connections and cater for larger capacity units and installations, the UK transmission system operators are devoted to raise the power in-feed loss limit (e.g. the amount of generation can be lost in a single event without causing undue system disturbances) from 1320 MW to 1800 MW by 2014 [11]. With such an increased power in-feed loss limit, if a large power plant trips, the system frequency is at greater risk of falling to an unacceptable level before frequency response control systems can mitigate the situation.

Moreover, the reduced controllability and uncertainty of wind power generations plus the unpredicted variations in future system power demand will also bring challenges to power system operations for load and generation balancing. In the future it may be compulsory for offshore wind farms to provide frequency support and participate in frequency response by their active power output control. For this reason, many European nations have adopted grid code requirements which specify offshore wind farm to provide not only frequency control but also voltage control and fault ride-through capability [5]. Along with the requirements, various control strategies aiming to

enable converters used for renewable power generations and transmissions are proposed and studied in [13]-[21], which will be demonstrated in next subsections.

3.5.2 Frequency support from wind power generators

Several control strategies for variable-speed wind power generators (WPG) and their HVDC connections to the AC grid(s), that can provide both inertial and primary frequency response functions have been proposed [13]-[21]. For the provision of an inertial response from WPGs, a sharp reduction in the speed of the rotating masses (i.e. the generator rotor and turbine blades) is normally activated by increasing the electrical torque in order to release the kinetic energy stored in the rotating masses, which acts to support and arrest the grid frequency drop. However, this requires an additional control loop which dictates the magnitude of turbine electrical torque or power output according to the level of grid frequency deviation, as illustrated in Figure 3.10.

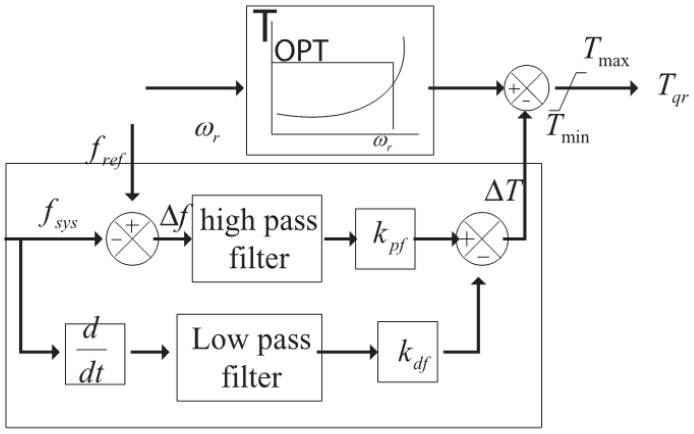

Figure 3.10 Wind turbine torque control with inertial and primary frequency response [13]

The WPG can virtually contribute to providing a grid **inertial response**. This is designed by designating a virtual inertia time constant H_{WPG} to the WPG to determine the amount of WPG electrical energy provided to the grid, as defined by differential gain k_{df} of the artificial control loop as illustrated in Figure 3.10:

$$\Delta T_{E1} = H_{WPG} \cdot \frac{df_{sys}}{dt} = k_{df} \cdot \frac{df_{sys}}{dt} \tag{13}$$

where ΔT_{E1} refers to the electrical torque change that defines the inertial response from the WPG, H_{WPG} refers to the turbine inertia time constant, and f_{sys} is the real-time system frequency.

Provision of inertial contribution by WPGs is proposed to significantly improve system frequency regulation. However, there are also adverse consequences, as wind turbines may stall if too much kinetic energy is trapped from the rotating masses. Furthermore, their power output after the provision of the initial inertial response may reduce due to the reduction in speed of the turbines and generators – in a realistic situation this could exacerbate the overall effects of the initial event (e.g. loss of a major generator) on the entire power system, perhaps negating any benefits offered by the initial inertial response.

The other control loop in parallel with the inertial control loop, as shown in Figure 3.10, is defined by the proportional gain of k_{pf} as shown in (14). This loop is required to provide the primary frequency response by constantly providing a torque offset as long as there is a frequency deviation.

$$\Delta T_{E2} = k_{pf} \cdot (f_{ref} - f_{sys}) \tag{14}$$

where ΔT_{E2} refers to the electrical torque contributing to the primary frequency response from the WPG and f_{ref} refers to the system nominal frequency.

A primary frequency response involves a linear variation of generated active power with grid frequency. The concerns with provision of **primary frequency response** from WPG are how long this incremental power for primary frequency response can be sustained. Additional adequate power reserve must be attainable from effectively reducing the "normal" power output from the WPGs; otherwise the rotor speed will reach the maximum limit due to a persistent difference between the electrical power required and the available mechanical power. Therefore, to provide such a primary frequency response, a power reserve is required for the WPGs in the wind farm. The control strategies proposed by others can be viewed as being divided into two distinct categories in terms of the control approaches adopted:

i. **Speed-controlled de-loaded mode**[14][15]:

This is a control strategy that allows a WPG to operate at active power outputs lower (or higher) than its nominal value by modifying the operational active power-rotor speed curve as far as possible, as long as the speed limit is not exceeded. The resultant active power reserve for inertial and frequency response can be delivered by decreasing the WPG rotor speed to support grid frequency drop through converter control, using the available reserve power form operating the turbine at less than maximum output.

Speed-controlled de-loaded mode is based on varying the *P-ω* curve as a function of grid frequency, as shown in Figure 3.11 and Figure 3.12. By shifting the optimal *P-ω* curve to the right at increased rotor speeds, the WPG is not operated at optimal speed at grid steady state in order to provide additional power support at grid frequency deviation for primary frequency response. As described in [16], the power reference P_{ref} can be defined as:

$$P_{ref} = P_1 + \frac{P_0 - P_1}{\omega_{r1} - \omega_{r0}}(\omega_{r1} - \omega_r) \tag{15}$$

where P_0 and P_1 refer to the maximum and de-loaded active powers for a given wind speed, respectively, and ω_{r0}, ω_{r1} and ω_r refer to the minimum, maximum and real-time WPG rotor speed.

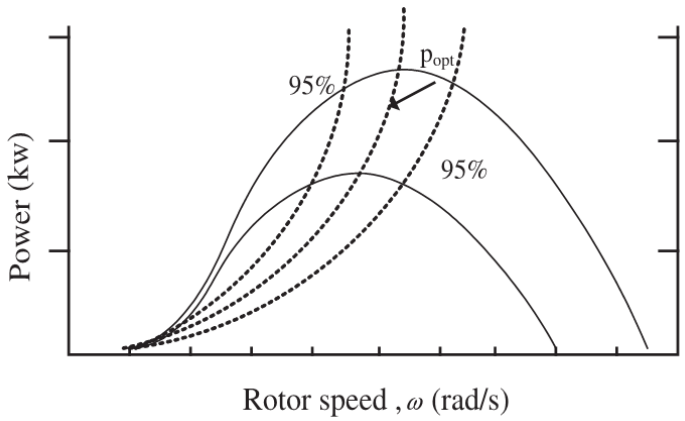

Figure 3.11 95% optimal power speed-controlled de-loaded mode [16]

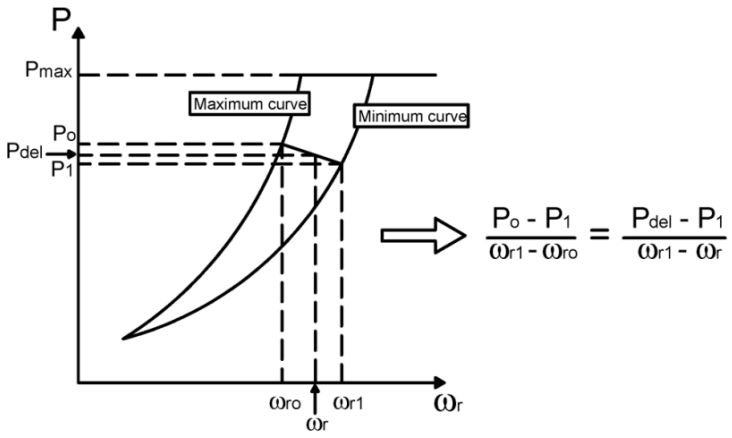

Figure 3.12 Schematic diagram of de-loaded active power curve [16]

The amount of active power defined by P_0-P_1 is the power reserve of the WPG for primary frequency support, whereas the kinetic energy released by moving the rotor speed from the higher speed ω_r to the lower speed ω_{r0} corresponding to optimal active power is available for inertial contribution to the grid.

ii. **Pitch-controlled de-loaded mode**[16][17]:

This is a control strategy where the WPG operates at active power outputs lower than its nominal value by controlling the pitch angle while keeping the rotor speed at optimal value. The resultant active power reserve for inertial and primary frequency response can be delivered by decreasing pitch angles to support grid frequency drops through pitch control.

Pitch-controlled de-loaded mode for WPG is designed in a similar fashion to a turbine governor of a synchronous generator [13], which provides the relatively long-term frequency response capability. The pitch control limits the active power output from the WPG to a level below its optimal value by adjusting the turbine speed, similar to the speed-controlled de-loaded mode. As system frequency drops, the active power reserve can be delivered by modifying the blade angle through the pitch control.

Ideally, the approaches described above can be employed to provide superior performance for WPG primary frequency response [16][17]. The resultant operational de-loaded characteristics of WPGs with services of inertial and primary frequency responses as shown in Figure 3.13 are alike for both speed-controlled de-loaded mode and pitch-control de-loaded mode, where the maximum turbine *P-ω* operating point curve at specific wind speeds is shifted from the optimal point A to point F (de-loaded –

to the right side of the figure) for cases where the wind speed is the same. During a grid frequency drop, the operating speed moves along the trace through points F>E>D>A>B>C. The slashed region as shown in Figure 3.13 is the inertial energy provided by the WPG during the operating point change, whereas the long-term power output reserve delivered by the two modes is the contribution of the WPG to grid primary frequency regulation.

The disadvantages of these two modes commonly include non-maximum power extraction of the WPG and the risk that excessive active power provided by the WPG for such services may exceed the power electronics converter ratings. For speed-controlled de-loaded mode, there is also another concern with the WPG operating speed exceeding the limit. As wind turbine generators are operated at levels of power output below the maximum power for specific wind speed, this may lead to reduced power efficiencies, incomplete utilisation of the existing assets and consequently a longer term of returning the investment in the WPG and wind farm – although system operators may pay for the provision/availability of inertial and frequency response.

3.5.3 Frequency support from HVDC transmission systems

The contributions of inertial and primary frequency response from HVDC systems integrating offshore wind farms are investigated in [19]-[21]. [19] presents a coordinated control method which enables offshore wind farms with line-commutating-converter based (LCC) based HVDC to provide inertial response and primary frequency control. The philosophy is based around sensing and feeding back grid frequency and the derivative of grid frequency to adjust the delivered power from the HVDC link using the rectifier controller and employing communications. When the grid frequency deviates from its nominal value, the active power flow through the HVDC link will be changed. In turn, the wind generation will adjust the blade angle to change the captured wind power through pitch control. [19] demonstrates the effectiveness of such a control strategy in reacting to load changes on the AC system by provision of both inertial response and primary frequency control, effectively reducing the deviation of the system frequency in response to events.

[20] investigates the support of frequency regulation (and power oscillation damping) from VSC-HVDC links used for wind farm integration. To achieve this goal, de-loading of the wind farm output power (as described for other techniques) is required, which can

be achieved by shifting the curve of maximum power point tracking (MPPT) towards the right (or left) using pitch control, as illustrated in Figure 3.13. When there is a frequency change in the power system, the grid side VSC will send out a signal to the wind farm via communications. The wind farm will then switch control mode from the MPPT curve to a de-loaded mode according to the frequency behaviour on the grid (shifting to the left to release reserve power in response to a frequency decrease, shifting to the right for frequency increase, to reduce wind farm power output, as shown in Figure 3.13). In this way, the generator electromagnetic torque will be changed with respect to the mechanical torque and the generator speed will be consequently modified to exchange the kinetic energy of the rotating masses with the power system. The disadvantage of this control strategy is that wind turbines are not always operating at the maximum power exporting point in order to reserve the power for frequency response. The simulation studies presented by the researchers validate the proposed control strategy and prove that VSC-HVDC with such a control strategy can reduce frequency deviations and improve the power system stability.

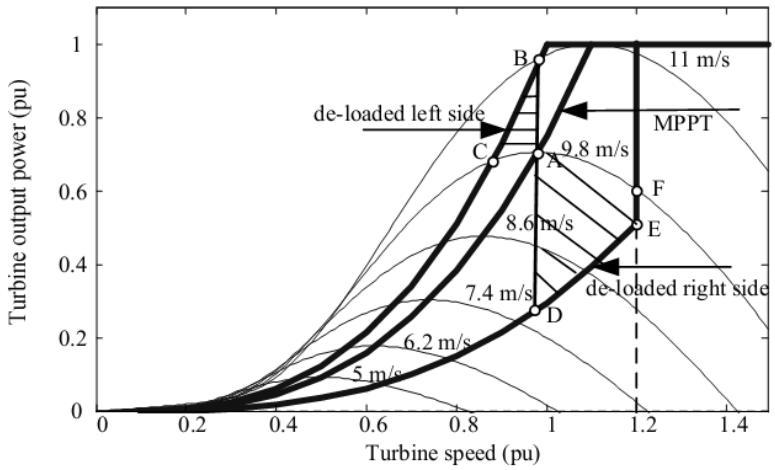

Figure 3.13 De-loaded characteristics for DFIG wind turbine[20]

In contract with the strategy presented in [20], which uses communications, [21] proposes a communications-free control strategy for multi-terminal VSC-HVDC (MTDC) to provide inertia emulation and primary frequency control from connected offshore wind farms. The DC voltage level of the HVDC network, which is regulated to vary along with grid frequency, acts as a physical indicator for the amount of power which the offshore wind farm should strive to provide. The DC voltage reference for onshore converters is generated in real time as follows:

$$U_{DC}^{*} = U_{DC}^{0} - k_{fv} \cdot f_{grid} \tag{16}$$

where U_{DC}* is the DC voltage reference, U_{DC0} is the nominal DC voltage, k_{fv} is the specified frequency/DC voltage droop constant and f_{grid} is the measured grid voltage.

For the control of the offshore converter, the strategy presented in [21] directly links the offshore power system frequency, which is regulated by the offshore HVDC converters, with the DC voltage level in the MTDC network, as shown in Figure 3.14 using DC voltage/offshore frequency droop. The additional control loops, similar to those presented in Figure 3.10 and [13], are implemented within the conventional control system of WPGs. The WPGs of the wind farms also operate at a de-loaded mode to ensure that power is held in reserve to provide the required service.

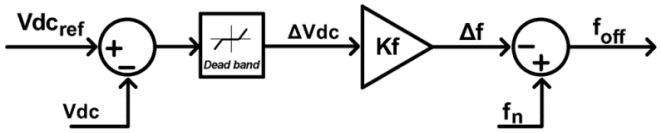

Figure 3.14 Droop control for the converter controlling offshore frequency [21]

In conclusion, with respect to inertia emulation and primary frequency response for HVDC connected offshore wind farms; HVDC transmission systems decouple the offshore wind power systems from the onshore grids. However, control strategies can be used to enable provision of inertia and frequency response services. Disadvantages of these strategies are similar to those associated with directly connected WPGs, such as reduced efficiency of electrical power production by the WPGs, increased risks of stalling WPGs due to excessive extraction of kinetic inertia during and following grid disturbances. These issues are important and must be addressed properly before being implemented in practice. To tackle these potential issues and reduce the potential for risk, this thesis proposes a distinctive inertia emulation control strategy purely using the DC side capacitor as the energy storage element, and this is demonstrated in Chapter 5.

3.5.4 Frequency support from energy storage, static Var compensator (SVC) and load shedding technologies

[22] studies the provision of dynamic frequency control support using ultra-capacitor banks for energy storage and shows that fast-acting storage can mitigate the impact of reduced system inertia on the dynamic performance of the studied "renewable dense"

power system in the case of a major generation outage. However, as the authors state in [22], many other aspects regarding the integration of renewables in power systems, such as variability and forecast accuracy, must be carefully studied before the frequency control support provided by energy storage can be viewed as a viable option.

[23] demonstrates a novel application of STATCOM with dynamic energy storage (in the form of a battery) as an add-on which is used for the purpose of frequency regulation. The schematic is shown in Figure 3.15. Although the simulations prove that battery energy storage is an effective means of providing primary frequency regulation, it is believed that the battery energy storage device may require large capital investment and there may be also other investments required to enhance the interfacing VSCs and maintain the life cycle of the implemented battery storage devices due to frequent charging and discharging of the batteries.

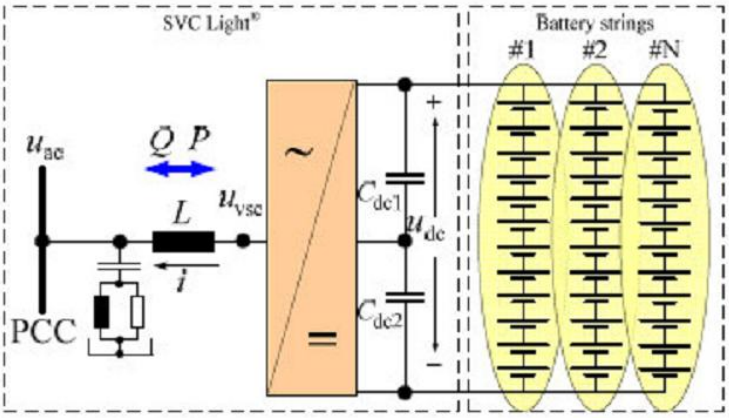

Figure 3.15 Schematic layout of STATCOM with energy storage [23]

In general, load shedding can be defined that as the amount of load that must be removed instantly from the grid to keep the frequency stable and the system operational. This can be illustrated by the blue curves in Figure 3.16. [24] compares two load shedding schemes with different speeds of response. With a faster response speed, as shown in the red line on Figure 3.16, the network frequency picks up more quickly to return to its nominal value. Various papers [24]-[26] have verified the effectiveness of load shedding techniques in assisting in the regulation of grid frequency, and it is believed that the research challenges are mainly centred upon the response speeds, and exactly when and how much capacity of load should be removed from the system. Of course, removing load from the system is generally undesirable, and load shedding schemes (of non-essential loads) can only have limited applicability.

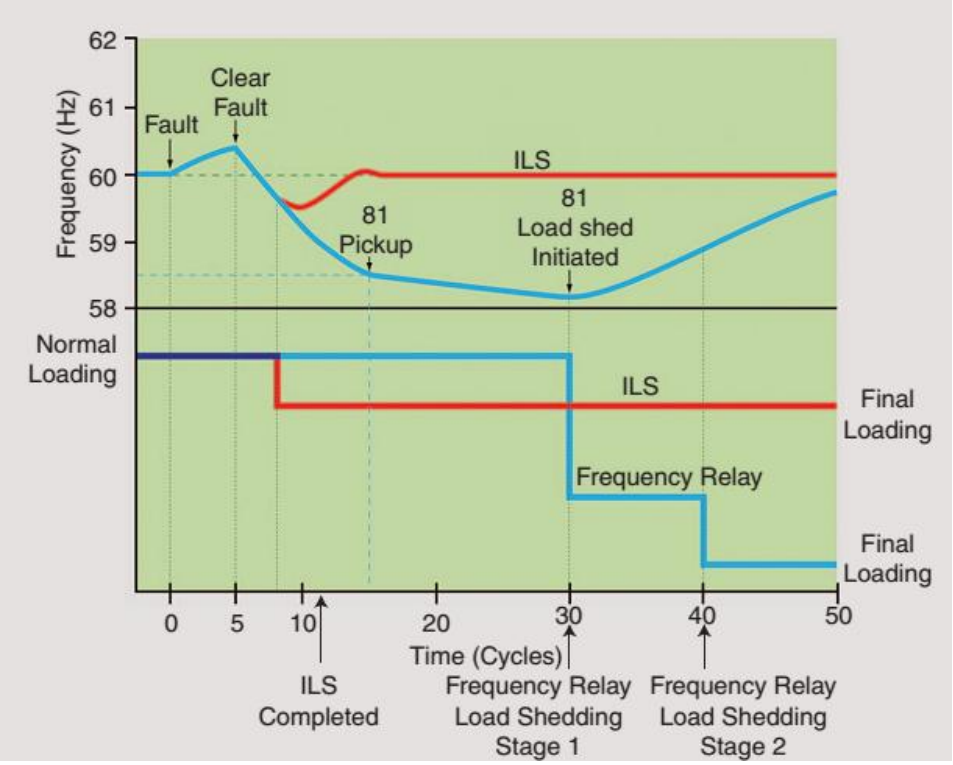

Figure 3.16 Load shedding schemes[24]

3.6 Research on Enhanced VSC Control Strategies

The applications of VSC based FACTS (Flexible AC Transmission Technology Systems) and HVDC technologies will continue to be implemented for improved power transmission system control and operation. These applications allow more efficient utilisation of existing transmission assets and facilitate existing power system to expand. The wide-range of VSC applications leads to numerous electrical benefits to power systems, from increased transmission capability at minimum cost to enhanced reliability through proven performance, from high-level security by means of sophisticated control and protection to improved system controllability with state-of-art technology [27]. They are summarised as follows:

- Continuous operation, compensation, and control to provide reactive power requirements and voltage control;
- Rapid and continuous response characteristics for enhanced dynamic control;
- Independent and automated control of active and reactive power transfer/production/consumption;

- Superior performance (e.g. black-start capability, voltage support, etc.) for weak system conditions with low short-circuit ratios;
- Advanced control methodologies for high-performance operation;
- Elimination or reduced requirements for harmonic filtering;
- Ability to add energy storage as the an energy source/sink (e.g. batteries, super-capacitors, flywheels, etc.);
- Additional functions such as damping of sub-synchronous and torsional power oscillations, unified power flow controllers, interconnection of independent but "weak" power systems, etc.

Regarding the connection methods of VSCs, three types of connections can be identified:

- Series connection of the VSC converter and the AC-system;
- Parallel/shunt connection of the VSC converter and the AC-system;
- Asynchronous infeed from the VSC converter into the AC-system.

With respect to power system issues to which a VSC is exposed, there are two major categories:

- Reactive power: influences voltage amplitude stability;
- Active power: influences voltage angle/ rotor angle stability.

As this dissertation focuses on HVDC transmission technology, and for completeness, this subsection highlights the system advantages of VSC-HVDC design concepts in accordance with the identified categories listed above.

3.6.1 Voltage support using VSC-HVDC systems

As demonstrated in the previous chapter, the phase reactor is important for independent active and reactive power control. The degree of reactive power flow is directly reflected to the voltage amplitude drop across the phase reactor and transformer,

as depicted in (17) which is commonly used to estimate the voltage drop across transmission and distribution lines according to active and reactive power flow:

$$\Delta v = |v_{conv}| - |v_{pcc}| = (R + jX)\frac{P - jQ}{v_{pcc}} = \frac{R \cdot P + X \cdot Q}{v_{pcc}} + j\frac{X \cdot P - R \cdot Q}{v_{pcc}} \approx \frac{R \cdot P + X \cdot Q}{v_{pcc}} \quad (17)$$

where $|v_{conv}|$ and $|v_{pcc}|$ are the converter end and PCC end voltage amplitudes respectively, X and R are the combined inductance and resistance of the phase reactor and transformer, P and Q are the active power and reactive power flow from the converter.

Normally the phase reactor and transformer tends to be sized relatively small, this results in a small imaginary component within equation (17), which can be neglected without significant loss of accuracy. For the phase reactor and transformer of a VSC-HVDC system, X>>R. Therefore (17) can be simplified to (18):

$$\Delta v \approx \frac{X \cdot Q}{v_{pcc}} \quad (18)$$

From (18) it can be deduced that, in order to provide voltage support, the reactive power generated by the VSC should be effectively controlled. [29]-[31] investigates the voltage support capability of VSC-HVDC systems in a number of different contexts.

[29] analyses the voltage stability of an AC network with a hybrid multi-infeed HVDC system. An AC voltage adjusting method is introduced, and simulations are carried out and verified using an RTDS (Real-Time Digital Simulator). It is shown that the proposed control method for VSCs improves the transient AC voltage stability by modulating the reactive power; however the VSC capability of exchanging reactive power in order to provide AC voltage support is not discussed or quantitatively studied in combination with its active power capability. In certain cases, if the VSC active power exchange is set to possess a higher priority than its reactive power exchange, it is likely that the VSC AC voltage support capability may be inhibited during severe network events (e.g. three-phase fault) which result in extreme AC voltage dips.

[30] presents analyses and comparisons between an AC line scenario and a VSC-HVDC link scenario when increasing the levels of power transmitted in the "Nordic

32A" test power system. Simulation results showed that, from an AC voltage support perspective, VSC-HVDC notably improves the stability of the system compared to the AC line connection. Voltage stability was greatly enhanced and the risk of system collapse due to lack of reactive power was shown to be mitigated. VSC-HVDC also facilitates reduced levels of stress in the excitation systems of generators and thereby can increase the stability margin of the machines. However, although the proposed control system for the VSC-HVDC link employs both active and reactive power damping to the grid as a key element of the strategy, it does not identify the priorities for the active and reactive power damping according to the circumstances of the connected power systems. The choice for active power damping priority is believed suitable for a power system where a VSC-HVDC link is connected as a tie line for two relatively "independent" areas. The choice for reactive power damping priority is believed suitable for a power system which lacks local Var compensation (e.g. does not possess generator automatic Var regulators) at the VSC's point of connection. There is also another choice for equal priority of active and reactive power damping which is proposed as being suitable for combination of both of the connection contexts described above.

[31] confirms the benefits of the ability of VSC-HVDC to provide voltage support through simulations which demonstrate that the power through a back-to-back asynchronous AC line can be increased by a factor of 1.68 when a VSC-HVDC system with AC voltage support replaces the AC line at the mid-point. However, more studies on the numerical ratio of the degree of voltage support that the VSC can provide through incremental reactive power output are required. Through this, the capability of voltage support can be specified for any VSC converter in per unit quantities and the capability can be further related to the increased power transfer across an AC grid that will be possible as a consequence of the VSC voltage support function.

3.6.2 Voltage angle oscillation damping using VSC-HVDC systems

Voltage angle oscillations can be damped effectively through modulation of VSC-HVDC output active power. The increasing numbers of HVDC links in modern power systems have led to interests in the ability to provide power oscillation damping (POD), as studied in [32]-[36]. These strategies all use power grid frequency as an indicator and guide for the required level of active power modulation. The basic principle is described as follows:

$$\Delta P = -K_{dmp}(\omega - \omega_{nom}) \tag{19}$$

where ΔP is the damping power provided by the HVDC terminal, K_{dmp} is the damping gain, ω and ω_{nom} are instantaneous and nominal network angular speed respectively.

[32] proposes a POD strategy for VSC-HVDC systems to use not only local grid frequency but remote frequency information for damping power oscillations, using a comparison of the frequency measurements. It also investigates the impact of HVDC converter locations on the POD functionality. With this POD, the VSC-HVDC can acto to increase the stability margins within the power system. This type of POD is described as:

$$\Delta P_i = -K_{dmp}(\omega_i - \omega_j) \tag{20}$$

where ΔP_i is the damping power provided by the HVDC terminal connection node i, ωi and ω_j are the network angular speeds at the HVDC connection node i and at the remote node j respectively.

[33] presents a new POD design for VSC-HVDC systems using a method called multi input single output Modal Linear Quadratic Gaussian, and shows that it can provide improved damping of power oscillations when compared to a power system stabiliser (PSS) based POD. It also demonstrates the robustness of this POD under a variety of operating conditions.

[34] and [35] describe the implementation of VSC stations with damping strategies, where the real power is proportional to frequency and reactive power is proportional to the rate of change of voltage, using the "Energy Function Method", which mathematically identifies the conditions for increasing the damping of a stable power system. It found that a combination of real and reactive power modulation yield the best provision of damping and the ability to damp through provision of real power becomes stronger when the VSC stations are located closer to the generators in the power system.

[36] investigates the issues associated with how best to coordinate the control actions at the two ends of a DC link without using a centralised control scheme in order to allow VSC-HVDC converter to perform power damping, which requires fast communication of control signals to remote converters. A fully centralised controller may result in a closed-loop performance worse than that of an open loop system in the event of the loss

of communicated feedback signal(s). Alternatively, with a block-diagonal control structure as presented in [36], the individual control loops are decoupled from each other, which is not only easier to implement in a decentralised fashion, but also acts to guarantee a certain level of performance as presented via simulations in [36]. It is shown in Chapter 5 that a localised control strategy for one VSC of the HVDC link (the inertia emulation control strategy), which is entirely independent from the other VSC, can avoid the aforementioned issue associated with loss of communications.

Rather than designing a POD controller, [37] proposes a power-synchronisation control strategy for VSC-HVDC systems, utilising the inherent synchronisation mechanism in AC systems. In principle, this is similar to the operation of a synchronous generator. The proposed power-synchronisation controller enables the active power control loop to integrate its errors to the phase angle increment of the PLL, which is used to perform Park and inverse-Park transforms. As verified in simulations in [37], the VSC avoids instability caused by a standard phase-locked loop in a weak AC-system connection, and can provide improved voltage support in a manner similar to that provided by a traditional synchronous machine.

In contrast with [37], [38] proposes a control strategy to enable VSC-HVDC systems to have the ability to provide damping power by incorporating a control loop which virtually mimics the application of static synchronous series compensation (SSSC). The power output using the proposed technique is actually another form of synchronising power provision by VSC-HVDC, but with a different behaviour. It is verified by simulations that VSC-HVDC systems with such a control support the recovery from fault disturbances and shorten the time taken to return to steady state conditions.

3.6.3 VSC-HVDC to correct unbalance in the AC systems

AC power systems normally operate under balanced three-phase AC voltage conditions. However, occasionally, unbalanced conditions may occur, for example, due to single-phase-to-earth faults, phase-to-phase faults, etc. During unbalanced grid supply voltage conditions, the corrective action of VSC-HVDC converters can be exploited in order to mitigate unbalanced voltage propagations and provide balanced three-phase supplies to loads on the AC system.

Conventional control, adopting only positive-sequence current transformations, is based on the assumption that three-phase AC voltages are balanced, so that an accurate control of P&Q can be achieved. With an unbalanced grid voltage, the ability to accurately control P&Q will be lost and there will be more DC voltage oscillations as illustrated in Figure 3.17. Two criteria should be fulfilled for VSC-HVDC systems during unbalanced voltage conditions [39]:

- DC voltage should not be significantly varied, in order not to trip the DC side protection;
- VSC-HVDC converters should be capable of improving the unbalanced voltage between each "side" of the HVDC.

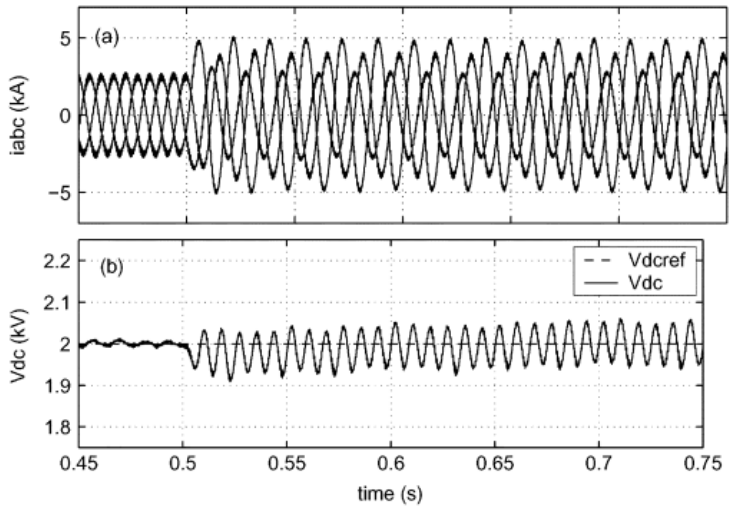

Figure 3.17 VSC Conventional control (positive-sequence only) (a) VSC unbalanced current; (b) VSC DC ripples [41]

Studies of VSC-HVDC operation during unbalanced grid voltage are presented in [39]-[41] and they all propose a dual controller which consists of two separate positive-sequence PI current control loop and negative-sequence PI current control loop in parallel, as illustrated in Figure 3.18. Consequently two synchronous reference frames are used to control the VSC positive-sequence and negative-sequence currents independently. As the grid voltage unbalance (e.g. single phase to earth fault) tends to result VSC unbalanced AC current waveforms or DC voltage ripples, the dual controller can have two different functional options, which are studied in [41]:

- **Option 1:** Enable VSC to output "unbalanced" three-phase current;
- **Option 2:** Enable VSC to get rid of DC voltage ripple.

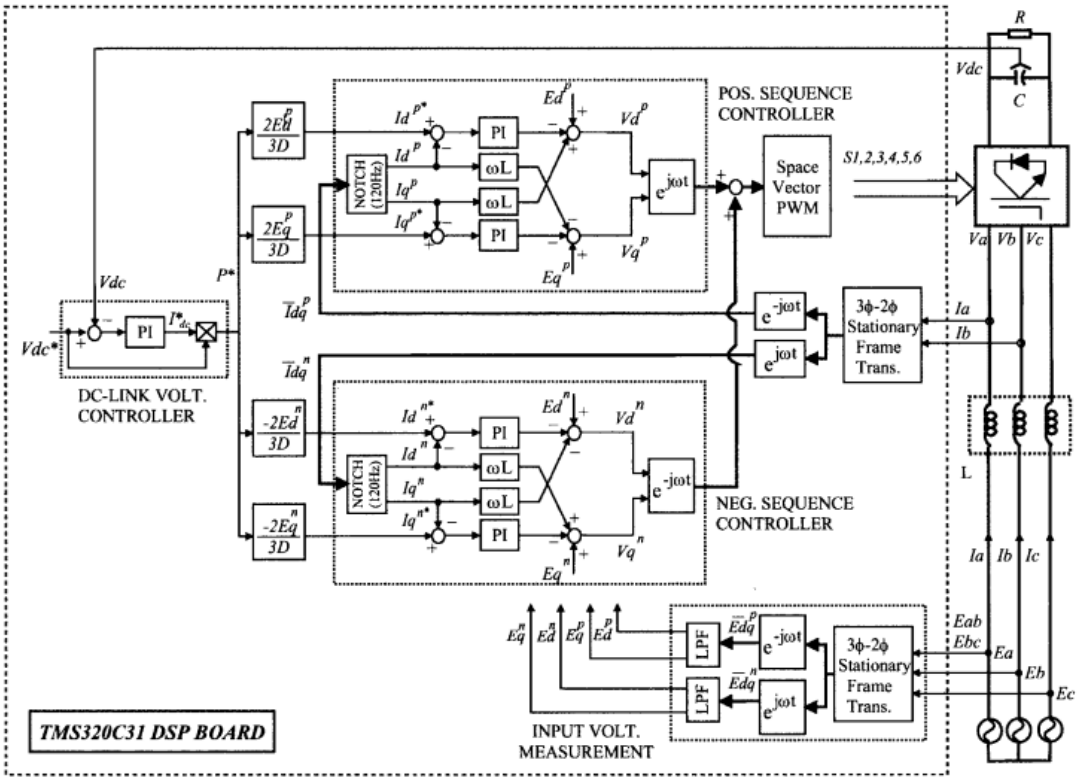

Figure 3.18 A VSC "dual" controller for unbalanced grid voltage, with a main positive-sequence and a compensating negative-sequence loop [40]

The control strategy option 1 which enables a three-phase balanced current under grid voltage unbalance is to eliminate the negative-sequence i_d^n and i_q^n by regulating their references i_d^{n*} and i_q^{n*} to be zero in the negative-sequence loop. As shown in Figure 3.19, with this control strategy the output three-phase current from VSC is perfectly balanced, in expense of small DC voltage ripples.

The control strategy option 2 which gets rid of the DC voltage ripple under grid voltage unbalance is to force active power P and reactive power Q to be zero by regulating the negative-sequence idn and iqn. As shown in Figure 3.20, with this control strategy the DC voltage ripple is much reduced compared to control strategy option 2, although there is slightly unbalanced output current.

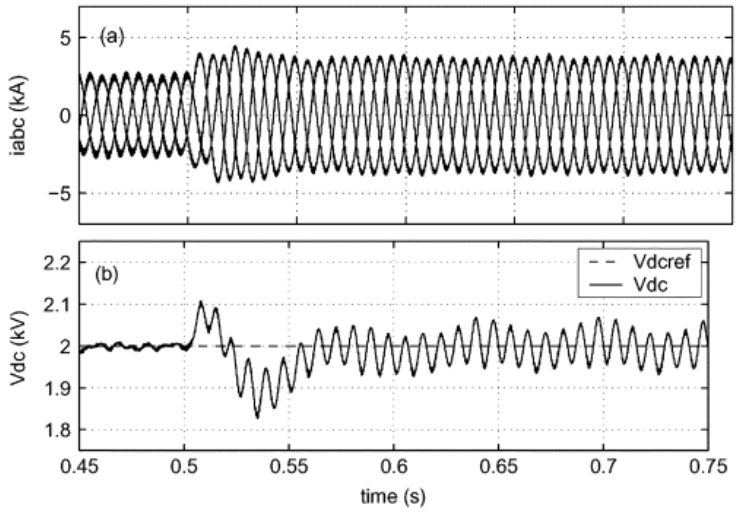

Figure 3.19 The VSC dual controller with target of outputting balanced three-phase current (option 1) [41]

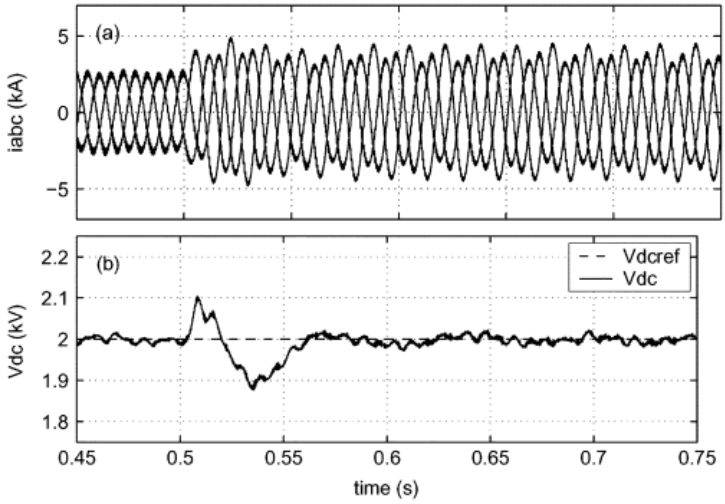

Figure 3.20 The VSC dual controller with target of reducing DC voltage ripples (option 2) [41]

3.7 Summary

In this chapter, a literature review relating to the work of others on the integration and control of large scale renewable generation connected via VSC-HVDC transmission technologies to traditional AC power systems has been presented. Firstly, the power system challenges associated with wind power development have been demonstrated in terms of transmission system interconnection options and the potential impacts on the system from increased wind penetration. Secondly, a dynamic model of power system frequency has been introduced with focus on the generators' inertial responses and the function of primary frequency control: the role of frequency-dependent loads is also described. Thirdly, a number of control strategies based upon provision of "artificial" or "synthetic" inertial responses and on how primary frequency contributions can be provided is reviewed. The reviewed technologies that may contribute such inertial responses include wind power generators, HVDC transmission systems, energy storage, SVCs and fast-acting load shedding schemes. Finally, a number of other applications of VSC converters to provide support and corrective actions to their connected AC systems are also briefly reviewed.

It is clear from the reviewed work that many researchers are working in the area of multi-terminal DC network operation, control and protection. However, there remains work to be done in ensuring that the integrated AC/DC networks will operate in a secure and stable fashion. The following chapters describe a number of control strategies that have been developed and demonstrated throughout the research reported in this thesis. These strategies help to address issues associated with stability and flexibility of controlling the future offshore multi-terminal network and the AC systems to which it will connect.

References

[1] Salic, G.; Rebours, Y., "Impact of German wind generation forecasts on net transfer capacities", *8th Inter. Conf. on the European Energy Market (EEM)*, 25-27 May 2011.

[2] Bresesti, P.; Kling, W.L.; Hendriks, R.L.; Vailati, R., "HVDC Connection of Offshore Wind Farms to the Transmission System", *IEEE Trans. Energy Convers.*, VOL.22, NO.l, March. 2007.

[3] Siemens report, *High Voltage Transmission Direct Current Transmission – Proven Technology for Power Exchange*. Online Available [assessed on 02/12/2012]: http://www.siemens.com/sustainability/pool/en/environmental-portfolio/products-solutions/power-transmission-distribution/hvdc_proven_technology.pdf

[4] Guo, H.; Rudion, K.; Styczynski, Z.A., "Integration of large offshore wind farms into the power system," *2011 EPU-CRIS Inter. Conf. on Science and Technol.*, vol., no., pp.1-6, 16-16 Nov. 2011.

[5] ENTSO-e, *Network Code on Requirements for Grid Connection applicable to All Generators*. Online Available [assessed on 29/07/2013]: https://www.entsoe.eu/major-projects/network-code-development/requirements-for-generators/

[6] EWEA statistic, *Operational Offshore Wind Farms in Europe*, 2010. Online Available [assessed on 04/12/2012]: http://www.ewea.org/fileadmin/ewea_documents/documents/statistics/110214_public_offshore_wind_farms_in_Europe_2010.pdf

[7] Anderson, P.; Fouad, A.A., *Power System Control and Stability*. Ames, Iowa, U.S.A: The Iowa State University Press, 1977.

[8] Anderson, G., *Dynamics and Control of Electric Power Systems*, Power Systems Laboratory, ETH Zurich, Feb 2011. Online Available [assessed on 01/01/2013]: http://www.eeh.ee.ethz.ch/fileadmin/user_upload/eeh/studies/courses/power_system_dynamics_and_control/Documents/DynamicsPartI_lecture_notes_2012.pdf

[9] Davies, M.; Moran, F.; Bird, J.I., "Power/frequency characteristics of the British grid system," *Proceedings of the IEE - Part A: Power Engineering*, vol.106, no.26, pp.154-162, April 1959.

[10] National Grid Electricity Transmission plc, *The Grid Code, Issue 5 Revision 0 – 17*, Online available [assessed on 05/12/2012]: http://www.nationalgrid.com/uk/electricity/codes/gridcode/gridcodedocs/

[11] GB National Electricity Transmission System Security and Quality of Supply Standard, *Largest Power Infeed Loss Amendment to GSR007 proposals,* Online Available [assessed on 05/12/2012]: http://www.nationalgrid.com/nr/rdonlyres/749c9fd8-1651-4059-8219-564940c4678c/44473/reporttoauthorityfinal.pdf.

[12] Pearmine, R.; Song, Y.H.; Chebbo, A.; Williams, T.G., "Identification of a load frequency characteristic for allocation of spinning reserves on the British electricity grid," *IEE Proc., Gener. Trans. Distr.*, 2006, 153, (6), pp. 633 – 638.

[13] Xue, Y.; Tai, N., "Review of contribution to frequency control through variable speed wind turbine," *ELSEVIER Renewable Energy*, 36 1671-1677, 2011.

[14] Ekanayake, J.; Jenkins, N., "Comparison of the response of doubly fed and fixed-speed induction generator wind turbines to changes in network frequency," *IEEE Trans. Energy Conv.*, vol.19, no.4, pp. 800- 802, Dec. 2004.

[15] Ramtharan, G.; Ekanayake, J.B.; Jenkins, N., "Frequency support from doubly fed induction generator wind turbines," *IET Renewable Power Gen.*, vol.1, no.1, pp.3-9, March 2007.

[16] De Almeida, R.G.; Lopes, J.A.P., "Participation of Doubly Fed Induction Wind Generators in System Frequency Regulation," *IEEE Trans. Power Syst.*, vol.22, no.3, pp.944-950, Aug. 2007.

[17] Kayikci, M.; Milanovic, J.V., "Dynamic Contribution of DFIG-Based Wind Plants to System Frequency Disturbances," *IEEE Trans. Power Syst.*, vol.24, no.2, pp.859-867, May 2009.

[18] Conroy, J.F.; Watson, R., "Frequency Response Capability of Full Converter Wind Turbine Generators in Comparison to Conventional Generation," *IEEE Trans. Power Syst.*, vol.23, no.2, pp.649-656, May 2008.

[19] Miao, Z.; Fan L.; Osborn, D.; Yuvarajan, S., "Wind Farms With HVdc Delivery in Inertial Response and Primary Frequency Control," *IEEE Trans. Energy Convers.*, vol.25, no.4, pp.1171-1178, Dec. 2010.

[20] Wang, Y.; Zhu, X.R.; Xu, L.; Li, H.M., "Contribution of VSC-HVDC connected wind farms to grid frequency regulation and power damping," *IECON 2010 - 36th Annual Conf. on IEEE Ind. Electron. Society*, vol., no., pp.397-402, 7-10 Nov. 2010.

[21] Silva, B.; Moreira, C.L.; Seca, L.; Phulpin, Y.; Lopes, J.A.P., "Provision of Inertial and Primary Frequency Control Services Using Offshore Multiterminal HVDC Networks," *IEEE Trans. Sustainable Energy*, vol.3, no.4, pp.800-808, Oct. 2012.

[22] Delille, G.; Francois, B.; Malarange, G., "Dynamic Frequency Control Support by Energy Storage to Reduce the Impact of Wind and Solar Generation on Isolated Power System's Inertia," *IEEE Trans. Sustainable Energy* , vol.3, no.4, pp.931,939, Oct. 2012.

[23] Holmberg, M.T.; Lahtinen, M.; McDowall, J.; Larsson, T., "SVC Light® with energy storage for frequency regulation," *2010 IEEE Conf. on Innovative Technol. for an Efficient and Reliable Electricity Supply (CITRES)*, vol., no., pp.317, 324, 27-29 Sept. 2010.

[24] Shokooh, F.; Dai, J. J.; Shokooh, S.; Tastet, J.; Castro, H.; Khandelwal, T.; Donner, G., "Intelligent Load Shedding," *IEEE Ind. Appl. Mag.*, vol.17, no.2, pp.44,53, March-April 2011.

[25] Rudez, U.; Mihalic, R., "Monitoring the First Frequency Derivative to Improve Adaptive Under frequency Load-Shedding Schemes," *IEEE Trans. Power Syst.*, vol.26, no.2, pp.839,846, May 2011.

[26] Huang S.J.; Huang C.C., "An automatic load shedding scheme including pumped-storage units," *IEEE Trans. Energy Conv.*, vol.15, no.4, pp.427, 432, Dec 2000.

[27] Reed, G.; Pape, R.; Takeda, M., "Advantages of voltage sourced converter (VSC) based design concepts for FACTS and HVDC-link applications," *2003 IEEE Power Eng. Society General Meeting*, vol.3, no., pp. 4 vol. 2666, 13-17 July 2003.

[28] Zhang, L.; Harnefors, L.; Rey, P., "Power System Reliability and Transfer Capability Improvement by VSC-HVDC," 2007 CIGRÉ Regional Meeting, Tallinn, Estonia.

[29] Liu Y.; Chen, Z., "Transient voltage stability analysis and improvement of a network with different HVDC systems," *2011 IEEE Power and Energy Society General Meeting*, vol., no., pp.1-8, 24-29 July 2011.

[30] Latorre, H.F.; Ghandhari, M., "Improvement of voltage stability by using VSC-HVdc," *2009 Trans. & Dist. Conf. & Expo.: Asia and Pacific*, vol., no., pp.1-4, 26-30 Oct. 2009.

[31] Huang, Z.; Ooi, B.T.; Dessaint, L.-A.; Galiana, F.D., "Exploiting voltage support of voltage-source HVDC," *Proceedings of IEE Gen., Trans. and Dist.*, vol.150, no.2, pp. 252- 256, March 2003.

[32] Latorre, H.F.; Ghandhari, M.; Soder, L., "Use of local and remote information in POD control of a VSC-HVdc,"*2009 IEEE Bucharest Power Technol.*, June 28 2009.

[33] Preece, R.; Almutairi, A.M.; Marjanovic, O.; Milanovic, J.V., "Damping of electromechanical oscillations by VSC-HVDC active power modulation with supplementary wams based modal LQG controller,"*2011 IEEE Power and Energy Society General Meeting*, 24-29 July 2011.

[34] Ruan, S.Y.; Li, G.J.; Ooi, B.T.; Sun, Y.Z., "Power system damping from energy function analysis implemented by voltage-source-converter stations," ELSEVIER Science Direct, 2007.

[35] Ruan, S.Y.; Li, G.J.; Ooi, B.T.; Sun, Y.-Z., "Power system damping from real and reactive power modulations of voltage-source-converter station," *IET Gen., Trans. & Dist.* , vol.2, no.3, pp.311-320, May 2008.

[36] Pipelzadeh, Y.; Chaudhuri, B.; Green, T. C., "Control Coordination Within a VSC HVDC Link for Power Oscillation Damping: A Robust Decentralized Approach Using Homotopy,", IEEE Trans. on Control Systs. Technol., accepted for inclusion in a future issue of the journal.

[37] Zhang L.D.; Harnefors, L.; Nee, H.P., "Power-Synchronization Control of Grid-Connected Voltage-Source Converters," *IEEE Trans Power Systs.*, vol.25, no.2, pp.809-820, May 2010.

[38] Jowder, F.A.Ra.; Ooi, B.T., "VSC-HVDC station with SSSC characteristics," *IEEE Trans. Power Electron.*, vol.19, no.4, pp. 1053- 1059, July 2004.

[39] Xu L.; Andersen, B.R.; Cartwright, P., "Control of VSC transmission systems under unbalanced network conditions," 2003 IEEE PES Trans. and Dist. Conf. and Expo., vol.2, no., pp. 626- 632 vol.2, 7-12 Sept. 2003.

[40] Song, H.S.; Nam, K., "Dual current control scheme for PWM converter under unbalanced input voltage conditions," *IEEE Trans. Ind. Electron.*, vol.46, no.5, pp.953, 959, Oct. 1999.

[41] Yazdani, A.; Iravani, R., "A unified dynamic model and control for the voltage-sourced converter under unbalanced grid conditions," *IEEE Trans. Power Del.*, vol.21, no.3, pp.1620, 1629, July 2006.

[42] Nakajima, T.; Irokawa, S., "A control system for HVDC transmission by voltage sourced converters," *1999 IEEE Power Eng. Soc. Summer Meeting*, vol.2, pp.1113-1119.

[43] Haileselassie, T.M.; Molinas, M.; Undeland T., "Multi-Terminal VSC-HVDC System for Integration of Offshore Wind Farms and Green Electrification of Platforms in the North Sea," *Nordic Workshop on Power and Ind. Electron.*, June 2008.

[44] Zhu, J.; Booth, C., "Future multi-terminal HVDC transmission systems using voltage source converters"*, 2010 45th Inter. Uni. Power Engineering Conf. (UPEC)*, vol., no., pp.1-6, Aug 2010.

[45] Xu, L.; Yao L., "DC voltage control and power dispatch of a multi-terminal HVDC system for integrating large offshore wind farms," *IET Renewable Power Gen.*, vol.5, no.3, pp.223-233. (May 2011)

[46] Whitehouse, R.S.; , "Technical challenges of realising multi-terminal networking with VSC,"*, Proc. 201114th European Conf. on Power Electron. and Appl. (EPE 2011)*, vol., no., pp.1-12, Aug. 30 2011-Sept. 1 2011.

[47] Adam, G.P.; Anaya-Lara, O.; Burt, G., "Multi-terminal DC transmission system based on modular multilevel converter," *Proc.2009 44th Int. Univ. Power Eng. Conf. (UPEC 2009).*

Chapter 4

A novel direct current matching control strategy for MTDC systems

4.1 Introduction

As introduced in Chapter 3, according to the established DC voltage margin and DC voltage droop control strategies, a multi-terminal HVDC (MTDC) transmission system should ideally be operated in a manner where no inter-terminal communication is required. However, as also demonstrated in Chapter 3, without communications, many of the reported control strategies have specific drawbacks, such as exposing the VSC responsible for DC voltage regulation to the risk of over-voltages and over currents – perhaps requiring it to be over-rated at significant cost. Without communications, it can be difficult to provide effective control due to limited knowledge of real-time DC power flows being available. This can result in control being overly complex and challenging due to fast and often unpredictable variations in the controlled system state. To tackle these disadvantages, a real-time communication-based control strategy, termed "Direct Current Matching Control" (DCMC), for MTDC systems has been developed and demonstrated.

This chapter is organised as follows: initially, a detailed control system for the wind farm terminal MTDC converters is designed and introduced. Secondly, to facilitate understanding of the VSC-MTDC system under study, a simplified but representative MTDC network model is presented. Thirdly, using the MTDC model, the dynamic behaviour of the DC voltage within the MTDC system is analysed and an important equation is derived which underpins and defines the operation of the proposed DCMC control strategy. A detailed explanation and demonstration of the DCMC system is then presented, through a step-by-step description of how individual converters' DC currents are estimated, and a description of the mode of operation of the direct current matching mechanism and the grid side converters' controllers. Finally, simulation studies are performed to validate the DCMC and demonstrate the advantages of the scheme in two main aspects: 1) flexibility and security of power dispatch to onshore AC grids; 2) improvement of DC voltage stability under variable levels of wind power generation.

4.2 Test MTDC System with Converter Control Systems

Figure 4.1 presents the MTDC configuration used to test and demonstrate the operation of the DCMC scheme. In this case, three independent wind farms inject power into a ring DC network via wind farm side converters $WVSC_1$, $WVSC_2$ and $WVSC_3$. The

grid side converters $GVSC_1$, $GVSC_2$ and $GVSC_3$ deliver power to AC power systems 1, 2 and 3. While the DC system is of a ring configuration, the DCMC would be applicable to other DC network layouts (e.g. radial configurations).

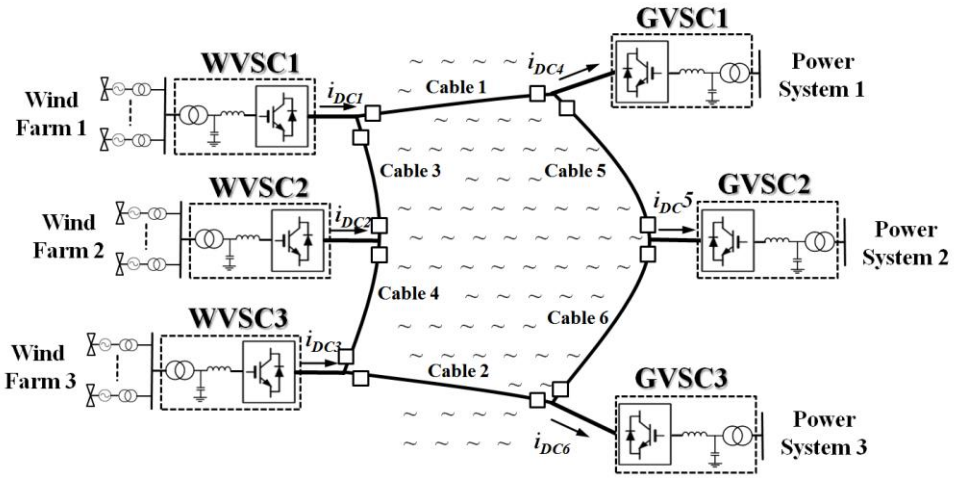

Figure 4.1 MTDC general configuration

4.2.1 Control of Grid side VSCs

As shown on the right hand side of Figure 4.2, the control system for the GVSCs in the MTDC is identical to the controllers that would be used within point-to-point VSC-HVDC converter control. These controllers have already been described in Chapter 2, and the reader is referred to this chapter for more details.

4.2.2 Control of Wind farm side VSCs

A coordinated control strategy between an MTDC wind farm interface converter station and the turbine and other controllers within the wind farm should be expected to facilitate wind power extraction, independent of the particular type of wind turbine generators employed. In [3], grid integration of a doubly-fed-induction-generator-based (DFIG) wind farm using a VSC-HVDC system is studied. The control of the turbines within the wind farm is based on maximum power point tracking (MPPT), which uses wind power versus turbine speed characteristics at different wind speeds to optimise the wind generator control[1]-[3]. A WVSC connected to an HVDC transmission system regulates performance to ensure a constant frequency and voltage amplitude for the AC-side power system to which the wind turbine generators are connected. As long as the frequency and AC voltage amplitude are maintained within limits (ideally constant), the

power generated by the wind farm is automatically absorbed by the WVSC and transferred to the DC link [3].

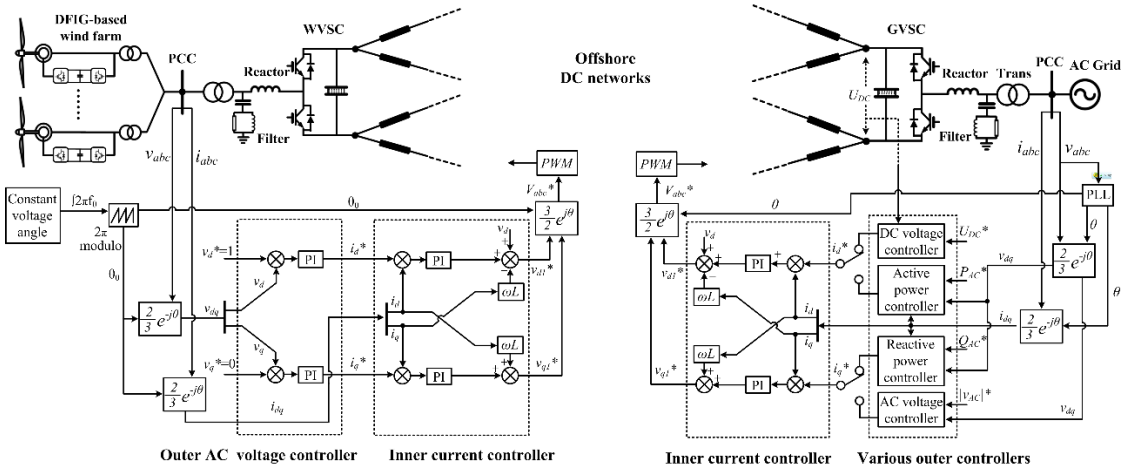

Figure 4.2 Control systems for WVSCs and GVSCs

The WVSC should act as an AC voltage source with a constant frequency for wind farm integration. The control systems for WVSCs proposed in [2]-[4] regulate frequency via a modulation index (M) without the use of inner current controllers. However, the disadvantage associated with this type of control is that the current through the WVSC is not effectively controlled due to the absence of the inner current control, with the possibility of resultant overcurrents which could stress the converter in certain circumstances.

In the research reported in this dissertation, the inner current controller, as employed in the GVSC controllers described in Chapter 2, is employed in order to provide a secure means of current control for WVSC operation. By regulating the AC voltage amplitude component v_d with a target value of 1 pu and the phase angle voltage component v_q with a target of 0, the WVSC can act as a "stiff" voltage source and i_{dq}* for the inner current control is generated. A constant phase angle θ_0 is provided for the Park and Inverse Park transformations by a virtual PLL which uses the grid frequency f_0 (e.g. 50 Hz) as input, as illustrated in Figure 4.2.

4.3 MTDC Network Simplification and Dynamic Analysis of DC Voltage

From the DC side perspective, each VSC can be regarded as a DC current source (whether exporting or importing from the network) [5]. Figure 4.3 presents a simplified network diagram for the six-terminal MTDC system presented in Figure 4.1. Converters $WVSC_1$, $WVSC_2$ and $WVSC_3$ act as input DC current sources i_{DC1}, i_{DC2} and i_{DC3} and converters $GVSC_1$, $GVSC_2$ and $GVSC_3$ act as output DC current sources (or effectively sinks)i_{DC4}, i_{DC5} and i_{DC6}. In this example, $GVSC_2$ is primarily responsible for regulating DC voltage.

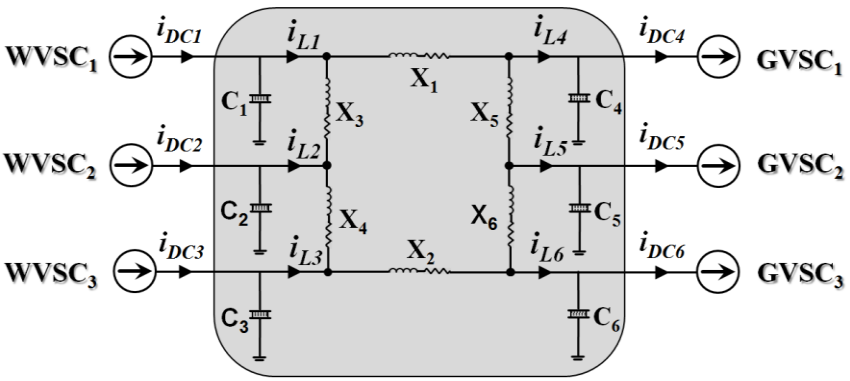

Figure 4.3 Simplified MTDC model

For a typical AC power system, frequency is a dynamic indicator of the power balance between generation and load, whereas for an MTDC system, the indicator is the instantaneous DC network voltage level with respect to some target level [6]. It is important that the DC voltage levels across the capacitors at all nodes in the MTDC system are maintained within limits, as transient DC over-voltage may damage the converter equipment and cables, while under-voltage may affect converter controllability [7].

Due to the relatively small DC cable impedances [9], the overall trend of DC voltage change for all converters is considered to be identical to the DC voltage level at the DC voltage regulating terminal $GVSC_2$. By neglecting the network impedance, the dynamics of the DC circuit can be approximated as expressed in equation (1):

$$NC \cdot \frac{dU_{DC}}{dt} = \sum i_{DCin} - \sum i_{DCout} \quad (1)$$

where $\sum i_{DCin}$ and $\sum i_{DCout}$ are the total input and output DC currents respectively.

The hypothesis underpinning the developed control strategy reported in this chapter is that the function of the DC voltage regulating terminal $GVSC_2$ (in terms of dealing with power mismatches in MTDC systems) can be improved by instantaneous matching of the input DC currents provided by the WVSCs with the output DC currents of the other two output converters $GVSC_1$ and $GVSC_3$. The scheme acts to reduce the total DC current mismatch in equation (1) for DC voltage regulating converter by "sharing" temporary DC current mismatch with the other two GVSCs. Using this technique, higher levels of DC voltage stability can be obtained.

4.4 Design of the Proposed DCMC Strategy

Wide-area (WA) control systems [11][12], and Supervisory Control and Data Acquisition (SCADA) systems [13]-[15] have been proposed for enhanced monitoring and operation of power systems in many areas, but not for MTDC system application. If MTDC control systems utilise such communication technologies, the aforementioned issues associated with DC voltage variations and power dispatch to the connected AC systems may be resolved. This section details the operation of the proposed DCMC scheme, with its operation being underpinned by a WA-SCADA system. The proposed control strategy also incorporates coordinated control capability, which accurately matches the DC current outputs of grid side VSCs (GVSC) with the cumulative current inputs of all wind side VSCs (WVSC), for improved power dispatch and DC voltage stability when compared to other strategies proposed in the literature. The operation of the scheme under loss of communications facilities is also described, as this of course must also be considered and catered for in any practically realisable system.

The proposed WA-SCADA based DCMC strategy continually estimates the total cumulative DC current injection being provided by all of the WVSCs and then matches this to the cumulative output of the GVSCs for the six-terminal MTDC system as illustrated in Figure 4.1. In addition, it uses configurable sharing factors to dispatch the power into the various AC grids (or individual injection points within a single grid) according to schedules set by system operators for $GVSC_1$ and $GVSC_3$, with $GVSC_2$

acting as a DC voltage regulating converter to stabilise the DC network by ensuring the algebraic sum of the DC current entering and leaving the system is always zero, thereby improving system voltage stability. The issues related to the DCMC algorithm, SCADA system, communications system latency and communications system failures will be discussed in the following subsections.

4.4.1 DC current estimation

Based on the power balance between the AC and DC sides of a VSC (assuming lossless conversion), the DC current contribution of each VSC in real time can be estimated from AC-side measurements as follows [17]:

$$i_{DC} = \frac{\frac{3}{2}(v_d \cdot i_d + v_q \cdot i_q)}{U_{DC}} \tag{2}$$

where v_d, v_q, i_d, i_q are the converter AC side vectors.

The reason to estimate the individual DC current instead of measuring is that this can reduce the cost of additional DC current sensor. Also as the upstream current of the DC capacitor, which is estimated from the converter AC end, tends to have more variations than the downstream current of the capacitor due to the capacitor energy storage effect, WVSC injected DC current can be "predicted" prior to the DC capacitor reaction.

In practice, the VSC and its associate equipment are not lossless. However, this may not significantly affect the accuracy of the DC current estimation in (2). In an attempt to substantiate this argument, the AC side current $WVSC_1$ of one VSC converter in the MTDC, as illustrated in Figure 4.1, with parameters presented in TABLE III and TABLE IV in the appendix, is controlled to vary significantly over a short period of time as shown in (a) (decreasing from 0.7 pu at t=0.1s until t=0.6s, increasing to 0.8 pu at t=0.9s, then decreasing again to 0.4 pu). Figure 4.4(b) and (c) show the other variables that are required by the estimation algorithm of (2), which include the AC voltage waveform v_{abc} produced by the VSC and the DC voltage U_{DC}. As observed in Figure 4.4(d), the error between the measured (in green) and estimated (in red) DC link currents is indiscernible during steady-state and transient conditions. The converter model used for Figure 4.4 is an average model where no actual switching actions take place, hence converter switching losses are not considered. As in practice these losses can be

estimated by the manufacture and easily calibrated in the DC current estimation algorithm, it will not affect the accuracy of the method.

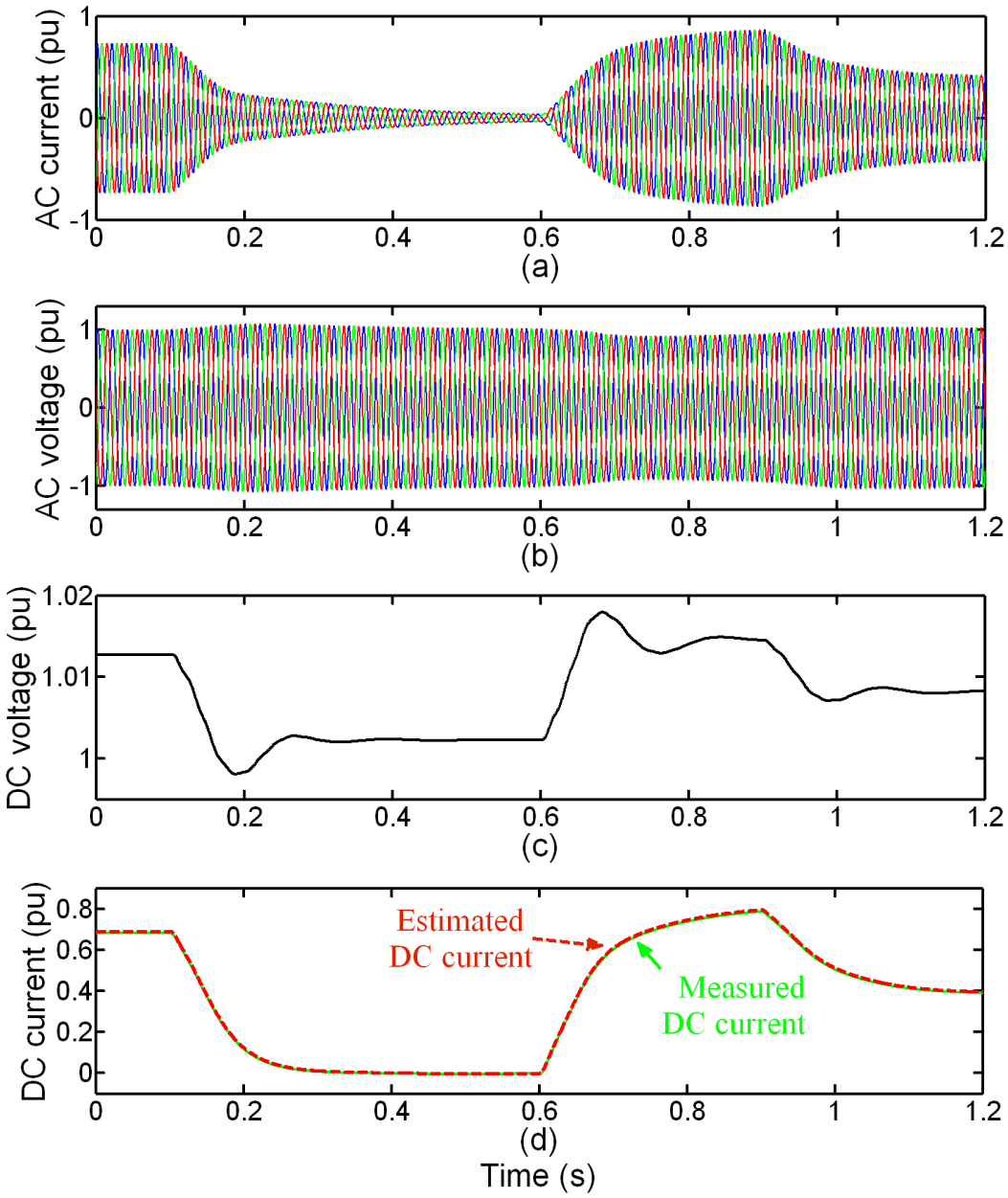

Figure 4.4 Effectiveness of DC current estimation algorithm for VSC AC current variations of $WVSC_1$

By applying (2) to all of the WVSCs shown in Figure 4.1, the individual DC current contributions from each of the three WVSCs can be estimated as presented in (3):

$$\begin{bmatrix} i_{DC1} \\ i_{DC2} \\ i_{DC3} \end{bmatrix} = \begin{bmatrix} \frac{3}{2}(v_{d1} \cdot i_{d1} + v_{q1} \cdot i_{q1}) / U_{DC1} \\ \frac{3}{2}(v_{d2} \cdot i_{d2} + v_{q2} \cdot i_{q2}) / U_{DC2} \\ \frac{3}{2}(v_{d3} \cdot i_{d3} + v_{q3} \cdot i_{q3}) / U_{DC3} \end{bmatrix} \quad (3)$$

4.4.2 Direct current matching mechanism

Based on (3), the DC current inputs from all WVSCs are estimated, remotely sent to the matching control centre (master terminal unit), and summed in the primary control server as shown in the central controller as shown in Figure 4.6. The value of total current injected is matched instantaneously to the output current using $\sum i_{DCin} = i_{DCout}$, and then allocated proportionally to the GVSCs according to the predetermined sharing factors as presented in (4). The sharing factors K_1, K_2 and K_3 are used to compute the current output references i_{DC4}*, i_{DC5}* and i_{DC6}* for $GVSC_1$, $GVSC_2$ and $GVSC_3$ respectively:

$$\begin{bmatrix} i^*_{DC4} \\ (i^*_{DC5}) \\ i^*_{DC6} \end{bmatrix} = \begin{bmatrix} K_1 \\ (K_2) \\ K_3 \end{bmatrix} \cdot \sum_{i=1}^{3} i_{DCi} \quad (4)$$

where $K_1 + K_2 + K_3 = 1.$

It must be emphasised that in (4), the DC voltage regulating converter $GVSC_2$ is not actually allocated with a current reference i_{DC5}*, as the control is implemented using a DC voltage controller as described previously. However, equation (4) can deduce the amount of DC current to $GVSC_2$ using knowledge of the other DC current flows in the MTDC network, with its sharing factor K_2then computed using the expression $(1-K_1-K_3)$. As such, the DC voltage regulating converter's DC current is also under control.

4.4.3 Grid side converter control

The AC side d-axis current references i_d^* for $GVSC_1$ and $GVSC_3$,representing the inputs into the inner current control as shown on the right hand side in Figure 4.2, are computed in a reverse manner to that presented in (2):

$$i_d^* = \frac{\frac{2}{3}U_{DC}i_{DC}^* - v_q i_q}{v_d} \tag{5}$$

Furthermore, i_q^* is controlled by regulating either the AC voltage amplitude or reactive power.

The consolidated equations for the local control of $GVSC_1$ and $GVSC_3$ are presented in (6):

$$\begin{bmatrix} i_{d4}^* \\ i_{d6}^* \end{bmatrix} = \begin{bmatrix} \frac{\frac{2}{3}U_{DC4}i_{DC4}^* - v_{q4}i_{q4}}{v_{d4}} \\ \frac{\frac{2}{3}U_{DC6}i_{DC6}^* - v_{q6}i_{q6}}{v_{d6}} \end{bmatrix} = \begin{bmatrix} \frac{\frac{2}{3}U_{DC4}K_1\sum_{i=1}^{3}i_{DCi} - v_{q4}i_{q4}}{v_{d4}} \\ \frac{\frac{2}{3}U_{DC6}K_3\sum_{i=1}^{3}i_{DCi} - v_{q6}i_{q6}}{v_{d6}} \end{bmatrix} \tag{6}$$

The entire DCMC process can be understood with reference to the flow chart shown in Figure 4.5, where MTU and RTU are referred to as "Master Terminal Unit" and "Remote Terminal Unit" commonly used for SCADA systems.

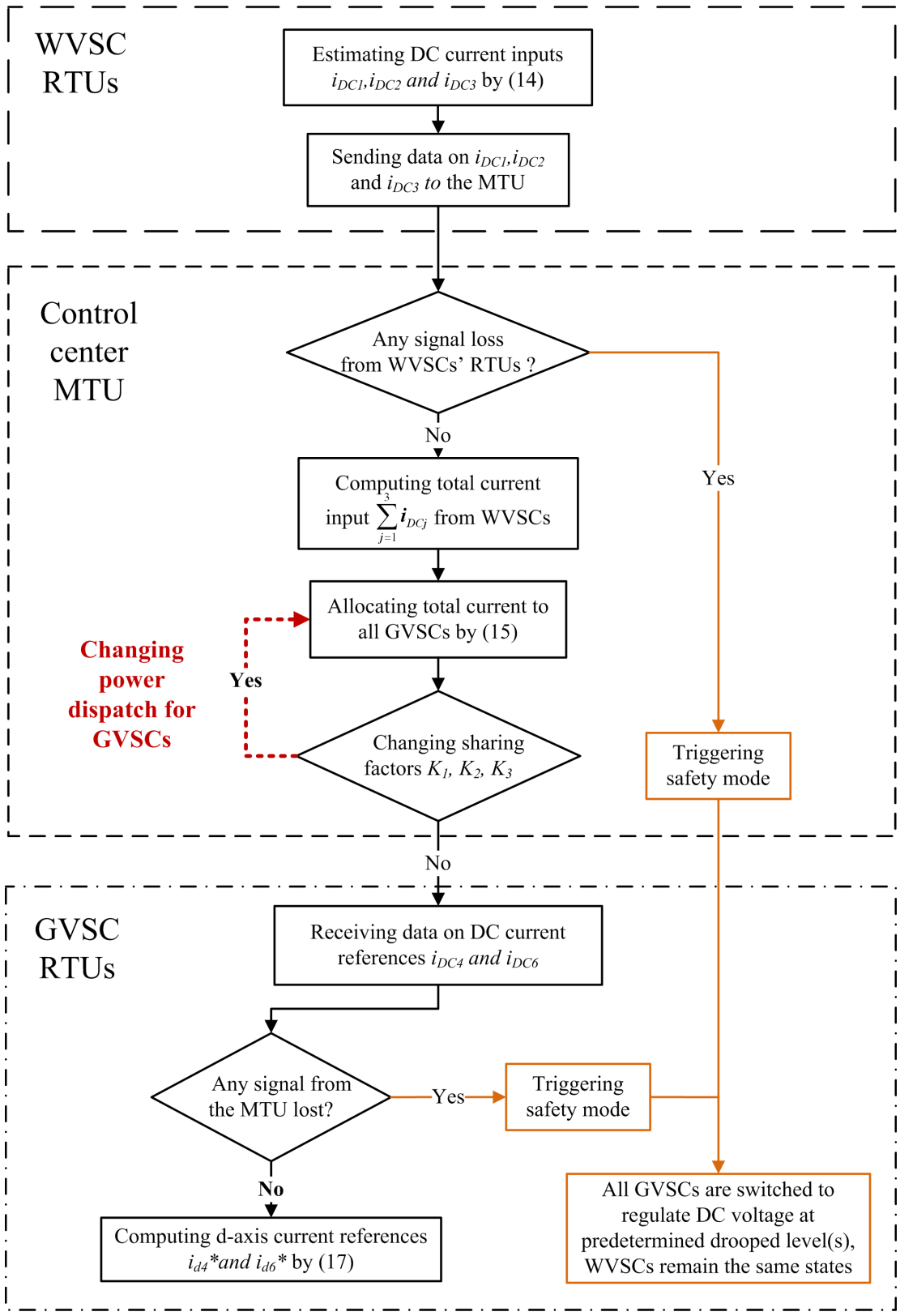

Figure 4.5 Flow chart of the DCMC process

4.4.4 SCADA communications system

A SCADA system typically consists of several data gathering and control execution devices (e.g. remote terminal units, programmable logic controllers), a central host computer server (e.g. master terminal unit), a communications system used to transfer data between RTUs and MTU, and Human Machine Interface software [14]. The data transmission media can be classified into two categories, dependent media (e.g. power line carriers, optical fibers) and independent media (e.g. satellites, microwave radio) [11][15].

Figure 4.6 illustrates a suitable WA-SCADA system that is applicable to the DCMC scheme. It consists of one master terminal unit (MTU) and six remote terminal units (RTUs). In the MTU, a local area network (LAN) connects a primary control server which implements the DCMC algorithms presented in (4) with configurable sharing factors which allow control operators to carry out intended control actions, a signal health monitoring system which can detect loss of communications, upon which "safety operation" mode can be enabled (this is described later).

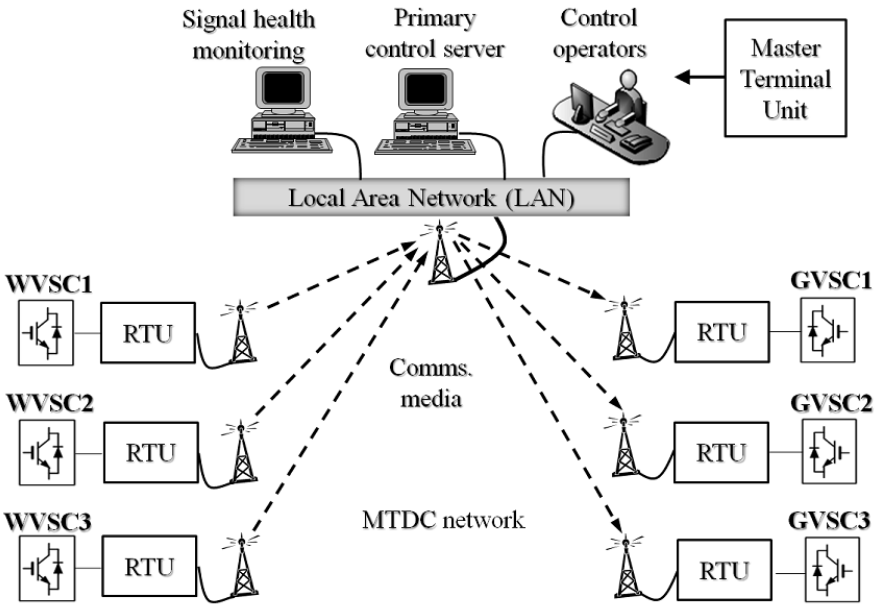

Figure 4.6 A suitable wide-area SCADA system for the DCMC strategy

Each of the three RTUs located at the wind farms collect data relating to measured (or estimated) DC current from the individual WVSCs' local controllers based on (3),

and sends this data to the MTU. The MTU collects data and sends control signals to the RTUs of $GVSC_1$ and $GVSC_3$. As $GVSC_2$ is a DC voltage regulating converter, there is, strictly speaking, no need to interface it to the SCADA system, although it will most likely be interfaced for other purposes. The communication media are likely to be radio, optical fiber or DC cable links, whereas satellite is less suitable because of its relatively high latency and jitter levels when used for data transmission between remote locations[15][16].

4.4.5 "Safety mode" to cater for communication failure

To prevent system collapse during communication failure, the system must have a "safety mode" to ensure secure and continuous operation in the event of communications problems. The operational philosophy of the safety mode is inferred from the non-communicating DC voltage droop method [6]-[8]: all GVSCs are operated at preset drooped DC voltage levels, so they all partially share the total DC current, preventing excessive current flow through any individual GVSC and preventing over-voltage on the DC system. The safety mode is triggered by detecting loss of communications signal availabilities as depicted in 0 and may require activation of auxiliary DC voltage controllers in the local controllers of $GVSC_1$ and $GVSC_3$.

4.5 Demonstration of DCMC Operation

The system shown in Figure 4.1 is modelled using SimpowerSystems in Matlab to demonstrate the effectiveness of the DCMC strategy in terms of providing flexible power dispatch to onshore AC grids using configurable sharing factors, the ability to permit exchange of power between onshore grids, and ensuring DC voltage stability by utilising the fast dynamic response and bidirectional power flow capabilities of the VSCs. The DCMC is compared with a conventional voltage margin control strategy. The parameters of the MTDC system and components are presented in TABLE III and IV in Appendix B.

The DCMC algorithms, as presented in (4), are implemented in the control centre to facilitate direct current matching and power sharing for the grid side converters as shown in Figure 4.7, with a large (representing worst-case) communications latency of 100ms included for each series channel as shown in Figure 4.7– this is extremely long and latencies of much shorter durations would probably be achievable in practice. The timer

as shown in Figure 4.7 represents the operator control actions for power dispatch by reconfiguring the set of sharing factors.

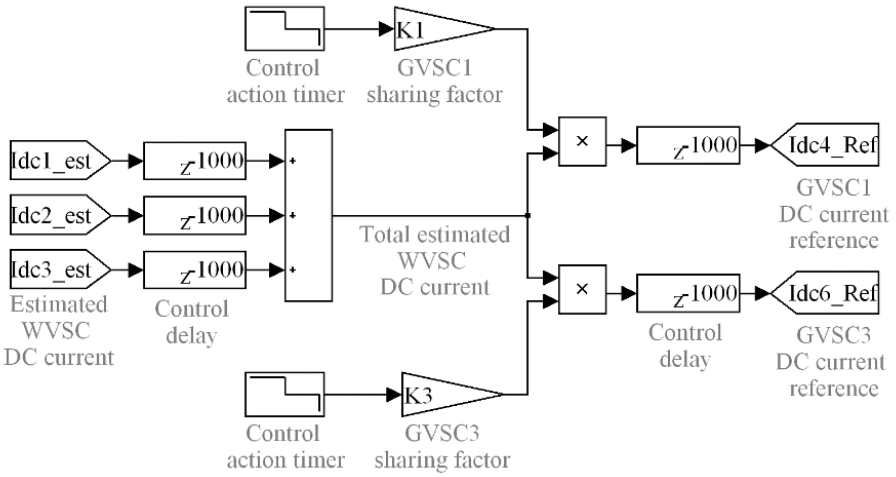

Figure 4.7 DCMC loops employed in the model

4.5.1 Flexibility and security of DC current dispatch

To demonstrate the increased flexibility of power dispatch with the DCMC, as opposed to using DC voltage droop control, four contingencies have been simulated. These include an increase in the power for one grid converter, reallocation of power sharing between two grid converters, power reversal for one grid converter and failure of the communications link with $WVSC_2$. These events, and the response of the system, are shown at specific times on the results plotted in Figure 4.8 and are described in the following text.

The $GVSC_1$ sharing factor K_1 is changed from 0.45 to 0.35 at t=0.5s. $GVSC_1$ reduces its DC current from 0.5 pu to 0.4 pu, and the DC voltage regulating converter $GVSC_2$ automatically compensates to increase its DC current from 0.38 pu to 0.48 pu as observed in Figure 4.8(c). The $GVSC_1$ sharing factor K_1 is changed from 0.2 to 0.4, with the sharing factor K_3 of $GVSC_3$ also being modified from 0.1 to 0.3 simultaneously at t=1s. Therefore, $GVSC_1$ is controlled by the DCMC scheme to reduce its DC current by 0.2 pu and $GVSC_3$ is controlled to take this share simultaneously as observed in Figure 4.8(c), whereas the DC voltage regulating converter $GVSC_2$ maintains the same DC current output. At t=1.5s, K_3 is modified from 0.15 to -0.25 and $GVSC_3$ reverses its power direction. In response to this, there is an increase in the DC currents of $GVSC_1$ and $GVSC_2$ through proportionally increasing K_1 and K_2; this reduces the risk of

overloading $GVSC_1$ or $GVSC_2$ as $GVSC_3$ rapidly reduces its DC current output from the MTDC network and begins to import power to the network, as seen in Figure 4.8(c). Using conventional DC voltage margin control, only the voltage regulating terminal $GVSC_2$ would passively respond to the power reversal of $GVSC_3$.

It can be observed that precise power sharing between the grid side converters is achieved using DCMC, whereas the DC currents injected by the WVSCs are not affected by changes in their operating points as demonstrated in Figure 4.8(b). Figure 4.8(a) presents DC bus voltage levels, with the DC voltage regulating converter $GVSC_2$ maintaining the voltage at 1 pu (600kV). It is observed that DC voltage levels experience small variations due to momentary power mismatches. The reason for the DC voltage variations can be described by referring to equation (1), which explains how the temporary non-zero MTDC network algebraic DC current of Figure 4.8(d) is essentially related to the dynamic behaviour of the voltage in the DC system. Such DC voltage variations are inevitable as each converter attempts to adjust its DC link voltage levels relative to the DC voltage regulating converter $GVSC_2$ in order to permit energy transfer between the DC side capacitors. The algebraic DC current is quickly reduced to zero by the DCMC for each contingency and consequently the amplitudes of any DC voltage variations are restricted to less than 0.01 pu.

To simulate a communications link failure, the signal health monitoring system in the control centre as shown in Figure 4.6 detects the loss of the signal containing estimated DC current from $WVSC_1$ at t=2.5s, and it instructs both $GVSC_1$ and $GVSC_3$ to enter safety mode as depicted in Figure 4.5. As observed in Figure 4.8(a), $GVSC_1$ and $GVSC_3$ are operated at predetermined DC voltage levels of 1.003 pu and 1.002 pu, while $GVSC_2$ continues to regulate DC voltage level with a target of 1 pu. As the predetermined DC voltage levels are the different values from the operating DC voltage level just prior to the communication failure, the adjustments causes small DC current transients as observed in Figure 4.8(c). The DC current share for GVSCs in Figure 4.8(c) is enabled by the conventional DC voltage droop approach. The DC voltage levels for all GVSCs involved in the safety mode must be properly set according to specific situations.

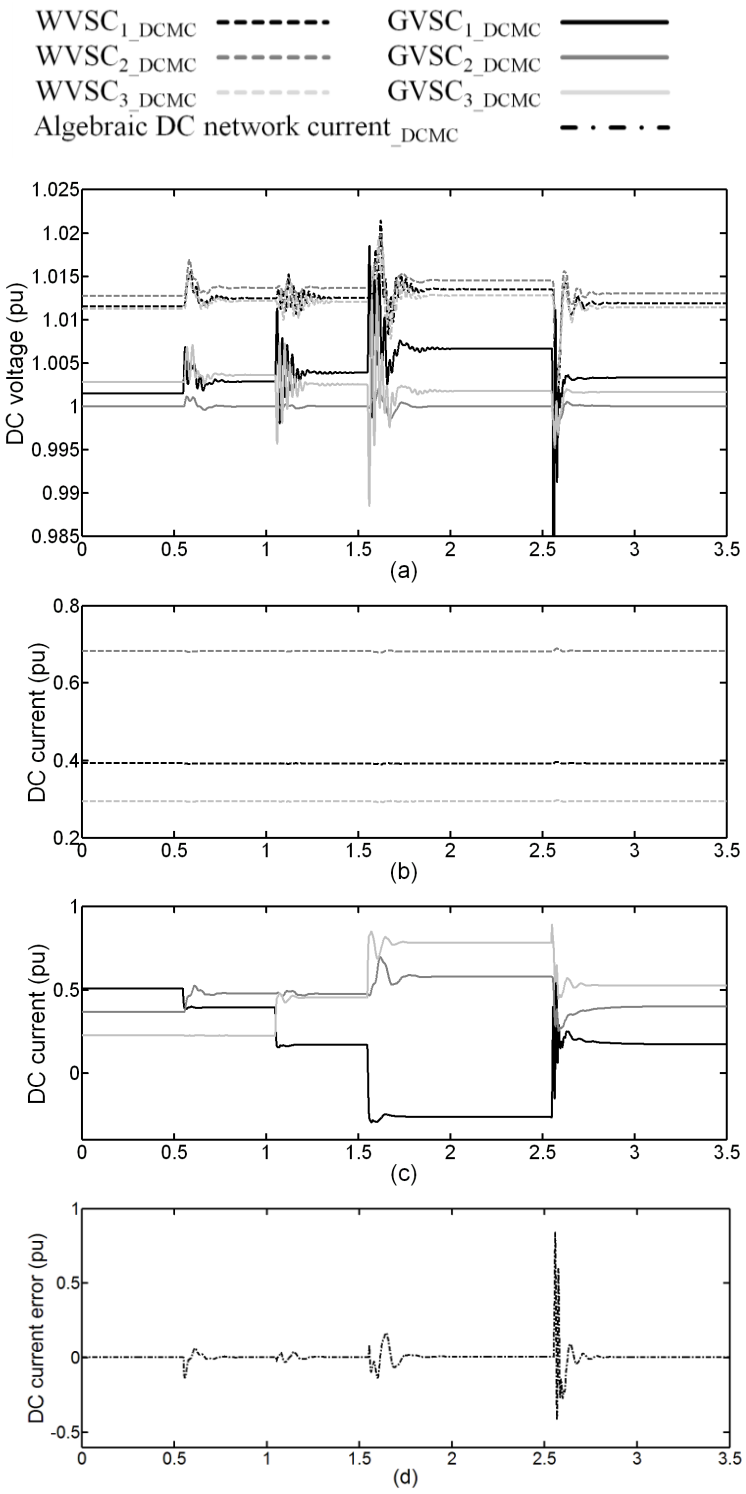

Figure 4.8 Power dispatch under the proposed DCMC strategy and safety mode

4.5.2 Restriction of amplitudes of DC voltage variations

In terms of DC voltage stability under wind power variations (resulting in significant DC power flow changes), DCMC and conventional voltage margin control strategies(where one converter ($GVSC_2$) regulates DC voltage and others act as power regulators [18]-[20]) are compared in Figure 4.9.

The solid and dashed lines represent the simulation results for DCMC and conventional approaches respectively. Both approaches allocate responsibility for DC voltage regulation to $GVSC_2$ and the remaining terminals operate in constant active power reference mode. To facilitate comparison, the test network in Figure 4.1 is simulated with the same initial conditions for both cases. Wind farm 1 increases its output power from 320MW to 640 MW from 0.5s to 1s, which results in an increase of $WVSC_2$'s DC current from 0.4 pu to 0.8 pu as shown in Figure 4.9(b). It can be seen in Figure 4.9(a) that the overall DC voltage levels under the proposed DCMC (solid lines) vary less from the initial values than those under the conventional control (the lines with box marks). The reason for this is that DCMC controls not only $GVSC_2$; but $GVSC_1$ and $GVSC_3$ are also controlled to respond to temporary DC power increases as observed in Figure 4.9(c), whereas under conventional control, $GVSC_2$ is solely responsible for managing power imbalances. Accordingly, the algebraic sum of DC current mismatches (Figure 4.9(d)) and DC voltage level variations (Figure 4.9(a)) using DCMC are much lower than under conventional control due to a reduction in the trapped energy in the DC side capacitors.

A wind power decrease from Wind Farm 2 is simulated at t=1.5s, from 560MW to 240MW, which results in $WVSC_2$'s DC current decreasing from 0.68 pu to 0.28 pu as shown in Figure 4.9(b). As before, lower overall DC voltage variations from the initial values for DCMC are obtained, when compared to conventional control.

The mechanism employed by the DCMC to restrict DC voltage variations is essentially the same as that used by DC voltage droop control: all grid side converters share any temporary power imbalance in the network. However, it is simpler to dispatch power using DCMC for systems with relatively high numbers of terminals.

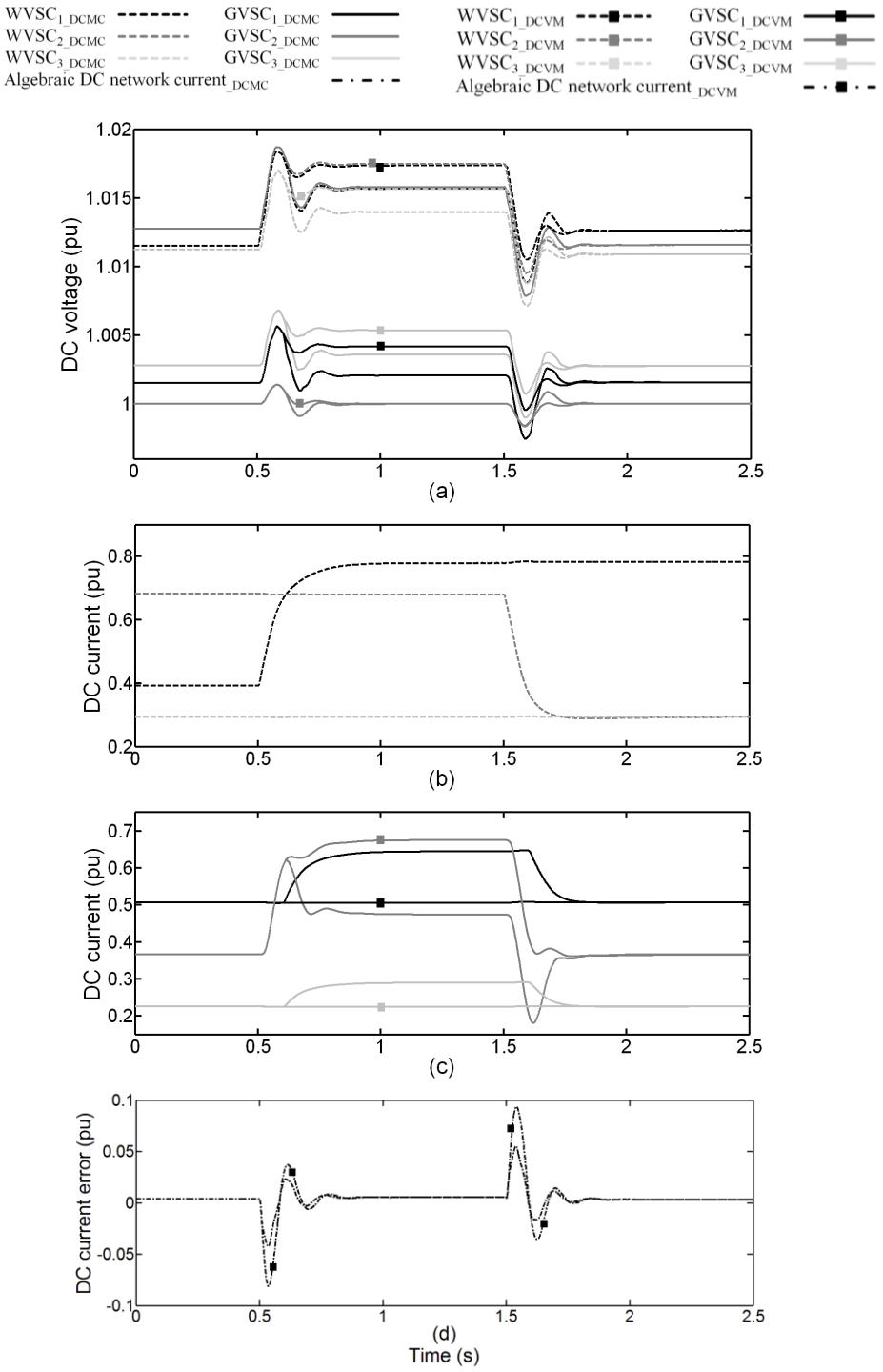

Figure 4.9 Comparison of the proposed DCMC strategy and DC voltage margin control (DCVM) under wind power increase and decrease

4.5.3 Test on a AC grid fault event and a wind farm loss

In addition, the proposed DCMC should robustly cope with temporary AC grid fault condition and the event of a wind farm loss. To test them, at t=0.5s a solid three-phase

fault is applied to the PCC of the GVSC1 for 0.14s (7 cycles) and cleared at t=0.64s. At t=1.5s, the wind farm which is connected to WVSC3 is constantly lost.

Figure 4.10 shows the corresponding simulation results. When the faulted $GVSC_1$ is inhabited with its active power output during its AC fault, in detecting fault condition $GVSC_2$ and $GVSC_3$ are controlled by the DCMC strategy to automatically share the initial power of $GVSC_1$, with the ratio of 50% to 50% set by the predefined sharing factors K_2=0.5 and K_3=0.5. It can be observed in Figure 4.10(a) from t=0.5s that all the terminal's DC voltage levels are experiencing adjusting variations, as the DC current output of $GVSC_1$ decrease to 0 due to the fault as seen in Figure 4.10(c). Due to the transients caused by $GVSC_1$'s AC fault, there is inevitably total DC current mismatch as shown in Figure 4.10. However the MTDC system under the proposed DCMC strategy manages to continue to deliver the offshore power to onshore GVSC2 and GVSC3 converters during the fault, and the overall DC voltage manages to restore to steady state immediately after the $GVSC_1$ fault is cleared.

At t=1.5s when the $WVSC_3$'s wind farm is lost, the total delivered wind power is reduced, and according to the unchanged sharing factors for all GVSCs (K_1=0.3, K_2=0.33 and K_3=0.37) by the DCMC control centre, all GVSCs briefly decreases their individual output DC currents as observed in Figure 4.10(c). There are small and negligible DC voltage variations, and the MTDC voltage under the DCMC strategy is verified to be stable in the event of the wind farm loss.

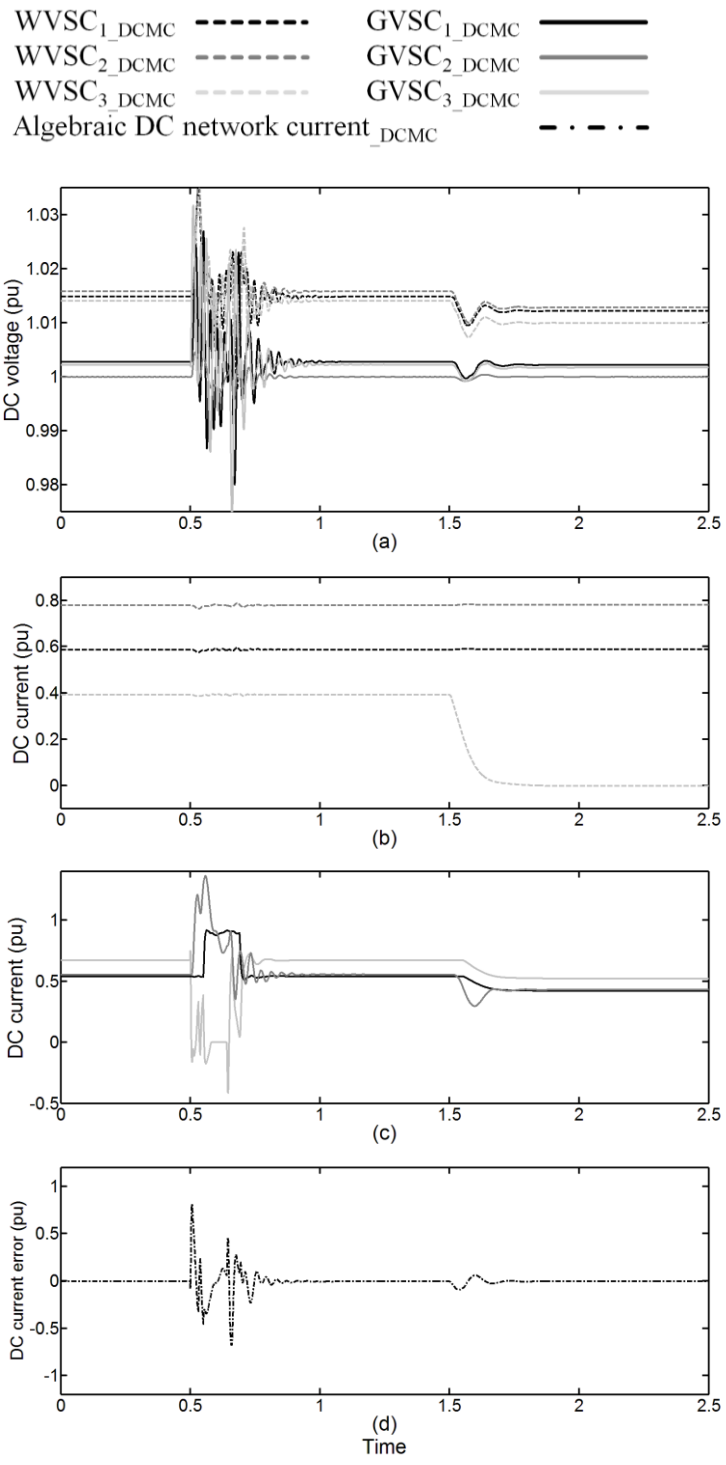

Figure 4.10 The proposed DCMC strategy under temporary fault on GVSC1's PCC at t=1s, and loss of WVSC3's wind farm at t=1.5s

4.6 Summary

This chapter has proposed a communication based DCMC scheme for multi-terminal HVDC transmission networks. The major advantages, in terms of the operational performance of the DCMC scheme, are summarised below:

The centrally implemented and configurable sharing factors result in great flexibility and convenience for dispatching GVSCs' DC currents. Furthermore, predictions of network current/power flows are obtained by the DCMC, which is an advantage over "DC voltage droop" schemes described in [6]-[8].

The scheme has the ability to implement near-real-time matching of the DC current outputs of GVSCs with those of the WVSCs, resulting in reduced voltage variations, when compared to other control schemes reported in [18]-[20].

It is proposed that the DCMC scheme employing communications, with further demonstration and prototyping, will be suitable for efficient operation of a practical MTDC system.

References

[1] Lu W.X.; Ooi, B.T., "Multiterminal LVDC system for optimal acquisition of power in wind-farm using induction generators," *IEEE Trans. on Power Electron.*, vol.17, no.4, pp.558-563, Jul 2002.

[2] Jovcic, D.; Strachan, N., "Offshore wind farm with centralised power conversion and DC interconnection," *IET Gen., Trans. & Dist.*, vol.3, no.6, pp.586-595, June 2009.

[3] Xu, L.; Yao, L.Z.; Sasse, C., "Grid Integration of Large DFIG-Based Wind Farms Using VSC Transmission," *IEEE Trans. on Power Syst.*, vol.22, no.3, pp.976-984, Aug. 2007.

[4] Feltes,C.; Wrede,H.; Koch, F.; ErlichI., "Fault ride-through of DFIG-based wind farms connected to the grid through VSC-based HVDC link," *2008 PSCC 16th Power Syst. Comput. Conf.*

[5] Cole, S.; Beerten, J.; Belmans, R., "Generalized Dynamic VSC MTDC Model for Power System Stability Studies," *IEEE Trans. on Power Syst.*, vol.25, no.3, pp.1655-1662, Aug. 2010.

[6] Whitehouse, R.S., "Technical challenges of realising multi-terminal networking with VSC,"*Proc. 2011 14th European Conf. on Power Electron. and Appl. (EPE 2011)*, vol., no., pp.1-12, Aug. 30 2011-Sept. 1 2011.

[7] Xu,L.;Yao, L., "DC voltage control and power dispatch of a multi-terminal HVDC system for integrating large offshore wind farms," *IET Renewable Power Gen.*, vol.5, no.3, pp.223-233. (May 2011)

[8] Adam,G.P.; Anaya-Lara, O.;Burt,G., "Multi-terminal DC transmission system based on modular multilevel converter," *Proc. 2009 44th Int. Univ. Power Eng. Conf. (UPEC 2009).*

[9] ABB, XLPE Land Cable Systems User´s Guide, pp.16-22, Available [assessed on 25/08/2012]: http://www05.abb.com/global/scot/scot245.nsf/veritydisplay/ab02245fb5b5ec4

1c12575c4004a76d0/$file/xlpe%20land%20cable%20systems%202gm5007gb%20rev%205.pdf.

[10] Pan J.P,; Nuqui, R.; Srivastava, K.; Jonsson, T.; Holmberg, P.; Hafner, Y.-J., "AC Grid with Embedded VSC-HVDC for Secure and Efficient Power Delivery," *IEEE Energy 2030 Conf.*, vol., no., pp.1-6, 17-18 Nov. 2008.

[11] Shahraeini, M.; Javidi, M.H.; Ghazizadeh, M.S., "Comparison Between Communication Infrastructures of Centralized and Decentralized Wide Area Measurement Systems," *IEEE Trans. on Smart Grid*, vol.2, no.1, pp.206-211, March 2011.

[12] Chaudhuri, B.; Majumder, R.; Pal, B.C., "Wide-area measurement-based stabilizing control of power system considering signal transmission delay," *IEEE Trans. on Power Syst.*, vol.19, no.4, pp. 1971- 1979, Nov. 2004.

[13] Bertsch, J.; Carnal, C.; Karlson, D.; McDaniel, J.; Vu, K., "Wide-Area Protection and Power System Utilization," *Proc. IEEE* , vol.93, no.5, pp.997-1003, May 2005.

[14] Valsalam, S.R.; Sathyan, A.; Shankar, S.S., "Distributed SCADA system for optimization of power generation," *2008 Annual IEEE India Conf.*, vol.1, no., pp.212-217, 11-13 Dec. 2008.

[15] Marihart, D.J., "Communications technology guidelines for EMS/SCADA systems," *IEEE Trans. on Power Del.*, vol.16, no.2, pp.181-188, Apr 2001.

[16] Shahraeini, M.; Javidi, M.H.; Ghazizadeh, M.S., "A new approach for classification of data transmission media in power systems,", *2010 Int. Conf. on Power Syst. Technol.*, vol., no., pp.1-7, 24-28 Oct. 2010.

[17] Zhu, J.; Booth, C.D.; Adam, G.P.; Roscoe, A.J.; Bright, C.G., "Inertia Emulation Control Strategy for VSC-HVDC Transmission Systems," *IEEE Trans. On Power Syst.*, vol.28, no.2, pp.1277, 1287, May 2013.

[18] Nakajima, T., Irokawa, S., "A control system for HVDC transmission by voltage sourced converters," *1999 IEEE Power Eng. Soc. Summer Meeting*, vol.2, pp.1113-1119.

[19] Haileselassie, T.M..; Molinas, M.; Undeland, T., "Multi-Terminal VSC-HVDC System for Integration of Offshore Wind Farms and Green Electrification of Platforms in the North Sea," *Nordic Workshop on Power and Ind. Electron.*, June 2008.

[20] Zhu, J.; Booth, C., "Future multi-terminal HVDC transmission systems using voltage source converters," *2010 45th Inter. Uni. Power Eng. Conf. (UPEC)*, Aug 2010.

Chapter 5

A Novel Inertia Emulation Control Strategy for VSC-HVDC Transmission Systems

5.1 Introduction

Power system frequency is an important indicator for any instantaneous imbalance between generation and demand. One of the major concerns with the rapid development and increase of renewable power relates to system frequency stability, as the majority of renewable power generation, normally connected via some form of power converter, contributes little or no inertial or frequency support response to network disturbances.

In order to address the reduction in system inertia that may be introduced by large scale penetrations of renewable energy interfaced via HVDC, the design of an Inertia Emulation Control (INEC) strategy for VSC-HVDC transmission systems is presented and simulation-based verifications of performance are discussed in this chapter. The applicability of INEC to both point-to-point direct HVDC links and for multi-terminal HVDC systems is demonstrated.

5.2 Inertia Emulation Control Strategy for back-to-back VSC-HVDC Systems

The proposed INEC uses stored energy in the HVDC DC capacitors to provide an inertial response, which can not only support frequency stability but also contribute to primary frequency control of the supplied AC network. Energy for the INEC is provided solely from DC link capacitors by using the converters to control the DC link voltage. In this section, the INEC will be introduced using the following steps, each of which is described in an associated subsection.

- Machine inertia time constant versus capacitor time constant;
- Capacitor DC voltage and emulated inertia time constant;
- VSC-HVDC INEC design loop;
- Frequency change versus DC voltage change.

5.2.1 Machine inertia time constant vs. capacitor time constant

The inertia constant H, which determines the response of SG angular speed to any changes in input power, can be expressed by (1):

$$H = \frac{W_K}{S_M} = \frac{\frac{1}{2} J\omega^2}{S_M} \tag{1}$$

Where W_K represents kinetic energy stored in the rotating mass of the machine (MVA·sec), J refers to the moment of inertia (kg·m^2) and S_M is the generator rating (MVA).

The capacity of the DC capacitors which are used in VSCs for DC voltage stability and filtering is characterised by a capacitor time constant τ , given in (2):

$$\tau = \frac{W_E}{S_{SVC}} = \frac{\frac{1}{2} C_T V_{DC}^2}{S_{VSC}} \tag{2}$$

where W_E represents the electro-static energy stored in the capacitor, S_{VSC} represents the VSC's rated power capability, C_T is the total capacitance in the DC link including capacitors and DC cables.

To some extent, the electro-static energy stored in DC capacitors is similar to the mechanical energy stored in the inertia of SGs, as both the angular speed ω of the SGs, and DC voltage V_{DC} of the VSC-HVDC capacitors are squared in (1) and (2) respectively.

5.2.2 Capacitor DC voltage and emulated inertia time constant

The electrical dynamics of a VSC's capacitor is given in (3):

$$\frac{NCV_{DC}}{S_{VSC}} \cdot \frac{dV_{DC}}{dt} = P_{in} - P_{out} = \Delta P_1 \qquad (pu) \tag{3}$$

where H is the inertia time constant in sec, f_0 is the nominal frequency in Hz, P_M is the mechanical power in pu, P_E is the electrical power in pu andP_1 is the kinetic power absorbed by or released from the inertia of the machine during a speed change (in pu).

In order to equate the available power of the DC capacitors to that of an electrical machine, the capacitor dynamics (in terms of DC voltage and output power) are presented in equation (4):

$$\frac{NCV_{DC}}{S_{VSC}} \cdot \frac{dV_{DC}}{dt} = P_{in} - P_{out} = \Delta P_2 \ (pu) \tag{4}$$

In equation (4), N represents the total number of capacitors (two in this case), S_{VSC} represents the VSC rated power capability in watts, P_{in} is VSC power input to the two capacitors in pu, P_{out} is the VSC power output in pu, and ΔP_2 is the dynamic electro-static power stored or released in or from the capacitors in pu.

Equation (4) indicates that any variation in DC voltage changes the stored energy in the capacitors. This energy is charged or discharged by varying the DC voltage according to the DC voltage controller as discussed in Chapter 2. Due to the low resistance of the DC cables, the DC voltage difference between the rectifier and inverter is negligible. For this reason, the DC voltages at the rectifier and inverter are assumed to be the same for the purposes of this analysis.

A further task is to assign a specific emulated "inertia" constant H_{VSC} to the HVDC system. Equating the SG power variation ΔP_1in (3) with capacitor power ΔP_2 in (4) yields:

$$\frac{2H_{VSC}}{f_0} \cdot \frac{df}{dt} = \frac{NCV_{DC}}{S_{VSC}} \cdot \frac{dV_{DC}}{dt} \tag{5}$$

Integrating both sides of (5) produces (6) below. This process cancels the df/dt and dV_{DC}/dt terms on either side of (5) and results in the following:

$$\int \frac{2H_{VSC}}{f_0} \cdot df = \int \frac{NCV_{DC}}{S_{VSC}} \cdot dV_{DC} \tag{6}$$

$$\frac{2H_{VSC} \cdot f}{f_0} = \frac{NCV_{DC}^2}{2S_{VSC}} + K_1 \tag{7}$$

The constant K_1 is the constant of integration which is calculated according to the specified values of H_{VSC}, total combined DC capacitance NC, the nominal DC voltage V_{DC0} and the converter power rating S_{VSC}. This is shown in (8):

$$K_1 = \frac{2H_{VSC} \cdot f_0}{f_0} - \frac{NCV_{DC0}^2}{2S_{VSC}} = 2H_{VSC} - \frac{NCV_{DC0}^2}{2S_{VSC}} \tag{8}$$

The full INEC equation can then be expressed in (9):

$$\frac{2H_{VSC} \cdot f}{f_0} = \frac{NCV_{DC}^2}{2S_{VSC}} + \left(\frac{2H_{VSC} \cdot f_0}{f_0} - \frac{NCV_{DC0}^2}{2S_{VSC}}\right) \tag{9}$$

Equation (7) can also be written in another format, shown in (12), that can be used to evaluate the influence of DC voltage change ΔV_{DC} on the VSC-HVDC emulated inertia time constant for a given change of network frequency Δf:

$$2H_{VSC} \cdot \frac{f - f_0}{f_0} = \frac{NC}{2S_{VSC}}(V_{DC}^2 - V_{DC0}^2) \tag{10}$$

$$2H_{VSC} \cdot \frac{\Delta f}{f_0} = \frac{NC \cdot V_{DC0}^2}{2S_{VSC}} \cdot \left[(\frac{\Delta V_{DC}}{V_{DC0}} + 1)^2 - 1 \right] \tag{11}$$

$$H_{VSC} = \frac{\frac{1}{2} \cdot \frac{NC \cdot V_{DC0}^2}{S_{VSC}} \left[\left(\frac{\Delta V_{DC}}{V_{DC0}} + 1 \right)^2 - 1 \right]}{2 \cdot \frac{\Delta f}{f_0}} \tag{12}$$

Equation (12) implies that, in order to emulate a specific inertia time constant H_{VSC}, the DC voltage level in VSC-HVDC link must vary according to the AC network frequency, although the relationship between network frequency variations and DC voltage variations will be non-linear. A large value of H_{VSC} will require a correspondingly large variation in DC voltage and this must be considered in the design of the VSC-HVDC system.

5.2.3 VSC-HVDC inertia emulation control loop

As already stated, the DC voltage of the VSC-HVDC must vary according to AC network frequency. Equation (7) is transformed to (13) to facilitate DC voltage control:

$$V_{DC}^* = \sqrt{\frac{4S_{VSC}H_{VSC}}{NCf_0} \cdot f - K_2} \tag{13}$$

where $K_2 = \frac{4S_{VSC}H_{VSC}}{NC} - V_{DC0}^2$.

Figure 5.1 illustrates the design of the INEC. The DC voltage reference V_{DC}* varies with AC network frequency f. The prevailing AC network frequency, which is estimated by the PLL, is used to compute the DC voltage reference through the gains and square root operations as shown in (13). Other variables, including the initial integration state factor K_2, the VSC rated power capability S_{VSC} and specified inertia time constant H_{VSC} are all included in the INEC loops.

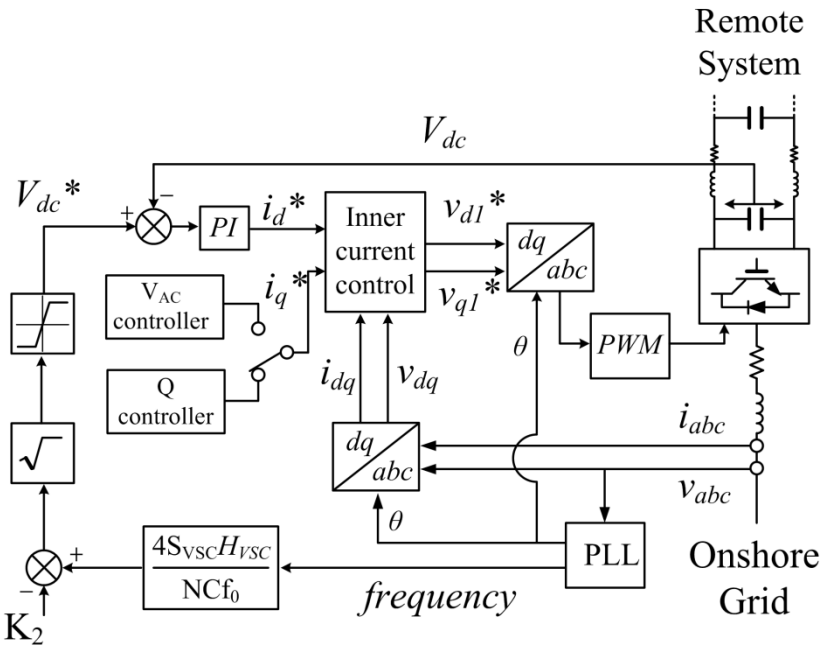

Figure 5.1 Proposed inertia emulation control system for VSC-HVDC

The DC voltage reference should be limited within upper and lower constraints, for example ± 15% of nominal DC voltage, although the exact figures would depend on insulation requirements, current ratings and PWM functionality.

Unlike the proposed inertia emulation control schemes presented in [2][13][19], the implementation of INEC in (13) avoids the processing of frequency differential terms df/dt with the consequent risk of measurement noise threatening stability, especially in response to step transients [4].

The INEC strategy has the potential for implementation in multi-terminal HVDC (MTDC) systems. In equation (13), N is the total number of capacitors present in the MTDC network. With the INEC strategy, the converter terminal that is responsible for DC voltage control is able to make an inertial contribution to its connected AC grid. In an HVDC link connecting two AC systems, it is not recommended that both terminals of the link employ INEC, as if both are attempting to dictate the DC voltage simultaneously, there is the potential for deterioration of DC voltage stability and DC link power flow control. Therefore, frequency support could only be provided to one AC system if the HVDC link was being used to connect to separate AC systems – but the terminal providing support could be switched as and when required. In an HVDC link providing power from an offshore wind farm(s), then obviously the terminal providing

frequency support and inertial response would always be allocated to the terminal at the AC grid end.

5.2.4 Frequency changes vs. DC voltage changes

It is clear from the previous discussions that VSC-HVDC has the potential to emulate a wide range of inertia time constants, if its DC voltage is allowed to vary by a wide margin. A range of inertia constants from 0s to 4s along with the associated resultant DC voltage changes for specific frequency changes is plotted in Figure 5.2. The maximum inertia time constant that can be provided will depend on the degree of permissible DC voltage variations, the value of DC link capacitors as shown in (22) and the converter's active power limit.

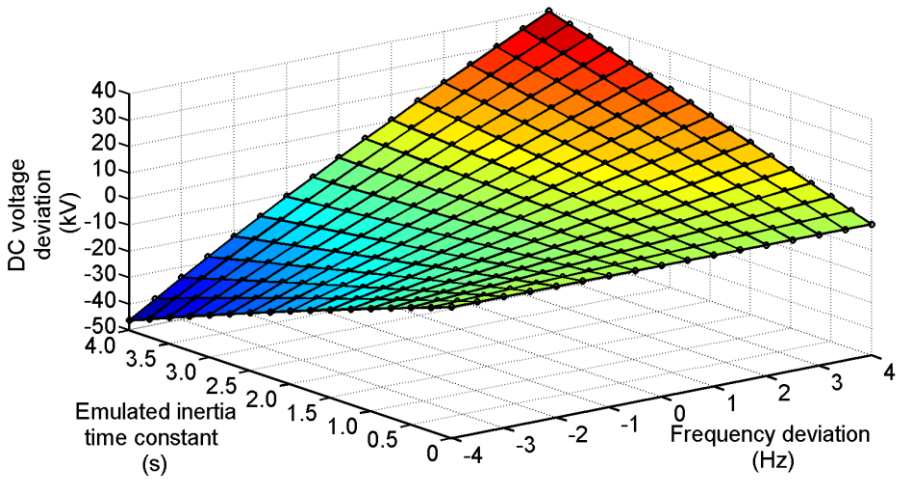

Figure 5.2 Three-dimensional relationship between emulated inertia, frequency and DC voltage deviations from rated value (total DC link capacitance=2*7.5mF for a 300 MW 300 kV VSC-HVDC link)

Equation (11) presents the relationship between the square of DC voltage variation and DC capacitance, which is inversely proportional in nature. Relatively large capacitors (e.g. 7.5 mF in this example) are used in order to lower DC voltage variations. Large DC capacitors will obviously require DC link protection; smaller values of DC capacitance could be used, with inertial responses being provided using larger DC voltage variations – refer to the next simulation section for examples of the use of different capacitor values. It is important to emphasise that the scheme reported in this dissertation is intended to provide an "instantaneous" inertial response, and would obviously be required to be backed up by a longer term controlled response for events involving major loss of generation/transmission capacity in the supplied AC system. DC links and

controllers could also be used for this purpose, with excess energy being delivered and sourced from other AC systems and/or wind farms (if available and permissible).

5.2.5 Simulation results

The evaluation scenario as illustrated in Figure 5.3 is simulated using SimpowerSystems in Matlab. A point-to-point VSC-HVDC link comprises three-phase converters VSC_1 and VSC_2, with parameters as presented in Table I in Appendix B. VSC_2, which is connected to the wind farm, regulates the active and reactive power by controlling offshore grid frequency and AC voltage amplitude in System 2. VSC_1 supplies power to System 1 at B_1 which represents a relatively weak system consisting of one synchronous generator and associated loads. The fixed load $P_{L1}+ Q_{L1}$ is 400 MW + 100 MVar, whereas the load $P_{L2}+ Q_{L2}$ can be switched in or out and is 20 MW + 5 MVar. The loads in System 1 are therefore being supplied by both the synchronous generator in System 1 and by System 2 via the HVDC system. The connected AC system is a relatively weak one consisting of one synchronous generator, in order to obviously show the inertial effect from VSC-HVDC converter (e.g. the system frequency trends with and without the proposed VSC-HVDC strategy).

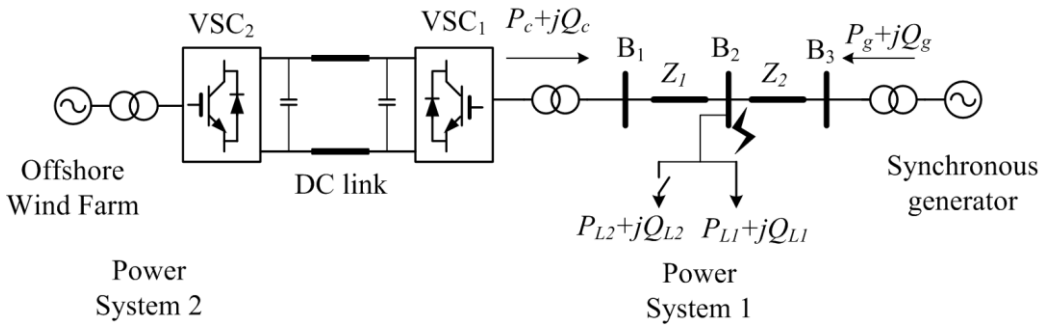

Figure 5.3 A single-line diagram of the simulated test system

The synchronous generator (SG) is modeled using a seventh-order model with IEEE parameters [5][6] as shown in Table II in Appendix B, where the electromagnetic transients and mechanical dynamics are incorporated. To illustrate the effectiveness of the proposed INEC strategy, the simulations comprise three different situations: emulated inertia time constants H_{VSC}=0 (i.e. conventional VSC-HVDC control with no inertial response), H_{VSC}=1s and H_{VSC}=3s, which are specified individually in the INEC design in Figure 5.1.

Two scenarios are considered:

- Sudden load changes using $P_{L2}+jQ_{L2}$ in System 1
- AC network side faults at busbar B_2in System 1

i. Sudden load changes

Figure 5.4 shows the obtained results for a load increase and decrease respectively. The switchable load at B_2 in Figure 5.3, which represents 5% of the pre-transient existing load, is introduced and then switched in and out to simulate changes in load.

Figure 5.4 presents the response to a total load increase. It is observed in Figure 5.4(a) that with an increased emulated inertia time constant (from the VSC-HVDC), the rate of change of the SG rotor speed is damped, demonstrating that the emulated inertia supplied by the VSC-HVDC improves system stability. The initial SG load angle perturbation, as illustrated in Figure 5.4(b), is reduced in magnitude as greater amounts of emulated inertia are supplied. The behavior of the SG load angle also shows the stability of the test power system as it settles at a new value following the load increase. Figure 5.4(c) illustrates that progressively larger values of emulated inertia result in greater variations of the DC link voltage.

Figure 5.4(d) shows the active power output from the converter VSC_1 during a load increase. The specified inertia constant H_{VSC} determines the magnitude and shape of the converter's inertial response. More active power is provided by VSC_1 for higher values of H_{VSC}. This shows how the INEC can provide frequency support.

From Figure 5.4(d)(e), it is clear that that the VSC_1 briefly increases its active power output by decreasing its DC voltage, until the SG increases its power to cope with the power demand from System 1. Once stable conditions are restored, the converter restores its active power to the original value. Therefore, the INEC enables the VSC-HVDC system to react fast enough to support the primary frequency control function. This also reduces the magnitude of the initial transient increase in output power demanded from the SG. Figure 5.4(f) illustrates the network frequency at VSC_1's Point of Common Connection (PCC) of B_1 and shows that an increase in the emulated inertia reduces the magnitude of the frequency transients. This is, potentially, a highly beneficial feature of the scheme, and this may become more important if renewable energy replaces conventional generation and especially if significant renewable energy is connected via

power electronics.

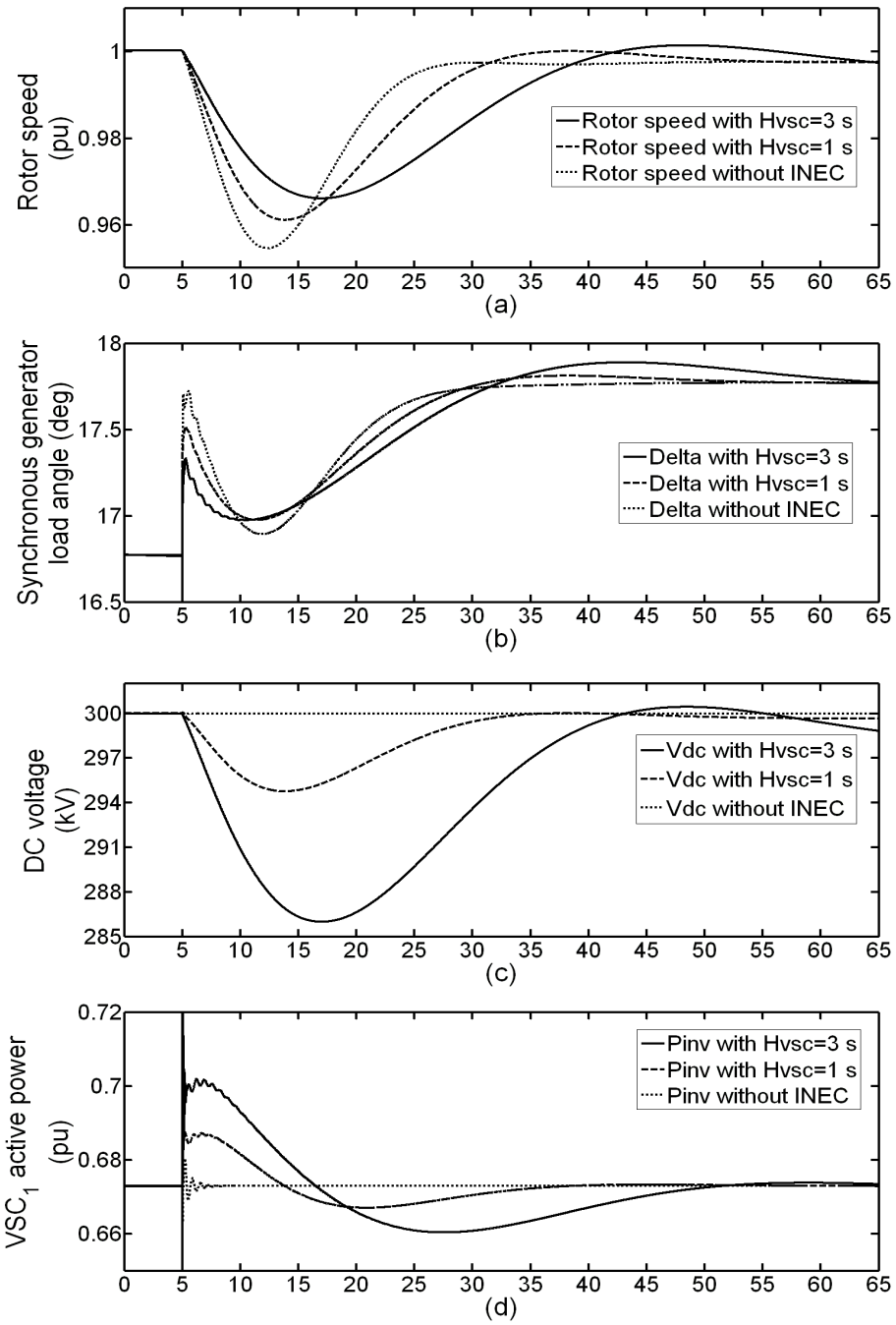

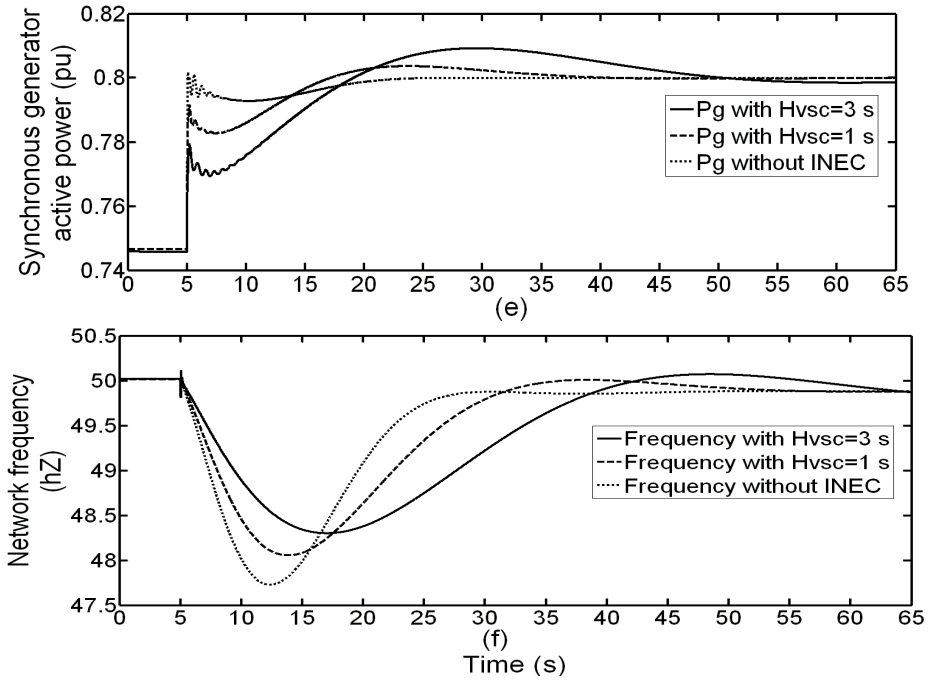

Figure 5.4 INEC response for 5% load increase: (a) SG rotor speed; (b) SG load angle (c) HVDC DC link voltage; (d) VSC_1 active power; (e) SG active power; (f) Network frequency.

Figure 5.5 presents the case of a sudden load reduction, which is simulated by switching out P_{L2}+ Q_{L2}. It is evident that the INEC scheme successfully damps the rotor speed deviation as presented in Figure 5.5(a). The magnitude of initial SG load angle perturbations is also significantly reduced due to the action of the INEC scheme, as shown in Figure 5.5(b). The INEC acts to increase DC link voltage as shown in Figure 5.5(c), with the capacitors absorbing the excess energy. This results in an instant decrease of the active power output from VSC_1 as shown in Figure 5.5(d), with the response of the SG shown in Figure 5.5(e). Figure 5.5(f) shows that increasing the value of H_{VSC} reduces the AC network frequency transients. In all cases, the DC link voltage is maintained within 5% (15 kV) of the nominal voltage level of 300 kV. Increasing the permissible limits on DC voltage variations (and possibly capacitor ratings) could offer higher emulated inertia.

Figure 5.6 shows that the active power input by VSC_2 from power system 2 remains unchanged for both load increase and decrease cases. It is clear that the offshore VSC_2 active power input is not affected by the variations in VSC_1 active power output, nor is it affected by the DC capacitor voltage variations. Therefore, the INEC retains the attractive HVDC attribute of decoupling systems 1and 2, avoiding transients in one system propagating through to another system(s). This feature will become more

important because of the continuing trend for AC power systems to interconnect via HVDC.

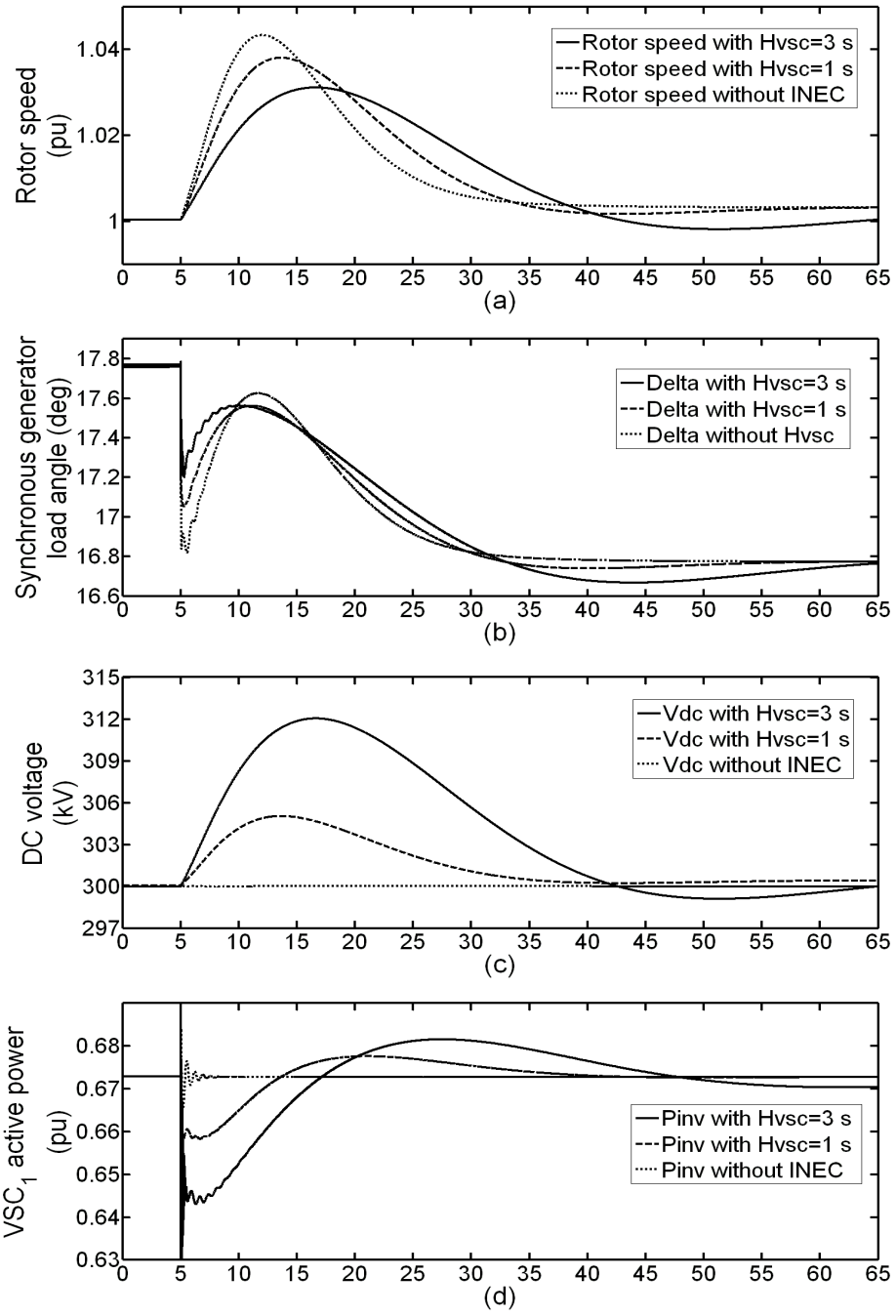

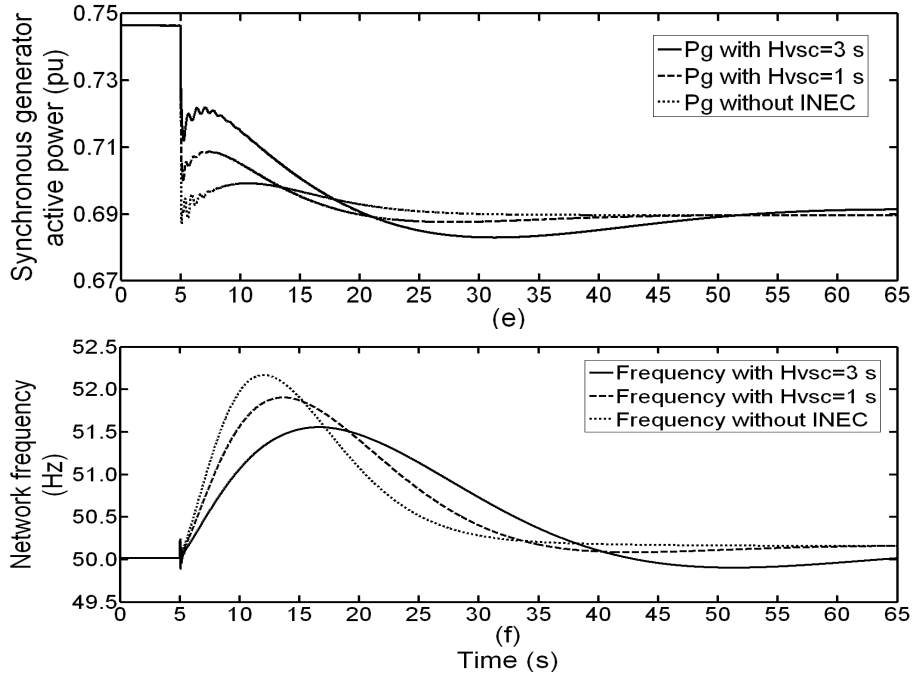

Figure 5.5 INEC response for 5% load decrease: (a) SG rotor speed; (b) SG load angle (c) HVDC DC link voltage; (d) VSC_1 active power; (e) SG active power; (f) Network frequency.

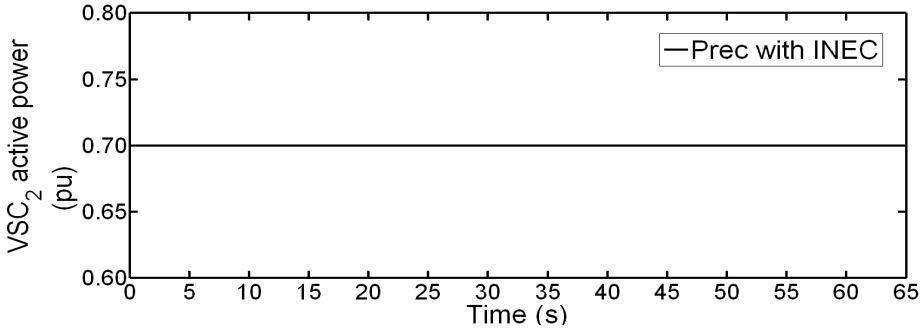

Figure 5.6 VSC_2 active power injected by the offshore wind farm

In order to illustrate the impact of DC link capacitor sizing on the INEC performance, difference capacitances for the DC capacitors, namely, C=7.5mF (for the base case), 4mF and 2mF, are used to synthesise the same inertia time constant H_{VSC}=1s for the case of a 5% load increase, as seen in Figure 5.7. These results have shown no differences in the system response for different values of DC link capacitances, as evident from SG rotor speed behavior in Figure 5.7(a), SG load angle in Figure 5.7(b), VSC_1 active power output in Figure 5.7(d), SG active power in Figure 5.7(e) and network frequency in Figure 5.7(f). However, it is noticeable that this performance is achieved at the expense of increased DC link voltage variation of the converter VSC_1 as the DC link capacitance reduces. These results indicate that the DC link capacitance must to be sized

taken into account the maximum permissible DC link voltage variation from the rated voltage to ensure proper system operation when INEC is implemented in one or more terminals.

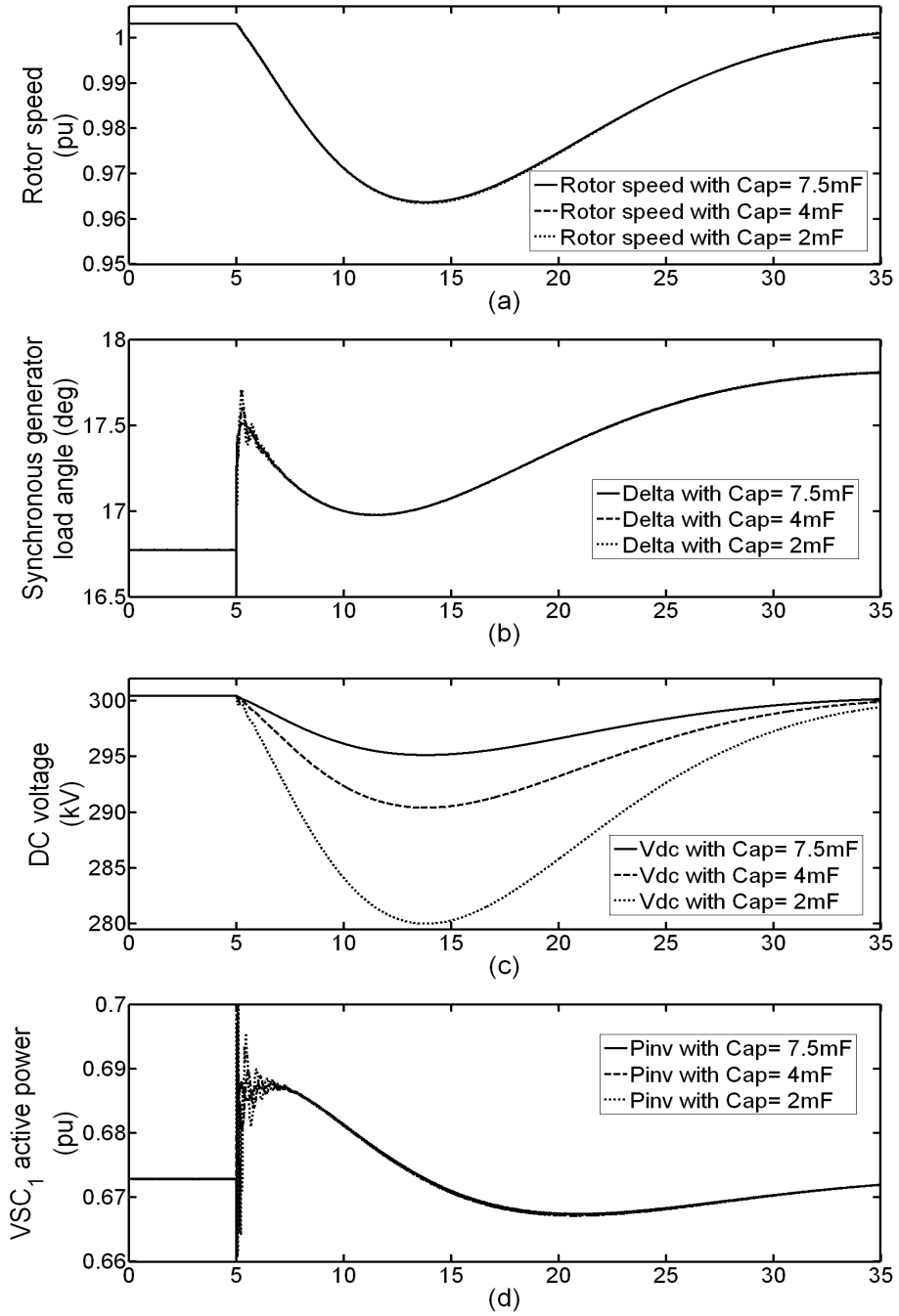

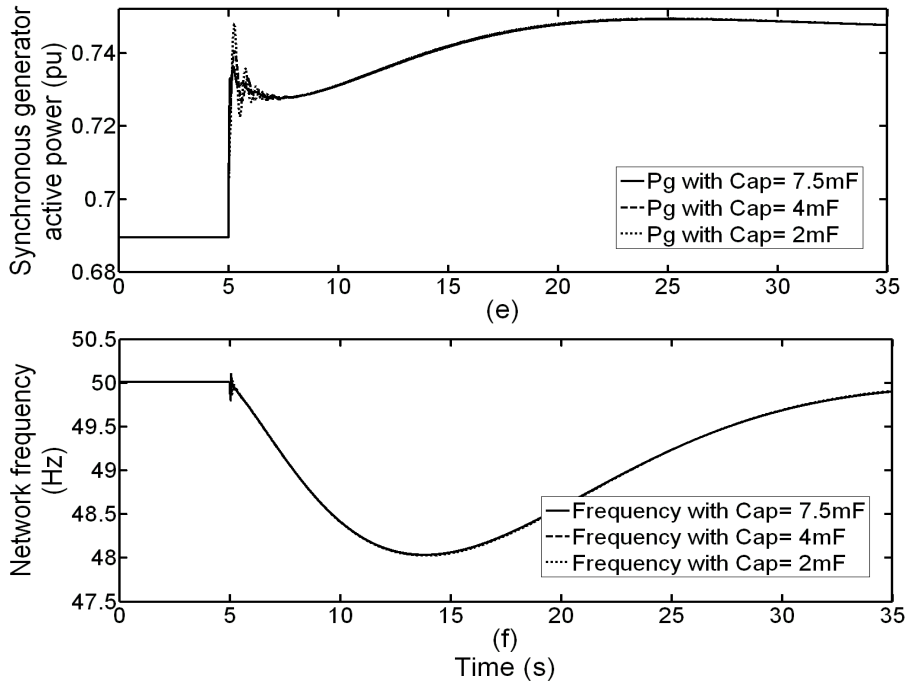

Figure 5.7 Comparison of different capacitance for the INEC: (a) SG rotor speed; (b) SG load angle (c) HVDC DC link voltage; (d) VSC_1 active power; (e) SG active power; (f) Network frequency.

ii.AC Faults

Figure 5.8 and Figure 5.9 compare the INEC performance for an electrically "close" fault (solidly connected short circuit, resulting in higher voltage drop) and a "remote" fault (a resistive fault with a value of 20 **Ω**, resulting in lower voltage drop). In both cases, three-phase faults are initiated at t=1s and cleared at t=1.14s. Note that power system stabiliser for the synchronous generator is disabled.

As shown in the zoomed Figure 5.8(a), the fault results in an AC voltage amplitude drop of 75% at busbar B_2. Generator rotor speed, with emulated inertia H_{VSC}=3s, recovers more slowly than for cases with lower values of H_{VSC} from the speed increase due to the fault, with relatively lower first and subsequent swing magnitudes, as observed in Figure 5.8(b). This actually exhibits the electro-mechanical effect of system inertia. Figure 5.8(c) illustrates the load angle of SG for different values of emulated inertia in the post-fault period. Figure 5.8(e) presents the VSC_1 active power output with and without INEC, which influences behavior throughout each of the three simulation cases. This is directly reflected in Figure 5.8(f), where the SG active power output with larger inertia H_{VSC}=3s changes less than for cases where H_{VSC}=1s and for the case where there is no INEC. During the fault, VSC_1's current is saturated (i.e. current limited) due to the

significant under-voltage, therefore the active powers for H_{VSC}=3s, 1s and 0 remain the same during this time. It is interesting to observe VSC_1's active power in the post-fault state with a larger inertia H_{VSC}=3s. The output power, immediately following fault clearance, is reduced (after an initial surge).This phenomenon is in accordance with the well-known equal area criterion for the SG, which specifies that the kinetic energy collected by the SG during the fault (when the machine is accelerating) must be released after the fault clearance (deceleration), and so the reduction of VSC_1's active power output aligns with this. This is important with respect to the first swing stability of a power system. The network frequency at B_2 is shown in Figure 5.8(g), which obviously has a similar trend to SG rotor speed.

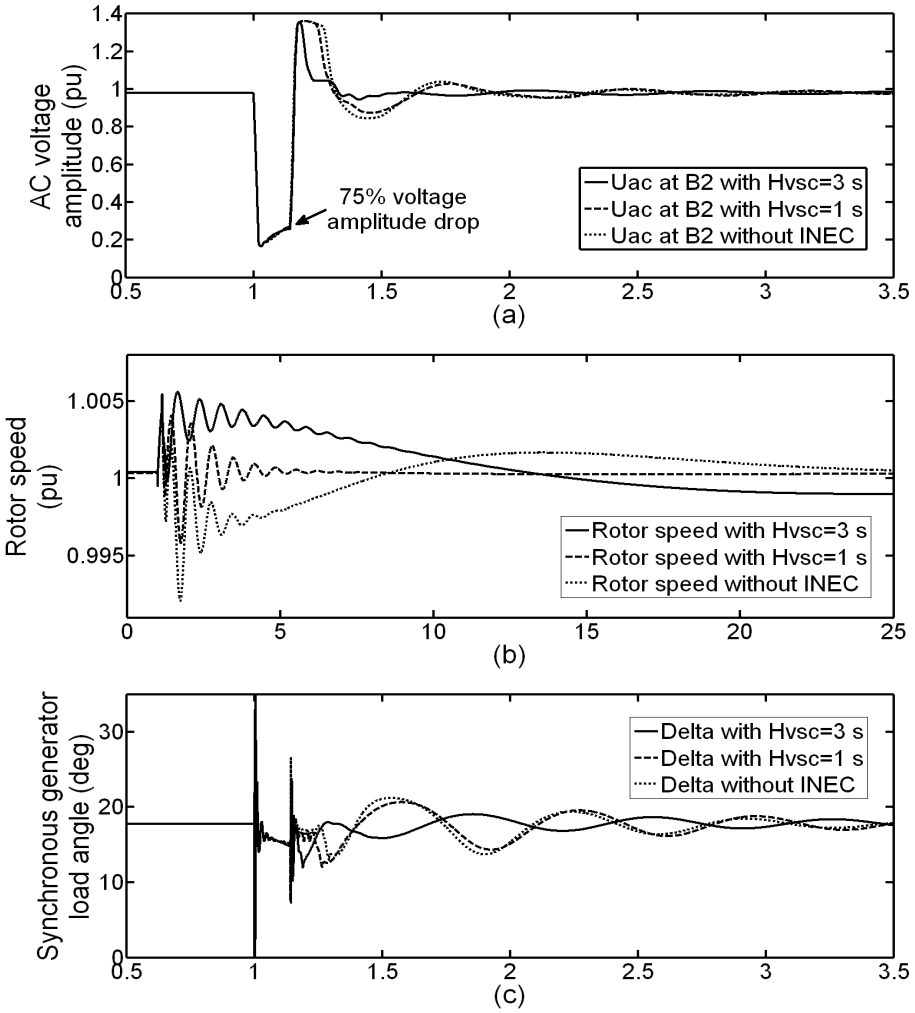

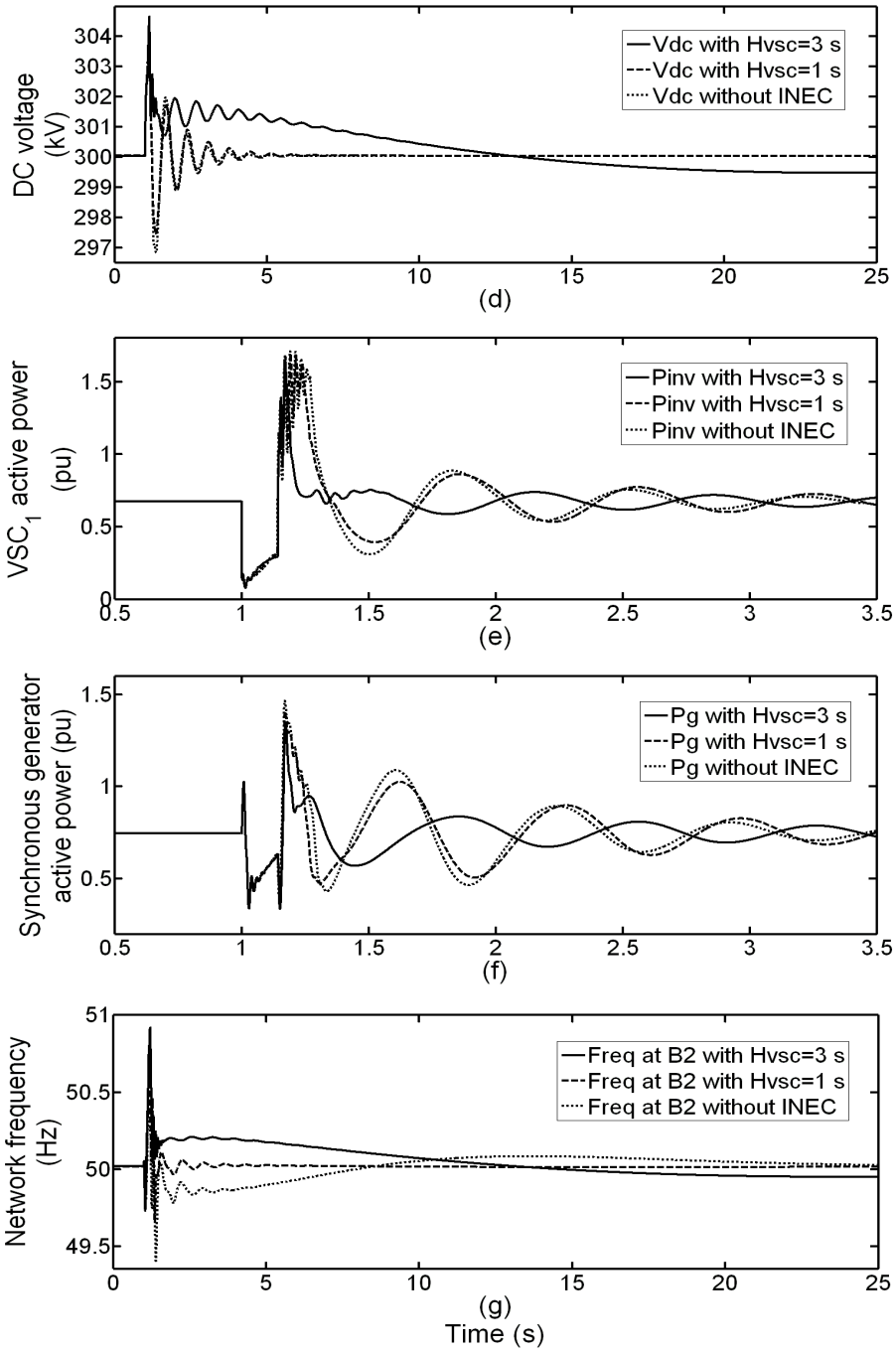

Figure 5.8 INEC response for 140-ms three-phase-to-ground close fault: (a) zoomed AC voltage amplitude at B2; (b) SG rotor speed; (c) zoomed SG load angle (d) HVDC DC link voltage; (e) zoomed VSC1 active power; (f) zoomed SG active power; (g) Network frequency.

The effectiveness of the INEC strategy in enhancing system stability for distant faults with relatively lower voltage drop of 25% is more obvious, as shown in Figure 5.9. The distant fault is represented by a resistive fault applied at B_2 leading to a voltage drop of 25% as shown in zoomed Figure 5.9(a). VSC_1's current output is not saturated due to the relatively smaller voltage drop. It is clear, in the circled region of Figure 5.9(e), that

during the fault (from t=1s to 1.14s) the VSC_1 effectively interacts with the network in terms of providing different instantaneous active power during the period of fault application for different emulated inertia time constants. This leads to different SG load angle and active power output behaviours as shown in Figure 5.9(c) and Figure 5.9(f). As illustrated in Figure 5.9(b) and Figure 5.9(g) respectively, the SG rotor speed and network frequency drops associated with larger emulated inertia H_{VSC}=3s are significantly less than for H_{VSC}=1s. As observed in Figure 5.9(d), the DC voltage drop for larger values of emulated inertia is higher in order to supply relatively higher values of instantaneous active power as shown in Figure 5.9(e). It is interesting to see that the network voltage at B_2 as shown in Figure 5.9(a), is also influenced by different values of emulated inertia due to the interactions between VSC_1 and the SG.

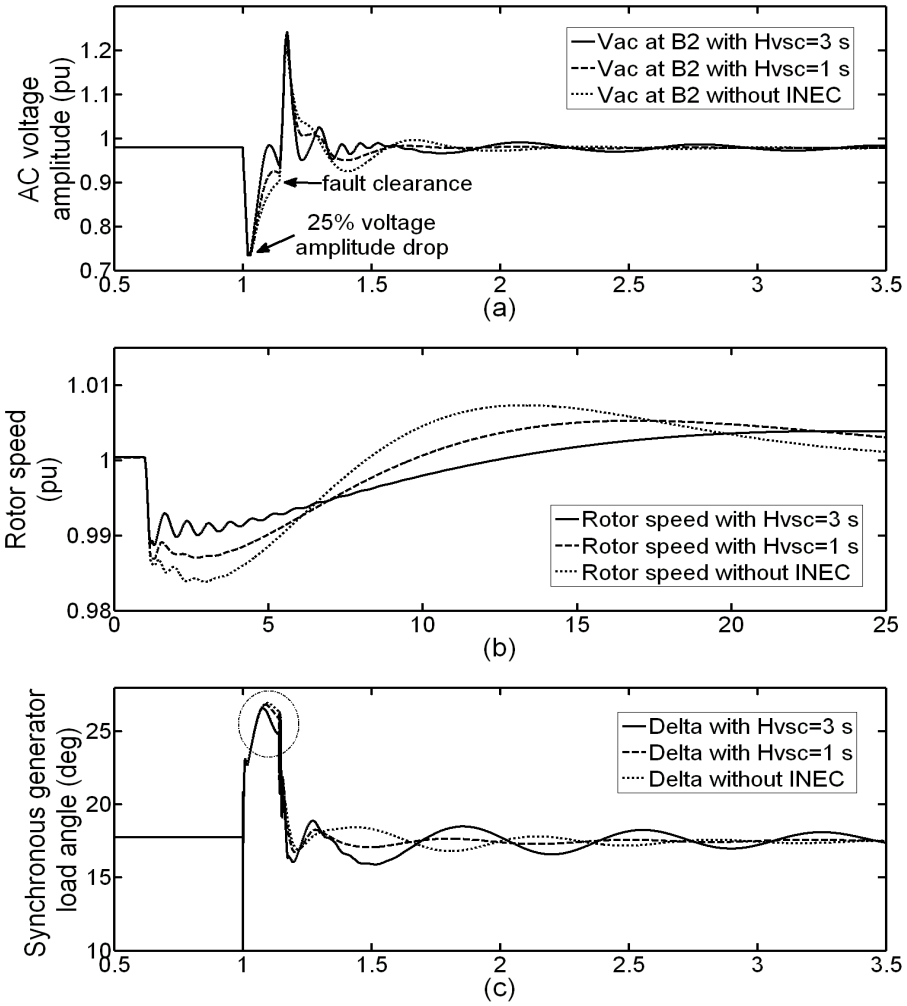

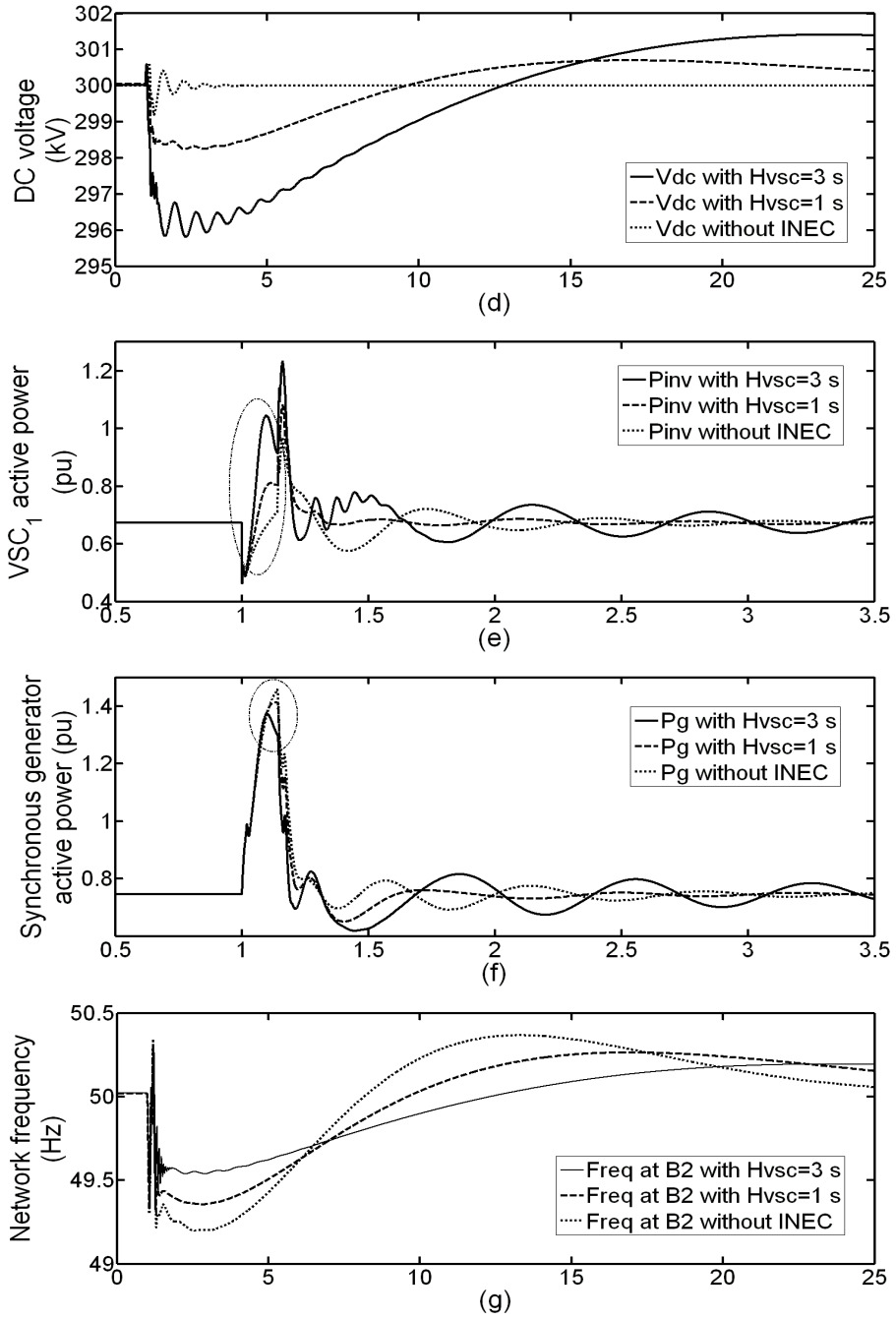

Figure 5.9 INEC response for 140-ms three-phase-to-ground distant fault: (a) zoomed AC voltage amplitude at B2; (b) SG rotor speed; (c) zoomed SG load angle (d) HVDC DC link voltage; (e) zoomed VSC1 active power; (f) zoomed SG active power; (g) Network frequency.

The AC fault simulation study clearly shows the INEC strategy can assist in increasing system fault ride-through capability. The inertial response from VSC-HVDC can be provided indefinitely, although the first few seconds are most important for assisting grid stability. This behaviour is therefore similar to the "natural" inertial response (from the kinetic energy of the rotor) provided by a synchronous machines, with the kinetic energy equivalent being the stored electrostatic energy in the capacitor of

the DC system – which is exercised according to the terminal voltage across the capacitor.

5.3 Inertia Emulation Control Strategy for Multi-terminal HVDC Systems

The inertia emulation control algorithm as designed in (23) can also be implemented in multi-terminal HVDC systems (MTDC). In an MTDC application, the capacitor number N as presented in (23) becomes the total number of capacitors in the entire MTDC network (e.g. N=4 for a four-terminal MTDC system). As a continuation of the INEC designed for point-to-point VSC-HVDC as demonstrated in section 5.2, this section extends the INEC application for point-to-point HVDC system to MTDC systems and studies the operation and impact of an MTDC system with INEC in a multi-machine power system using simulations.

5.3.1. INEC implementation within an MTDC converter

In order to enable an MTDC converter to provide an inertial response in response to grid disturbances, the overall DC voltage will obviously not be maintained constant at all times. Instead, the INEC dictates the MTDC network voltage; therefore the MTDC should have one and only one grid side VSC (GVSC) equipped with a DC voltage regulator that would be modified to provide the INEC response functionality. The control loops for this converter's INEC are expected to be the same as those shown in Figure 5.1 for the point-to-point VSC-HVDC's converter.

5.3.2. Trade-off between C_{DC} and V_{DC}

Based on (23) within the description of the INEC algorithm, a range of inertia constants from 0s to 4s along with the associated resultant DC voltage changes for specific frequency changes are plotted in Figure 5.10. For each MTDC terminal, the capacitance of 5 mF, as shown in Figure 5.10(a), is compared to another case where the capacitance at each terminal is 2mF, as shown in Figure 5.10(b). It can be observed that for a specific frequency deviation, relatively large capacitors can be used in order to lower DC voltage variations to provide the same emulated inertia time constants. The tradeoff between capacitor size and maximum allowable DC voltage variation has to be investigated further and the selection of the appropriate capacitance justified. Increased

capacitance could have detrimental effects in the event of a DC-side fault, as the stored energy from the capacitor will discharge into the fault.

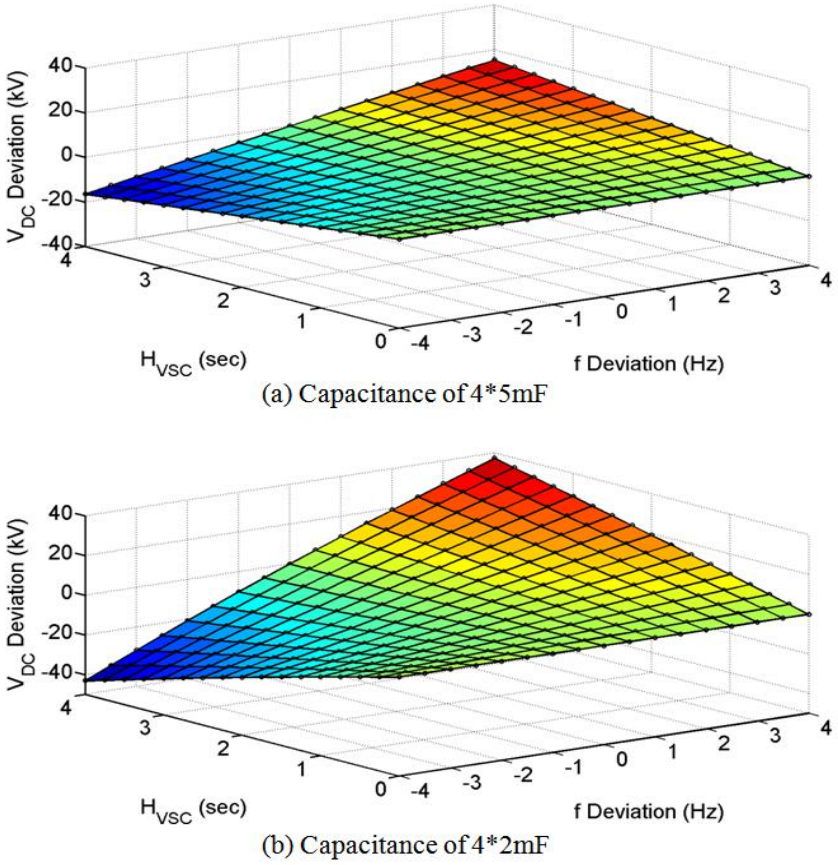

Figure 5.10 Three-dimensional relationship between emulated inertia, frequency and DC voltage deviations from rated value (comparing effect of 2mF and 5mF for 400 MVA 400 kV MTDC VSC converter)

5.3.3. Simulation results

Simulation scenarios as illustrated in Figure 5.11 are carried out in SimPowerSystems in Matlab to validate the INEC for the MTDC systems and verify the effectiveness of contributing emulated inertial responses. The four VSCs for the MTDC system are each rated at 400 MVA. The 600 MVA rated SG_1 and 200 MVA rated SG_2, which possess inertia time constants of 1.5s and 3s, respectively, are modeled using a seventh-order model with IEEE parameters in accordance with those stated in [7]. The 400 kV transmission network interconnects two MTDC GVSCs and two SGs with loads (1, 2 and 3), via lines with specific lengths as shown in Figure 5.11. All the parameters on the simulated MTDC and the connected AC system can be found in TABLE V and TABLE VI in the Appendix.

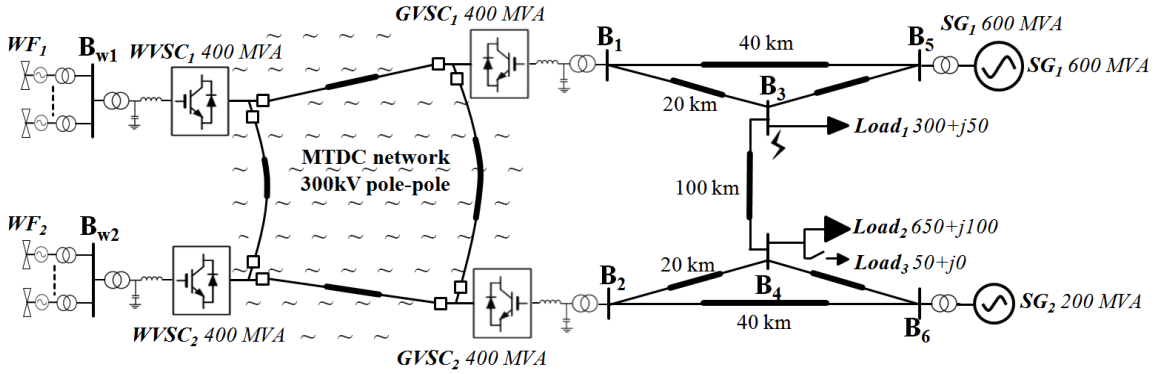

Figure 5.11 Test scenario for the INEC implementation in the MTDC system

i. Load increase

Figure 5.12 shows the simulation comparisons between $G_{VSC1}$when a DC voltage controller is used, regulating its node DC voltage level to a constant reference value of 301 kV (H_{VSC1}=0), and the same G_{VSC1} when equipped with INEC, emulating an inertia time constant of H_{VSC1}=3s and H_{VSC1}=1.5s. The load increase is initiated by switching in Load3 (50 MW), representing 5%of the total load. Figure 5.12(a) illustrates the voltage change resulting from the sudden load increase, and a minor voltage drop of 0.02 pu can be observed. As shown in Figure 5.12(b) and (c), the MTDC terminal DC voltage level remains constant under the traditional control scheme when the sudden load change is initiated, whereas those with the INEC are controlled to drop. As observed in Figure 5.12(d), a sharp power impulse is output from $GVSC_1$ when the INEC is applied. This is to facilitate the inertial response, whereas $GVSC_1$using traditional DC voltage control does not change. Due to the inertial interactions between $GVSC_1$ and both of the SGs connected to the MTDC network, the output active power from SG_1 and SG_2 are significantly reduced as observed in Figure 5.12(c) and (d). By comparing the active power outputs of $GVSC_1$ and the two SGs, similarities are found in the first 2s after the load change for both. However as SG_1 and SG_2 are configured with primary controllers (steam turbine governors in this case), the extra active power required by the increased load is ultimately provided by the SGs. In contrast, $GVSC_1$ provides a short-term inertial active power impulse using the inherent energy storage and exchange characteristics of the MTDC capacitors. The rotor speed drops of both SGs are as shown in Figure 5.12(h), and the load angles (with respect to SG_1's emf angle) of the GVSCs and SGs are shown in Figure 5.12(i)(j)(k) respectively, as well as the network frequency drop at busbar B_3. As shown in Figure 5.12(l), the frequency drops are reduced by the emulated inertia

contribution from $GVSC_1$ of the MTDC. Despite only providing an inertial response for a relatively short time period, there is a significant benefit to the dynamic frequency response of the connected multi-machine system.

Figure 5.12(e) shows that the active powers of $WVSC_1$, $WVSC_2$ and $GVSC_2$ do not response to the load increase. It verifies that the INEC decouples the effects of the disturbances from the onshore grid side to the offshore wind farm side, while still contributing an emulated inertia, an attractive feature of the INEC. The INEC can be equally applied to $GVSC_2$ also; this will be studied in the next section relating to fault tests.

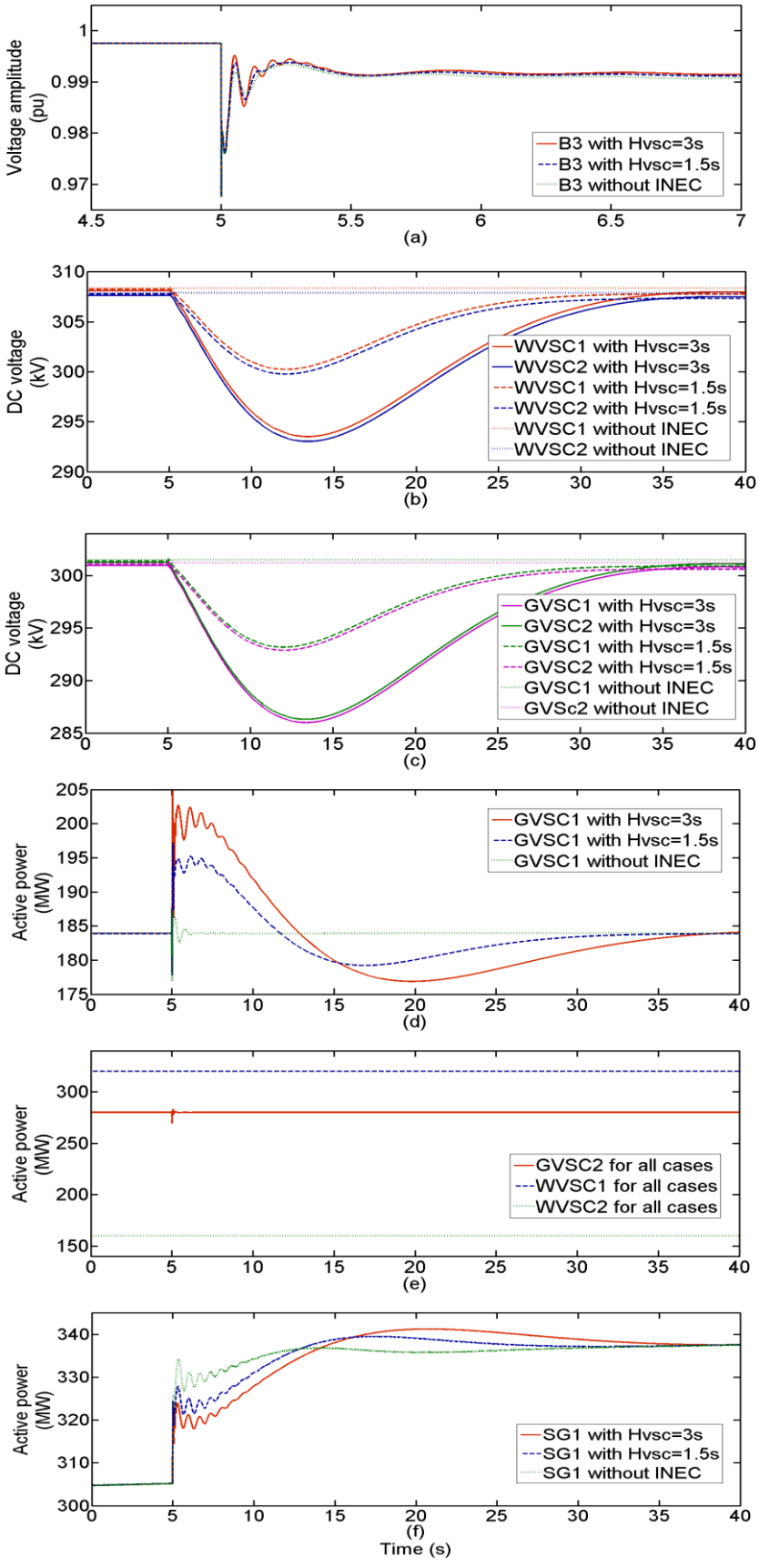
Voltage amplitude (pu)
B3 with Hvsc=3s
B3 with Hvsc=1.5s
B3 without INEC
(a)
DC voltage (kV)
WVSC1 with Hvsc=3s
WVSC2 with Hvsc=3s
WVSC1 with Hvsc=1.5s
WVSC2 with Hvsc=1.5s
WVSC1 without INEC
WVSC2 without INEC
(b)
DC voltage (kV)
GVSC1 with Hvsc=3s
GVSC2 with Hvsc=3s
GVSC1 with Hvsc=1.5s
GVSC2 with Hvsc=1.5s
GVSC1 without INEC
GVSc2 without INEC
(c)
Active power (MW)
GVSC1 with Hvsc=3s
GVSC1 with Hvsc=1.5s
GVSC1 without INEC
(d)
Active power (MW)
GVSC2 for all cases
WVSC1 for all cases
WVSC2 for all cases
(e)
Active power (MW)
SG1 with Hvsc=3s
SG1 with Hvsc=1.5s
SG1 without INEC
(f)
Time (s)

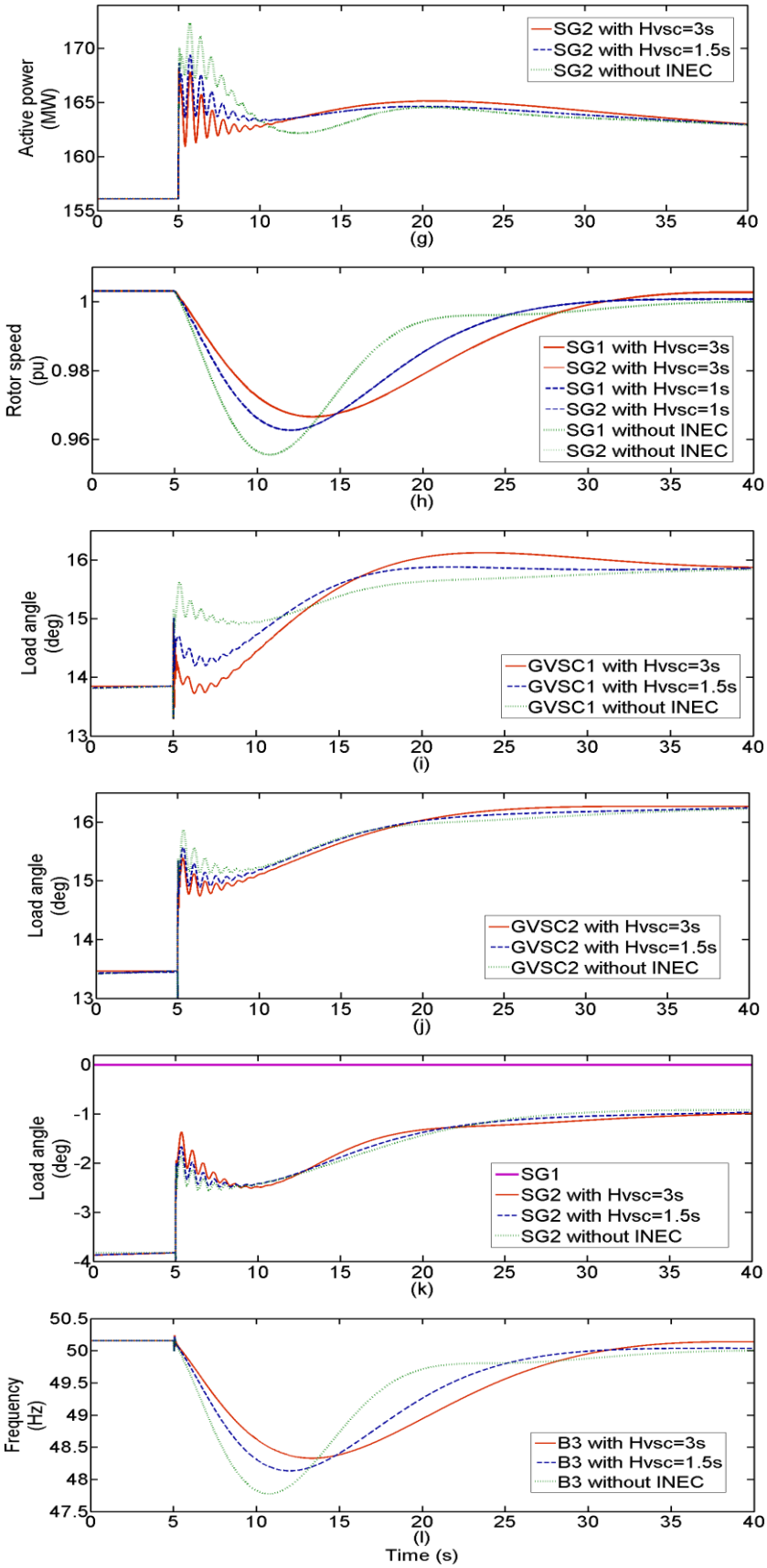

Figure 5.12 5% Load increase by switching on Load3

ii.Fault study

Figure 5.13 shows the simulation results from fault studies with the INEC applied to $GVSC_2$ (H_{VSC2}=3s, 1.5s and 0). The fault is triggered at busbar $B_{3,}$ as illustrated in Figure 5.13, and lasts for 140 ms before being cleared. As demonstrated in section 5.2, INEC can cater for bolted short circuit faults due to current limiting from the VSC. In the case study reported here, a resistive fault is applied. This results in a 0.5 pu voltage amplitude drop at B3, as shown in Figure 5.13(a).

It is clearly shown in Figure 5.13(b) and (c) that the DC voltage levels for each of the four VSC nodes are not affected by the fault when "traditional" control is applied, whereas when $GVSC_2$ has INEC enabled, with H_{VSC2}=3s and H_{VSC}=1.5s as shown in Figure 5.13, the voltage varies. It is clear that the active power interactions between $GVSC_2$ and the SGs as shown in Figure 5.13(d)(f)(g) respectively, and the rotor speed variations and frequency variations at busbar B_3, as illustrated in Figure 5.13(h) and (k) respectively, are significantly damped and by the emulated inertia provided by $GVSC_2$. The lower degree of load angle variations for the case with H_{VSC2}=3s than those with H_{VSC2}=1.5s and 0, observed in Figure 5.13(i)(j)(h) verify the stabilising effect of the INEC for the fault tests. It is clear that the GVSCs equipped with INEC interact and counter-balance the transient and dynamic changes resulting from the fault. The active power levels of $WVSC_1$, $WVSC_2$ and $GVSC_1$ remain the same for all three cases, as shown in Figure 5.13(e).

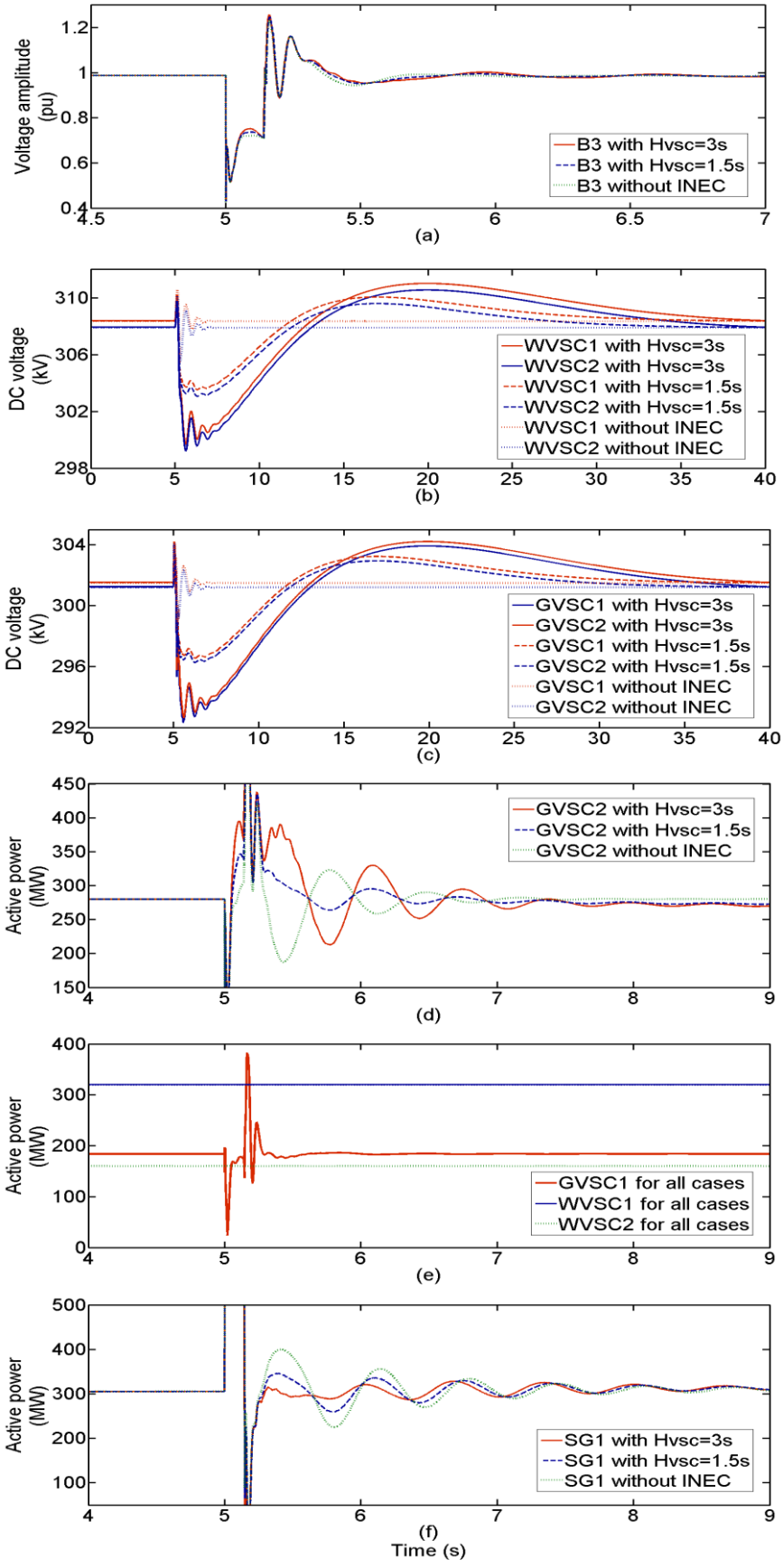
Voltage amplitude (pu)
B3 with Hvsc=3s
B3 with Hvsc=1.5s
B3 without INEC
(a)
DC voltage (kV)
WVSC1 with Hvsc=3s
WVSC2 with Hvsc=3s
WVSC1 with Hvsc=1.5s
WVSC2 with Hvsc=1.5s
WVSC1 without INEC
WVSC2 without INEC
(b)
DC voltage (kV)
GVSC1 with Hvsc=3s
GVSC2 with Hvsc=3s
GVSC1 with Hvsc=1.5s
GVSC2 with Hvsc=1.5s
GVSC1 without INEC
GVSC2 without INEC
(c)
Active power (MW)
GVSC2 with Hvsc=3s
GVSC2 with Hvsc=1.5s
GVSC2 without INEC
(d)
Active power (MW)
GVSC1 for all cases
WVSC1 for all cases
WVSC2 for all cases
(e)
Active power (MW)
SG1 with Hvsc=3s
SG1 with Hvsc=1.5s
SG1 without INEC
(f)
Time (s)

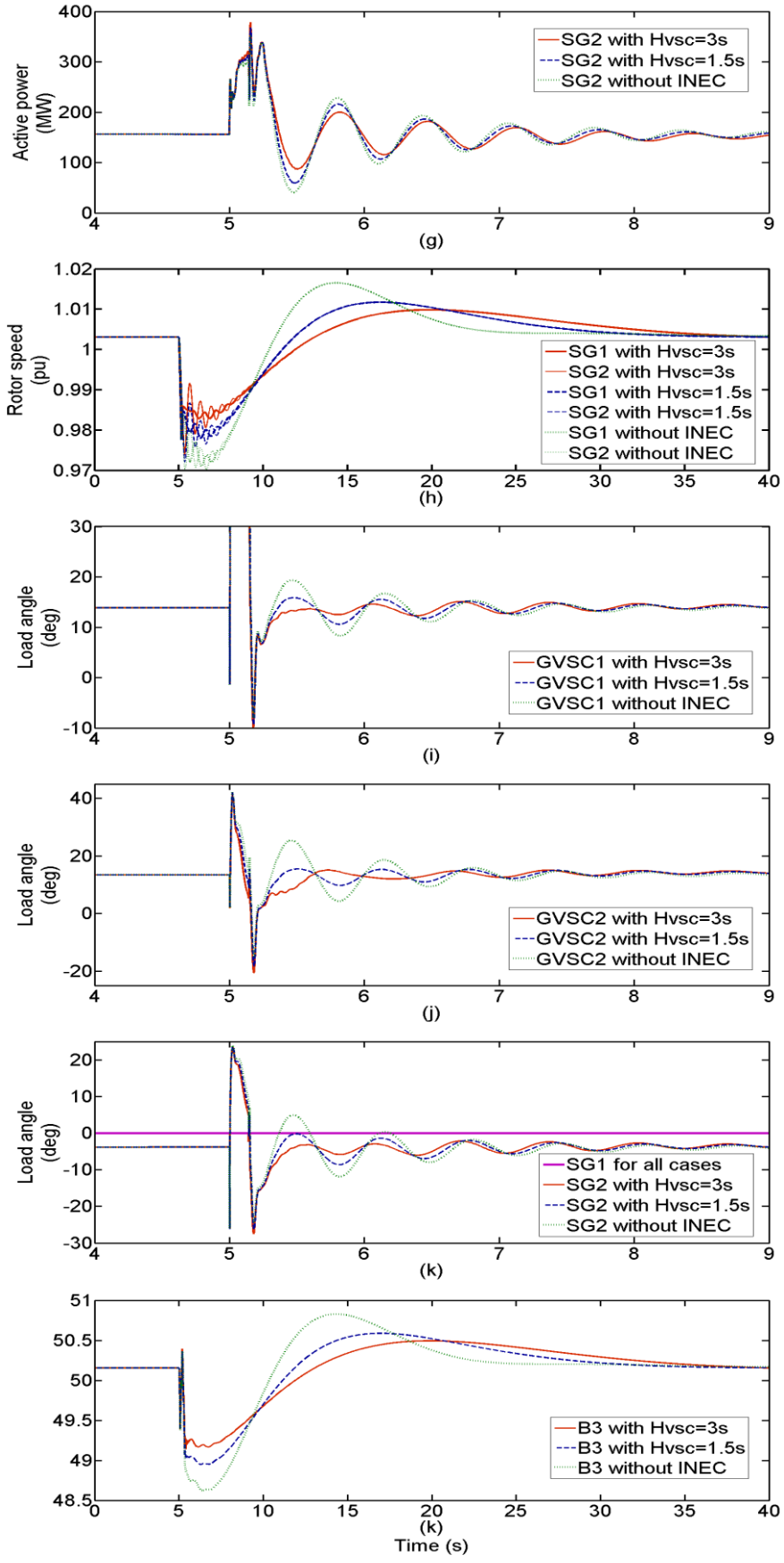

Figure 5.13 Resistive fault test (30% voltage drop for 140ms)

5.4 Summary

An inertia emulation control (INEC) strategy for both conventional point-to-point VSC-HVDC and multi-terminal VSC-HVDC transmission systems has been proposed and demonstrated in this chapter. In summary, INEC possesses the following significant features:

- Inertia time constants, H_{VSC}, can be specified and varied;
- DC voltage variations can be limited to fall within a specified range during transients using INEC;
- The INEC provided at the inverter terminals of the HVDC links or MTDC networks has no impact on the rectifier-side offshore wind power system.

Simulations verify that the INEC for VSC-HVDC and VSC-MTDC transmission system is capable of interacting with connected generators, counteracting, and damping generator rotor speed (and system frequency) changes. It allows the VSC-HVDC or VSC-MTDC converter to contribute to both the damping of low-frequency oscillations, enhancement of the primary frequency control of the AC networks and consolidation of system fault ride-through capability. In future, this is likely to become more important due to the continuing trend of HVDC interconnections and use of MTDC networks and also to address the anticipated replacement of conventional generation with renewable generation.

References

[1] Kayikci, M.; Milanovic, J.V., "Dynamic Contribution of DFIG-Based Wind Plants to System Frequency Disturbances," *IEEE Trans. Power Syst.*, vol.24, no.2, pp.859-867, May 2009.

[2] Conroy, J.F.; Watson, R., "Frequency Response Capability of Full Converter Wind Turbine Generators in Comparison to Conventional Generation," *IEEE Trans. Power Syst.*, vol.23, no.2, pp.649-656, May 2008.

[3] Miao, Z.X.; Fan L.L.; Osborn, D.; Yuvarajan, S., "Wind Farms With HVdc Delivery in Inertial Response and Primary Frequency Control," *IEEE Trans. Energy Convers.*, vol.25, no.4, pp.1171-1178, Dec. 2010.

[4] Bennett, S., "Development of the PID controller," *IEEE Trans. Control Syst.*, vol.13, no.6, pp.58-62, 64-5, Dec 1993.

[5] MathWorks, "Hydraulic Turbine and Governor," Online Available [assessed 01/08/2011]: http://www.mathworks.com/.

[6] IEEE Working Group on Prime Mover and Energy Supply Models for System Dynamic Performance Studies, "Hydraulic Turbine and Turbine Control Models for Dynamic Studies," *IEEE Trans. Power Syst.*, Vol.7, No.1, pp. 167-179, February, 1992.

[7] Anderson, P.; Fouad, A.A., *Power System Control and Stability*. Ames, Iowa, U.S.A: The Iowa State University Press, 1977.

Chapter 6

Conclusions and future work

6.1 Conclusion

Environmental concerns, economic incentives and political pressures are acting to increase the amount of power sourced from renewables. VSC-HVDC transmission systems, as a flexible and proven technology, will be progressively employed within future transmission grids to both facilitate the connection of renewables and to increase the interconnection between previously separate systems.

This thesis has firstly introduced the present power system context, with a focus on the UK and European situations. In particular, the development of complex offshore DC networks to accommodate wind farms and system interconnection has been described, and the impact that this will have, in terms of an overall reduction in the effective inertia within the power system due to the power converter interfaced renewable generation, has been highlighted as a key future challenge.

To underpin the work reported in the thesis, a comprehensive review of power electronics technology, covering semiconductor devices, converter configurations, and control systems was presented. With specific relevance to the contributions reported in the thesis, a detailed treatment of fundamental control system for HVDC VSC converters was included, which encompassed VSC power capabilities, control vectors, inner controllers and various outer controllers. The range of applications of VSC technologies to power systems was also briefly described.

Moving on to the main body of the thesis, a comprehensive literature review focussed upon control system designs for VSC-HVDC systems was presented, and the range of topics addressed included synthetic inertia control schemes, primary frequency regulation strategies for renewable generation, energy storage, and load shedding schemes. One of the main findings of the review is that "short-term" synthetic inertia associated with wind power generation is normally provided by varying the generator rotor speed with grid frequency, whereas "longer-term" primary frequency support/response functions is often achieved (or proposed as being achievable by) routinely operating the generators at power outputs less than optimal value to give power "headroom" that can be called upon to provide long-term frequency support. The provision of synthetic inertia contribution from an LCC-HVDC converter connecting a wind farm to a host AC system was reviewed: this is achieved by communicating the grid frequency derivatives to the wind farm to release extra power when necessary, using the

LCC-HVDC to deliver this to the main system. However, the provision of synthetic inertia from VSC-HVDC converters is rarely covered in the literature, although some manufacturers are now developing products that are claimed to provide this function.

The literature review also covers conventional control strategies for multi-terminal HVDC networks. An example of a six-terminal HVDC system is used to demonstrate the operation of two previously reported "DC voltage margin control" and "DC voltage droop control" schemes. The advantages and disadvantages for each of these schemes are demonstrated, and it is concluded that the existing schemes are generally effective methods for controlling multi-terminal DC grids, but with some drawbacks. This justifies the requirement for an improved means of control that address the identified disadvantages of the aforementioned schemes.

Consequently, a communication-based direct current matching control (DCMC) scheme for multi-terminal HVDC networks has been proposed. The major advantages, in terms of the operational performance of the DCMC scheme, are summarised below:

- The centrally implemented and configurable sharing factors result in great flexibility and convenience for dispatching Grid side VSCs' DC currents. Furthermore, predictions of network current/power flows are obtained by the DCMC, which is an advantage over "DC voltage droop control" schemes.

- The scheme has the ability to implement near-real-time matching of the DC current outputs of grid side VSCs with those of the wind farm side VSCs, resulting in reduced voltage variations, when compared to "DC voltage margin control" schemes.

It is proposed that the DCMC scheme employing communications, with further demonstration and prototyping, will be suitable for operation of a practical MTDC system.

To address the aforementioned issues of reduced system inertia, the second main contribution reported in the thesis is concerned with the development of a novel inertia emulation control (INEC) system for VSC-HVDC transmission systems. INEC employs the electro-static energy stored in the DC capacitors to enable the inverter to provide an inertial response to load and frequency changes in the power system, in a manner similar to that exhibited by a synchronous generator. The INEC varies the DC voltage to exploit

the energy stored in the DC link capacitance; the amount of energy exercised varies with the magnitude of the inertia time constants being emulated. INEC possesses the following significant features:

- Inertia time constants can be specified and varied;
- DC voltage variations can be limited to fall within a specific range;
- The INEC provided at the inverter terminals of the HVDC links has no impact on the rectifier-side offshore wind power system (or remotely connected AC system in a point-to-point or multi-terminal system linking separate AC systems).

Simulations verify that the INEC system is capable of supporting and reducing the impact of system transients on connected generators; counteracting, and damping generator rotor speed (and system frequency) changes. It allows the VSC-HVDC system to contribute to the damping of low-frequency oscillations, enhancement of the primary frequency control of the AC networks and support overall system fault ride-through capability. In the future, this is likely to become more important due to the increasing amounts of HVDC interconnections and also that conventional generation is likely to be replaced by renewable generation (with lower, or no, inherent inertia) in future. The challenges of the proposed method are believed to be the large value of the DC capacitance which has to be added. Consequently more practical constraints need to be considered in terms of additional capital investment, DC circuit protections and converter and cable insulation and reinforcement.

The thesis paper also proposes a *generic* inertia emulation controller for multi-terminal HVDC transmission system, which extends the applicability from point-to-point systems. The INEC allows any specific AC grid-interface converter within a multi-terminal DC grid to contribute an inertial response, through varying the DC voltage levels on the DC side to exchange energy with the AC side, without modification being required for the multi-terminal DC hardware. The multi-terminal INEC system possesses the following features:

- Interconnected synchronous generators' rotor speed variations during system disturbances (e.g. load changes, faults) are effectively damped by the INEC;

- Power network frequency deviations, and busbar load angle deviations, during system disturbances are effectively stabilised by the INEC;

- The INEC retains the attractive decoupling feature of VSCs, which isolates disturbances on one system from the other(s).

6.2 Future Work

VSC-HVDC converters can obviously provide a number of system advantages due to their abilities to control real and reactive power flow magnitudes and directions, their inherent high-performance control systems and fast converter switching speeds, allowing rapid reactions to detected system conditions and requirements. Future areas of activity, which follow on naturally from the activities and outcomes reported in this thesis, are listed below:

- The DC side capacitors on VSC-HVDC DC side act as temporary energy storage, and their characteristics play a critical role in defining the HVDC systems' DC dynamic performance. These capacitors and their capabilities can also be exploited for provision of further AC side support. For example, in addition to the synthetic inertia contribution, DC capacitors in the VSC-HVDC DC link could be also used as voltage harmonic filters or power ripple filters for the connected AC systems.

- VSCs using DC capacitor energy storage capability could also be used for power damping purposes. For example, they can be exploited to damp the AC side low-frequency sub-synchronous power oscillations, by designing a proper VSC converter system and choosing an appropriate value for DC capacitance;

- The proposed INEC strategy can be accompanied and extended by primary frequency support functions from wind farm side (or indeed from other connected AC systems if permissible) to provide an AC system(s) with not only synthetic inertia but also primary frequency control and support.

- The INEC strategy could be extended to application to back-to-back converter pairs using fully rated converters used with wind power generators to contribute a similar inertial response to the grid. To do this, similar modifications to those applied in the HVDC INEC needs to be applied to the grid connected wind VSC's DC voltage controller.

- The INEC strategy may be applied to doubly fed induction generator (DFIG) based wind turbines; however, many modifications to the INEC strategy would be required to achieve this, such as taking account of the power flow through both the VSC converter pair and the directly coupled stator winding. The INEC algorithm for HVDC system would require to be significantly modified in order to be adapted to the specific properties of DFIGs.

- The INEC strategy could be used for VSC converter interfaced energy storage devices and compensation devices with DC capacitors on the DC side (e.g. fuel cells, static compensators, etc.). Similarly, the INEC algorithm could be applied to the VSC DC voltage controller of these devices to synthesise inertia.

- The DCMC control scheme for multi-terminal HVDC networks could be applied to lower voltage multi-terminal DC distribution systems (or micro-grids) and DC distribution systems as proposed for use on marine and aircraft applications. With shorter geographical distances between converters, the communications system requirements and latency problems would be less pressing, which may result in better performance and more attractive economic arguments for adoption of the DCMC scheme.

Appendices

Appendix A Park Transformation

The Park Transformation is a mathematical technique which is used to simplify three-phase circuits. It has been commonly employed in the modelling of electric machines and more recently to facilitate the control of three-phase converters. In the situation where there are balanced three-phase voltages or currents, the Park transformation can be used to reduce three time-varying AC quantities to two DC quantities by projecting the three-phase quantities to a rotating reference frame.

The transformation equations are described in a matrix as follows:

$$T = \frac{2}{3}\begin{bmatrix} \sin(\omega t) & \sin(\omega t - \frac{2}{3}\pi) & \sin(\omega t + \frac{2}{3}\pi) \\ \cos(\omega t) & \cos(\omega t - \frac{2}{3}\pi) & \cos(\omega t + \frac{2}{3}\pi) \\ 1/2 & 1/2 & 1/2 \end{bmatrix} \quad (1)$$

where **T** is the Park Transformation matrix, ω is the voltage angular speed.

In the control of inverters, the voltages are expressed in dq coordinates under the rotating reference frame which is synchronised with the angular frequency of the AC system voltages. To transfer the three-phase voltages from abc coordinates to dq coordinates as shown in Figure A1, the Park Transformation is performed:

$$\begin{bmatrix} v_d \\ v_q \end{bmatrix} = T \begin{bmatrix} v_a \\ v_b \\ v_c \end{bmatrix} \quad (2)$$

where v_d and v_q is d-axis and q-axis voltage vector.

To recover the three-phase voltages from dq coordinates, the Inverse Park Transformation is performed:

$$\begin{bmatrix} v_a \\ v_b \\ v_v \end{bmatrix} = T^{-1} \begin{bmatrix} v_d \\ v_q \end{bmatrix} \quad (3)$$

A three-phase voltage phasor rotating at synchronous speed ω_s can be expressed as:

$$\begin{cases} v_a = \sqrt{2} \cdot V \cos(\omega_s t) \\ v_b = \sqrt{2} V \cdot \cos(\omega_s t + \frac{2}{3}\pi) \\ v_c = \sqrt{2} V \cdot \cos(\omega_s t - \frac{2}{3}\pi) \end{cases} \quad (4)$$

where V refers to the three phase rms voltage.

The application of the Park Transformation results in voltage vectors in dq coordinates as follows:

$$\begin{cases} v_d = \frac{2\sqrt{2}}{3} V\left[\cos(\omega_s t)\sin(\omega t) + \cos(\omega_s t + \frac{2}{3}\pi)\sin(\omega t + \frac{2}{3}\pi) + \cos(\omega_s t - \frac{2}{3}\pi)\sin(\omega t - \frac{2}{3}\pi)\right] \\ v_d = \frac{2\sqrt{2}}{3} V\left[\cos(\omega_s t)\cos(\omega t) + \cos(\omega_s t + \frac{2}{3}\pi)\cos(\omega t + \frac{2}{3}\pi) + \cos(\omega_s t - \frac{2}{3}\pi)\cos(\omega t - \frac{2}{3}\pi)\right] \end{cases} \quad (5)$$

Equation (5) is further simplified into (6):

$$\begin{cases} v_d = \sqrt{2} \cdot V \cos(\omega_s - \omega) \\ v_q = \sqrt{2} \cdot V \sin(\omega_s - \omega) \end{cases} \quad (6)$$

Focusing on the control of a VSC converter, the phase-locked loop (PLL) provides a dynamic angular speed ω_s that is synchronous with the grid voltage ω for Park Transformation, therefore (6) can be express in (7) with $\omega_s = \omega$.

$$\begin{cases} v_d = \sqrt{2} \cdot V \cos(\omega - \omega) = \sqrt{2} \cdot V \cos(0) = \sqrt{2} V \\ v_q = \sqrt{2} \cdot V \sin(\omega - \omega) = \sqrt{2} \cdot V \sin(0) = 0 \end{cases} \quad (7)$$

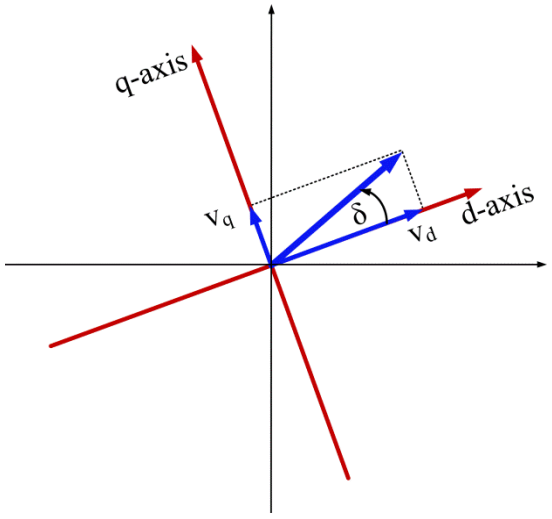

Figure A1 Three phase voltage under dq coordinate

From (7), it can be ascertained that v_d represents the amplitude of the three phase voltages in a steady state without voltage phase angle transient change or unbalance. In contrast, v_q actually represents the three-phase voltage phase angle, which is equal to 0 in the reference conditions, but a non-zero value appears whenever there is a voltage phase change from the reference value (0).

This can be illustrated in Figure A1 where an abc to dq transformation is performed. When at t=0.05s the three-phase voltage amplitude is increased from 1 pu to 1.5pu; it can be seen that d-axis vector v_d is increased accordingly. When at t=0.1s, the voltage phase angle is shifted forward by 30 degree, the q-axis vector v_q begins to increase from 0 to 0.8 pu. It should note that the conventional PLL normally assumes a three-phase "balanced" voltage to derive the voltage vectors v_d and v_q as depicted in (1), when there is a voltage unbalance (as in the example as shown in Figure A2 from t=0.15s), the voltage vectors will oscillate resulting in unstable control of the converter. This voltage unbalance should be corrected immediately to ensure the correct performance of a VSC converter.

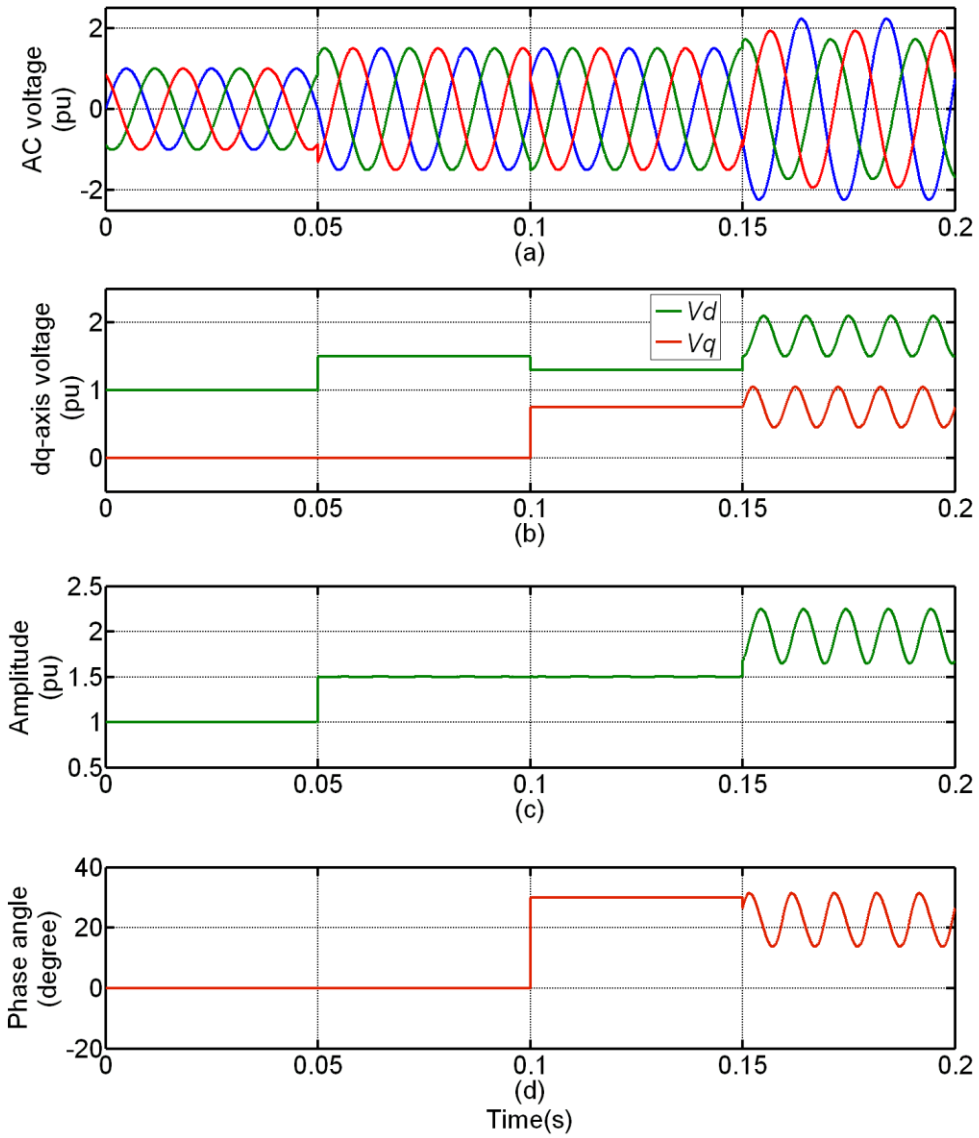

Figure A2 Examples of abc to dq transformations in response to voltage amplitude changes, phase angle changes and voltage unbalance conditions

Appendix B Simulation Parameters

TABLE I

PARAMETERS FOR THE VSC-HVDC LINK

Item	*Value*
Rated VSC power S_{VSC}	300 MW
Rated VSC AC rms voltage V_{vsc}	150 kV
Nominal DC voltage V_{dc}	300 kV
Reactor inductance L	0.15 pu
Reactor resistance R	0.005 pu
DC capacitor C_{dc}	7.5 mF
Total capacitor number N	2
Switching frequency f_{sw}	1350 Hz
Rated AC rms voltage in System 1	150 kV

TABLE II

PARAMETERS FOR SYNCHRONOUS GENERATOR [1]

Item	*Value*
Rated MVA S_g	200 MVA
Terminal Voltage V_g	13.8 kV
Inertia time constant	3.2 s
x_d , x_d', x_d''	1.305, 0.296, 0.252
x_q , x_q'', x_l	0.474, 0.243, 0.18
τ_d',τ_d'',τ_q'	1.01, 0.053, 0.1
Stator resistance R_s	2.8544e-3 pu
Pole pairs p	32
Turbine permanent droop R_p	0.05
Turbine time constant T_w	2.67 s
Servo-motor time constant	0.07 s
Exciter regulator gain	300
Exciter time constant	0.001 s

TABLE III

PARAMETERS FOR THE MTDC SYSTEM

Item	*Value*
Rated VSC power S_{VSC}	800 MW
Nominal DC voltage V_{DC0}	±300 kV (600 kV)
Nominal 3-ph AC voltage V_{AC0}	400 kV
DC capacitor C_{dc}	300μF
Total capacitor number N	6
Switching frequency f_{sw}	1350 Hz
Rating of Wind Farm 1	800 MW
Rating of Wind Farm 2	750 MW
Rating of Wind Farm 3	700 MW

TABLE IV

PARAMETERS FOR DC CABLES [2]

DC Cable parameters	*Resistance Ω per km*	*Inductance H per km*	*Capacitance F per km*
	9e-3	3.3e-4	3.1e-7
DC Cables	*Length*	*DC Cables*	*Length*
X1	300	X4	50
X2	300	X5	50
X3	50	X6	50

TABLE V

PARAMETERS FOR THE MTDC SYSTEM

Item	*Value*
Rated MTDC VSC power S_{VSC}	400 MVA
Nominal DC voltage V_{DC0}	±150 kV (300 kV)
Converter side RMS AC voltage V_{AC0}	150 kV
DC capacitor C_{dc}	5mF
Total number of capacitor N	4
Switching frequency f_{sw}	1350 Hz
Power Rating of Wind Farm WF_1	380 MVA
Power Rating of Wind Farm WF_2	360 MVA

TABLE VI

PARAMETERS FOR THE AC SYSTEM

Item	*Value*

AC network line-to-line voltage	400 kV
AC network impedance per km	5.29e-2Ω, 1.4e-3H, 8.7e-9F
SG_1 rated power	400 MVA
SG_1 Terminal line-to-line voltage	13.8 kV
SG_1 inertia time constant	3.3 s
SG_1 turbine time constant T_w	2.67 s
SG_1 servomotor time constant T_a	0.1 s
SG_1 exciter time constant	0.001 s
SG_2 rated power	200 MVA
SG_2 Terminal line-to-line voltage	13.8 kV
SG_2 inertia time constant	3.2 s
SG_2 turbine time constant T_w	2.43 s
SG_2 servomotor time constant T_a	0.07 s
SG_2 exciter time constant	0.001 s

Appendix C Worldwide HVDC Project List up to 2012

TABLE VII

HVDC projects installed in the globe by end of 2011 [3]

System / project	Hvdc supplier	Year commis-sioned	Power rating (mw)	DC voltage (kv)	Line/ cable (km)	Mercury/ thyristor/ transistor	Location
MOSOW-KASHIRA (retired from service)	RUSSIAN	1951 (____)	30	±100	100	MERC	RUSSIA
GOTLAND I (retired from service)	ASEA	1954 (1986)	20	±100	96	MERC	SWEDEN
GOTLAND EXTENSION (retired from service)	ASEA	1970 (1986)	30	±150	96	THY	SWEDEN
GOTLAND II	ASEA	1983	130	150	100	THY	SWEDEN
GOTLAND III	ASEA	1987	260	±150	103	THY	SWEDEN
GOTLAND HVDC LIGHT	ABB	1999	50	±60	70	TRA	SWEDEN
ENGLISH CHANNEL (retired from service)	ASEA	1961 (1984)	160	±100	64	MERC	ENGLAND-FRANCE
VOLGOGRAD-DONBASS	MINISTRY FOR ELECTROTE CHNICAL INDUSTRY OF USSR	1962/65	720	±400	473	MERC/THY	RUSSIA
NEW ZEALAND HYBRID INTER ISLAND LINK	ASEA	1965	600	±250	609	MERC	NEW ZEALAND
NEW ZEALAND HYBRID INTER ISLAND LINK	ABB	1992	1240	+270/-350	612	THY	NEW ZEALAND
KONTI-SKAN 1	ASEA	1965	250	±250	180	MERC	DENMARK-SWEDEN
KONTI-SKAN 1	AREVA	2005	250	±250	180	THY	DENMARK-SWEDEN
KONTI-SKAN 2	ASEA	1988	300	285	150	THY	DENMARK-SWEDEN
SAKUMA (retired from service)	ASEA	1965 (1993)	300	2x125	B-B	MERC	JAPAN
SACOI 1	ENGLISH ELECTRIC	1965	200	200	385	THY	ITALY
SACOI TAP ON CORSICA (LUCCIANA)	CGEE/ALST HOM	1985	50	200	415	THY	ITALY-CORSICA-SARDINIA
SACOI (CODRONGIANOS AND SUVERETO)	ANSADO/GE NERAL ELECTRIC	1993	300	±200	385	THY	ITALY-CORSICA-SARDINIA
SARDINIA (retired from service)	ENGLISH ELECTRIC	1967 (1992)	200	200	413	THY	ITALY
VANCOUVER I	ASEA	1968/69	312	±260	74	MERC	CANADA
VANCOUVER II	GENERAL ELECTRIC	1977/79	370	±280	74	THY	CANADA
PACIFIC INTERTIE	ASEA/GE	1970	1440	±400	1362	MERC	U.S.A
PACIFIC INTERTIE	ASEA/GE	1982	1600	±400	1362	MERC	U.S.A
PAC INTERTIE UPGRADE	ASEA	1985	2000	±500	1362	THY	U.S.A

PACIFIC INTERTIE EXPANSION	ABB	1989	3100	±500	1362	THY	U.S.A
PACIFIC INTERTIE SYLMAR REFURBISHMENT	ABB	UNDER CONSTRUCTION 2010	3100	±500	1362	THY	U.S.A.
KINGSNORTH (retired from service)	ENGLISH ELECTRIC	1972 (1987)	640	±266	82	THY	UNITED KINGDOM
EEL RIVER	GENERAL ELECTRIC	1972	320	±80	B-B	THY	CANADA
NELSON RIVER 1	ENGLISH ELECTRIC/GEC ALSTHOM	1973	1854	±463	890	MERC	CANADA
NELSON RIVER 1	GEC ALSTHOM	1992/93	1854	±463	890	MERC/THY	CANADA
NELSON RIVER 1	SIEMENS	2001/02	1854	±463	890	THY	CANADA
NELSON RIVER 2	AEG/BBC/SIEMENS	1978	900	±250	940	THY	CANADA
NELSON RIVER 2	AEG/BBC/SIEMENS	1985	2000	±500	940	THY	CANADA
SKAGERRAK I	ASEA	1976	275	±250	240	THY	NORWAY-DENMARK
SKAGERRAK II	ASEA	1977	275	±250	240	THY	NORWAY-DENMARK
SKAGERRAK III	ABB	1993	500	±350	240	THY	NORWAY-DENMARK
SHIN-SHINANO 1	HITACHI/TOSHIBA/NISSHIN	1977	300	125	B-B	THY	JAPAN
SHIN-SHINANO 2	HITACHI/TOSHIBA/NISSHIN	1992	300	125	B-B	THY	JAPAN
SQUARE BUTTE	GENERAL ELECTRIC	1977	500	±250	749	THY	U.S.A.
DAVID A. HAMIL	GENERAL ELECTRIC	1977	100	±50	B-B	THY	U.S.A
CAHORA-BASSA	AEG/BBC/SIEMENS	1975/1998	1920	±533	1456	THY	SOUTH AFRICA/MOZAMBIQUE
CAHORA-BASSA	ABB	2008	1920	±533	1420	THY	SOUTH AFRICA/MOZAMBIQUE
CU	ASEA	1979	1000	±400	701	THY	U.S.A
HOKKAIDO-HONSHU	ASEA	1979	150	125	167	THY	JAPAN
HOKKAIDO-HONSHU	HITACHI/TOSHIBA	1980	300	250	167	THY	JAPAN
HOKKAIDO-HONSHU	HITACHI/TOSHIBA	1993	600	±250	167	THY	JAPAN
ACARAY	SIEMENS	1981	55	±25	B-B	THY	PARAGUAY-BRAZIL
VYBORG	MINISTRY FOR ELECTROTECHNICAL INDUSTRY OF USSR	1981	355	1X170(±85)	B-B	THY	RUSSIA-FINLAND
VYBORG	MINISTRY FOR ELECTROTECHNICAL INDUSTRY OF USSR	1982	710	2x170	B-B	THY	RUSSIA-FINLAND
VYBORG	MINISTRY FOR ELECTROTECHNICAL	1984	1065	3x170	B-B	THY	RUSSIA-FINLAND

	INDUSTRY OF USSR						
VYBORG	MINISTRY FOR ELECTROTECHNICAL INDUSTRY OF USSR	1999	4x405	±85	B-B	THY	RUSSIA-FINLAND
ZHOU SHAN PROJECT		1982	50	100	42	THY	CHINA
INGA-SHABA	ASEA/GE	1982/83	560	±500	1700	THY	ZAIRE
DUERNROHR 1 (retired from service)	BBC/SIEMENS	1983 (1997)	550	145	B-B	THY	AUSTRIA
EDDY COUNTY	GENERAL ELECTRIC	1983	200	82	B-B	THY	U.S.A.
POSTE CHATEAUGUAY	BBC/SIEMENS	1984	2x500	145	B-B	THY	CANADA-U.S.A.
CHATEAUGUAY UPGRADE	ABB	2009	2x500	145	B-B	THY	CANADA
OKLAUNION	GENERAL ELECTRIC	1984	200	82	B-B	THY	U.S.A
ITAIPU 1	ASEA	1984	1575	±300	785	THY	BRAZIL
ITAIPU 1	ASEA	1985	2383	±300	785	THY	BRAZIL
ITAIPU 1	ASEA	1986	3150	±600	785	THY	BRAZIL
ITAIPU 2	ASEA	1987	3150	±600	805	THY	BRAZIL
BLACKWATER	BBC	1985	200	57	B-B	THY	U.S.A.
HIGHGATE	ASEA	1985	200	±56	B-B	THY	U.S.A.
MADAWASKA	GENERAL ELECTRIC	1985	350	130.5	B-B	THY	CANADA
MILES CITY HVDC SYSTEM (MCCS)	GENERAL ELECTRIC	1985	200	82	B-B	THY	U.S.A
BROKEN HILL	ASEA	1986	40	2x17 (±8.33)	B-B	THY	AUSTRALIA
INTERMOUNTAIN POWER PROJECT (I.P.P.)	ASEA	1986	1920	±500	785	THY	U.S.A.
I.P.P. UPGRADE	ABB	UNDER CONSTRUCTION 2010	2400	±500 kV	785	THY	USA
CROSS CHANNEL BP 1+2	CGEE ALSTHOM/GEC	1985/86	2000	±270	70	THY	FRANCE-U.K.
DES CANTONS-COMFERFORD	GENERAL ELECTRIC	1986	690	±450	172	THY	CANADA-U.S.A.
QUEBEC-NEW ENGLAND (THREE TERMINAL)	ABB	1990-92	2250	±450	1500	THY	CANADA-U.S.A.
VIRGINIA SMITH	SIEMENS	1987	200	50	B-B	THY	U.S.A
GESHA (GEZHOUBA-SHANGHAI)	BBC/SIEMENS	1989	600	500	1000	THY	CHINA
GESHA (GEZHOUBA-SHANGHAI)	BBC/SIEMENS	1990	1200	±500	1000	THY	CHINA
VINDHYACHAL	ASEA	1989	500	2x69.7	B-B	THY	INDIA
McNEILL	GEC ALSTHOM	1989	150	42	B-B	THY	CANADA

FENNO-SKAN	ABB/ALCATEL	1989/98	500	400	303	THY	FINLAND-SWEDEN
FENNO-SKAN II	ABB/NEXANS	2011	800	500	303	THY	FINLAND-SWEDEN
BARSOOR LOWER SILERU	BHEL	1989/91	100	±200	196	THY	INDIA
RIHAND-DELHI	ABB/BHEL	1991	750	500	814	THY	INDIA
RIHAND-DELHI	ABB/BHEL	1992	1500	±500	814	THY	INDIA
Inter-Island NZ 2		1992	640	350	610	THY	NewZ (Benmore - Haywards)
SAKUMA	HITACHI/TOSHIBA/MITSUBISHI/NISSHIN	1993	300	±125	B-B	THY	JAPAN
ETZENRICHT (retired from service)	SIEMENS	1993 (1997)	600	160	B-B	THY	GERMANY-CZECH REPUBLIC
VIENNA SOUTH-EAST (retired from service)	SIEMENS	1993 (1997)	600	145	B-B	THY	AUSTRIA-HUNGARY
URUGUAIANA	TOSHIBA	1994	50	15	B-B	THY	BRAZIL-ARGENTINA
BALTIC CABLE	ABB	1994	600	450	261	THY	SWEDEN-GERMANY
WELSH	SIEMENS	1995	600	170	B-B	THY	U.S.A
KONTEK	ABB/NKT CABLES	1995	600	400	171	THY	DENMARK-GERMANY
SYLMAR EAST (VALVE RECONSTRUCTION)	SIEMENS	1995	550	500	1200	THY	U.S.A.
HAENAM-CHEJU	GEC ALSTHOM	1997	300	±180	101	THY	KOREA
CHANDRAPUR-RAMAGUNDUM	GEC ALSTHOM	1997/98	1000	2x205	B-B	THY	INDIA
CHANDRAPUR BACK-TO-BACK	ABB	1998	1500	±500	736	THY	INDIA
LEYTE-LUZON	ABB/MARUBENI	1998	440	350	455	THY	PHILIPPINES
WELCH-MONTICELLO	SIEMENS	1998	600	162	B-B	THY	U.S.A.
MINAMI-FUKUMITZU	HITACHI/TOSHIBA	1999	300	125	B-B	THY	JAPAN
VIZAG 1	GEC ALSTHOM	1999	500	205	B-B	THY	INDIA
VIZAG 2	ABB	2005	500	±88	B-B	THY	INDIA
VISBY-NAS	ABB	1999	50	80	70	THY	SWEDEN
SWEPOL LINK	ABB	2000	600	±450	254	THY	SWEDEN-POLAND
DIRECTLINK	ABB	2000	3 x 60	±80	59	TRA	AUSTRALIA
KII CHANNEL	HITACHI/TOSHIBA/MITSUBISHI	2000	1400	±250	102	THY	JAPAN
GARABI 1	ABB	2000	1100	±70	B-B	THY	ARGENTINA-BRAZIL
EAGLE PASS	ABB	2000	36	15.9	B-B	TRA	U.S.A.

TJAEREBORG	ABB	2000	7	9	4.3	TRA	DENMARK
GARABI 2	ABB	2002	2000	±70	B-B	THY	ARGENTINA-BRAZIL
RIVERA	GEC ALSTHOM	2000	70	20	B-B	THY	URUGUAY-BRAZIL
GRITA	PIRELLI/ABB	2001	500	400	316	THY	GREECE-ITALY
TIAN-GUANG	SIEMENS	2001	1800	±500	960	THY	CHINA
HIGASHI-SHIMIZU	HITACHI/TOSHIBA	2001	300	125	B-B	THY	JAPAN
MOYLE INTERCONNECTOR	SIEMENS	2001	2x250	2x250	64	THY	NORTHERN IRELAND-SCOTLAND
THAILAND-MALAYSIA	SIEMENS	2001	300	±300	110	THY	THAILAND-MALAYSIA
CROSS SOUND	ABB	2002	330	±150	40	TRA	U.S.A
MURRAYLINK	ABB	2002	200	±150	176	TRA	AUSTRALIA
SASARAM	GEC ALSTHOM	2002	500	205	B-B	THY	INDIA
RAPID CITY TIE	ABB	2003	2 x 100	±13	B-B	THY	U.S.A.
EAST-SOUTH INTERCONNECTOR II	SIEMENS	2003	2000	±500	1450	THY	INDIA
EAST-SOUTH INTERCONNECTOR II UPGRADE	SIEMENS	2007	2500	±500	1450	THY	INDIA
THREE GORGES-CHANGZHOU	ABB/SIEMENS	2003	3000	±500	860	THY	CHINA
THREE GORGES-GUANGDONG	ABB	2004	3000	±500	940	THY	CHINA
GUI-GUANG I	SIEMENS	2004	3000	±500	980	THY	CHINA
GUI-GUANG II	SIEMENS	2007	3000	±500	1200	THY	CHINA
TROLL A	ABB	2004	2x40	±60	70	TRA	NORWAY
CELILO (VALVE REPLACEMENT)	SIEMENS	2004	3100	±400	1200	THY	U.S.A.
LAMAR	SIEMENS	2005	210	±64	B-B	THY	U.S.A.
LINGBAO		2005	360	168	B-B	THY	CHINA
BASSLINK	SIEMENS	2006	500	400	350	THY	AUSTRALIA
ESTLINK	ABB	2006	350	±150	105	TRA	ESTONIA-FINLAND
THREE GORGES-SHANGHAI	ABB	2006	3000	±500	900	THY	CHINA
NEPTUNE	SIEMENS	2007	660	500	105	THY	U.S.A.
SHARYLAND	ABB	2007	150	±21	B-B	THY	USA - MEXICO
THE APOLLO CONVERTER STATION	ABB	REFURBISHED 2008	2500	±533	1420	THY	SOUTH AFRICA
LEVIS DE-ICER	AREVA	2008	250	±17.4	27 to 242	THY	CANADA

NORNED	ABB	2008	700	±450	580	THY	NORWAY-NETHERLANDS
BALLIA - BHIWADI	SIEMENS	2010	2500	500	800	THY	INDIA
OUTAOUAIS	ABB	2009	2x625	315	B-B	THY	CANADA
NORDE.ON 1	ABB	2009	400	150	203	TRA	GERMANY
VALHALL	ABB	UNDER CONSTRUCTION 2011	78	150	292	TRA	NORWAY
AL FADHILI	AREVA	2009	3 x 600	3 x 222	B-B	THY	SAUDI ARABIA
CAPRIVI	ABB	2010	300	350	950	TRA	NAMIBIA
SAPEI	ABB	UNDER CONSTRUCTION 2011	1000	±500	435	THY	ITALY MAINLAND-SARDINIA
BRITNED	SIEMENS	2011	1000	±400	260	THY	UK - NETHERLANDS
YUNNAN-GUANGDONG	SIEMENS	2010	5000	±800	1418	THY	CHINA
STOREBAELT	SIEMENS	2010	600	400	56	THY	DENMARK
XIANJIABA-SHANGHAI	ABB	2010	6400	±800	1980	THY	CHINA
TRANS BAY CABLE	SIEMENS AND PIRELLI	2010	400	200	88	TRA	U.S.A.
HULUNBEIR-LIAONING HVDC LINK	ABB	2010	3 000	±500	920	THY	CHINA
HULUNBEIR (INNER MONGOLIA) - SHENYANG		2010	3000	± 500	920	THY	CHINA
LINGBAO II EXTENSION PROJECT	ABB/ALSTOM	2010	750	168	B-B	THY	CHINA
BORWIN1	ABB	SCHEDULED 2012	400	±150	200	TRA	GERMANY
JINDO-JEJU	ALSTOM	2011	400	±250	105	THY	KOREA
COMETA	PRYSMIAN/NEXANS/SIEMENS	UNDER CONSTRUCTION 2011	400	250	247	THY	SPAIN
RIO MADEIRA	ABB (BIPOLE 1) &ALSTOM (BIPOLE 2)	UNDER CONSTRUCTION 2012 (BIPOLE 1) 2013 (BIPOLE 2)	2 x 3150	±600	2375	THY	BRAZIL
EAST-WEST INTERCONNECTOR	ABB	UNDER CONSTRUCTION 2012	500	±200	261	TRA	IRELAND-UNITED KINGDOM
BISWANATH-AGRA	ABB	UNDER CONSTRUCTION 2014-2015	6000	±800	1728	THY	INDIA
RIO MADEIRA	ABB	PLANNED 2012	800 (2x400 BTB)	100	B-B	THY	BRAZIL
SUMATRA-JAVA		UNDER CONSTRUCTION 2013	3000	±500	700	THY	INDONESIA
MUNDRA - HARYANA	SIEMENS	UNDER CONSTRUCTION 2012	2500	±500	960	THY	INDIA

SKAGERRAK 4	ABB	UNDER CONSTRUCTION 2014	700	500	244	TRA	NORWAY - DENMARK
JINPING - SUNAN (SGCC)	ABB	SCHEDULED 2013	7200	±800	2090	THY	CHINA
THREE GORGES - SHANGHAI 3	ALSTOM	2010	3000	±500	1000	THY	CHINA
NINGDONG - SHANGDONG	Alstom	2011	4000	±660	1335	THY	CHINA
ESTLINK 2	SIEMENS	SCHEDULED 2014	670	±450	171	THY	ESTONIA-FINLAND
BLACK SEA TRANSMISSION NETWORK	SIEMENS	SCHEDULED 2013	2x350	96	B-B	THY	GEORGIA - TURKEY
INTER ISLAND CONNECTOR	SIEMENS	SCHEDULED 2013	700	±350		THY	NEW ZEALAND
HIGHGATE CONVERTER STATION REFURBISHMENT	ABB	SCHEDULED 2012	200	57	B-B	THY	USA - CANADA
HUDSON TRANSMISSION	SIEMENS / PRYSMIAN	SCHEDULED 2013	660	±345	12	THY	USA
NUOZHADU-GUANGDONG	SIEMENS	SCHEDULED 2013	5000	800	1500	THY	CHINA
XILUODU-HANZHOU	SIEMENS	SCHEDULED 2013	6400	800	1300	THY	CHINA
QINGHAI-TIBET	CET/SGCC	SHEDULED 2012	1500	±400	1038	THY	CHINA-TIBET
MELO INTERCONNECTOR	ALSTOM	SCHEDULED 2012	500	525	B-B	THY	URUGUAY-BRAZIL
FRANCE - SPAIN INTERCONNECTION LINK	SIEMENS	UNDER CONSTRUCTION 2013	2000	±320	65	THY	FRANCE - SPAIN

References

[1] Anderson, P.; Fouad, A.A., *Power System Control and Stability*. Ames, Iowa, U.S.A: The Iowa State University Press, 1977.

[2] ABB, XLPE Land Cable Systems User´s Guide, pp.16-22, Available [assessed on 25/08/2012]: http://www05.abb.com/global/scot/scot245.nsf/veritydisplay/ab02245fb5b5ec41c12575c4004a76d0/$file/xlpe%20land%20cable%20systems%202gm5007gb%20rev%205.pdf.

[3] University of Uidaho, *HVDC Projects List Prepared for the HVDC and Flexible AC Transmission Subcommittee of the IEEE Transmission and Distribution Committee*, Online Available [assessed on 09/06/2013]: http://www.ece.uidaho.edu/hvdcfacts/Projects/HVDCProjectsListingMarch2012-existing.pdf.